Fall 2016

Analysis and mitigation of wellbore breakout and fracturing

Reza Rahimi

ANALYSIS AND MITIGATION OF WELLBORE BREAKOUT AND FRACTURING

By

REZA RAHIMI

A DISSERTATION

Presented to the Faculty of the Graduate School of the

MISSOURI UNIVERSITY OF SCIENCE AND TECHNOLOGY

In Partial Fulfillment of the Requirements for the Degree

DOCTOR OF PHILOSOPHY

in

PETROLEUM ENGINEERING

2016

Approved by:

Runar Nygaard, Advisor
Andreas Eckert
Ralph Flori
Peyman Heidari
John Hogan

PUBLICATION DISSERTATION OPTION

This dissertation consists of following five articles, formatted in the style used by the Missouri University of Science and Technology:

Pages 24 to 54 are published in the INTERNATIONAL JOURNAL OF ROCK MECHANICS AND MINING SCIENCES.

Pages 55 to 84 are submitted to the JOURNAL OF ROCK MECHANICS AND ROCK ENGINEERING.

Pages 85 to 110 are submitted to the JOURNAL OF NATURAL GAS SCIENCE & ENGINEERING.

Pages 111 to 131 are published in proceeding of 2016 AADE FLUIDS TECHNICAL CONFERENCE AND EXHIBITION held in Houston, TX, USA, 12-13 April 2016.

Pages 132 to 156 are submitted to the 2017 OFFSHORE TECHNOLOGY CONFERENCE (OTC).

ABSTRACT

Mechanical wellbore integrity problems while drilling are mainly due to wellbore shear failure or tensile failure. To ensure wellbore integrity, breakout and fracture geomechanical analysis is conducted to estimate minimum and maximum drilling fluid densities. Currently, there is no agreement as to which rock failure criterion to use for estimating breakout or fracture criteria to use for analyzing drilling induced fractures. However, when wellbore integrity issues arise while drilling, mitigation strategies can be applied to rectify these problems.

This dissertation analyzes criteria for wellbore breakout and fracturing. Also, mitigation strategies for breakout and fracturing while drilling were experimentally investigated. Thirteen rock failure criteria were compared based on estimating borehole breakout for field reported wellbore failure cases. Five fracture width models were investigated, compared, and experimentally evaluated. Hydraulic fracturing experiments were carried out to evaluate the impact of LCM addition on enhancing both; breakdown and re-opening pressure. Coal Combustion Residuals particles evaluated as shale inhibitor additive in water-based drilling fluid system using pressure transient test.

The results showed the estimated borehole breakout by Mogi-Coulomb, Modified Lade, and Modified Wiebols Cook criteria is close to field reported shear failure. Carbonell and Detournay's fracture width model estimated close to the measured fracture width of core samples. The addition of different LCM blends enhanced the breakdown pressure up and the re-opening pressure. Using fine grained Coal Combustion Residuals in water-based drilling fluid reduced the pressure transient rate in Catoosa shale samples.

ACKNOWLEDGMENTS

It has been a long journey, enjoyable and sometimes painful but at the end of the day so special. My name is shining in the first page but many people have contributed to this achievement in their own particular way and for that, I want to give them special thanks. First and foremost I want to thank my advisor, Dr. Runar Nygaard. I appreciate all his contributions of time, ideas, and funding to make my time in graduate school so special. His mix of straightforward criticism combined with heart-warming support have given me great confidence as a researcher, and at the same time made me realize that I am only a beginner in this exciting profession. I would like to thank my committee members, Dr. Andreas Eckert, Dr. Ralph Flori, Dr. Peyman Heidari, and Dr. John Hogan for their valuable feedback. I am especially grateful for the fun group of original members in the drilling research group who stuck it out in grad school with me: Dr. Mohammed Al Dushaishi and Dr. Mortadha Alsaba. For all experimental works, Jeff Heniff made a significant contribution. My time at Missouri S&T was made enjoyable in large part due to the many friends that became a part of my life. I especially thank my mom, dad, and sisters. My hard-working parents, Ensieh and Hamid, have sacrificed their lives for my sisters and myself and provided unconditional love and care. I love them so much, and I would not have made it this far without them. My sisters, Masoomeh and Maedeh, have been my best friends all my life and I love them and thank them for all their support. I know I always have my family to count on when rough times come. The best outcome from these past four years is finding my best friend and soul-mate. Desiree has been a true and great supporter and has unconditionally loved me during my good and bad times. I truly thank Desiree for sticking by my side all the time.

TABLE OF CONTENTS

Page

PAPER

LIST OF ILLUSTRATIONS

SECTION Page

PAPER II

PAPER III

LIST OF TABLES

PAPER V

NOMENCLATURE

Symbol	Description
UCS	Uniaxial Compressive Strength
CDP	Circumscribed Drucker-Prager
ML	Modified Lade
MG	Mogi-Coulomb
MWC	Modified Wiebols-Cook
MR	Murrell
HB	Hoek-Brown
SD	Stassi D'Alia
MC	Mohr-Coulomb
MGR	Modified Griffith
IDP	Inscribed Drucker-Prager
GR	Griffith
VM	Von Mises
TR	Tresca
LCM	Lost Circulation Material
PSD	Particle Size Distribution
G	Graphite
SCC	Sized Calcium Carbonate
NS	Nutshells
CF	Cellulosic Fiber
HPA	High Pressure Apparatus

HPHT	High Pressure High Temperature
WBM	Water-Base Mud
OBM	Oil-Base Mud
P_B	Breakdown Pressure
T_0	Tensile Strength
C_0	Uniaxial Compressive Strength
c	Cohesion
ϕ	Internal Angle of Friction
μ	Coefficient of Internal Angle of Friction
q	Flow Factor
σ_V	Overburden Stress
σ_H	Maximum Horizontal Stress
σ_h	Minimum Horizontal Stress
W_c	Fracture Width
L	Fracture Length
E	Young's Modulus
v	Poisson's Ratio
P_f	Pressure along the fracture surface
P_w	Wellbore Pressure
r_w	Wellbore Radius
x	Distance from the fracture mouth
P_0	Pore Pressure

1. INTRODUCTION

Wellbore integrity problems while drilling are well-known and costly, including wellbore instability problems and fluid loss events. Mechanical failure, insufficient hole cleaning, differential sticking, tight hole, stuck pipe, and wellbore trajectory problems are often the consequence of wellbore instabilities. Partial and total losses of drilling fluid are the consequence of fluid loss events. It is believed that the principal reason of wellbore instability is the borehole compressive failure, especially for shales (Hale et al., 1993; Bol et al., 1994; Gazianol et al., 1995). Root cause diagnosis of drilling instabilities is of key importance in prevention or remediation approaches. For example, keyseat (i.e. borehole wear due to lateral force from the drill stem when the dogleg is too sharp in deviated wellbores) causes borehole enlargement on one side of the wellbore and is not symmetric as borehole breakouts are. Fluid losses and fractures around the wellbore walls are other major concerns for wellbore integrity and also for operational safety purposes. Drilling induced tensile fracture and presence of pre-existing fractures around wellbore are root cause of fluid loss events. Drilling fluids are expensive and availability of fluid in the rig site is limited, especially for offshore operations. More importantly, a drop in wellbore pressure due to fluid losses will enhance the likelihood of well control issues and kick. In addition to consequences while drilling, out-of-gauge wellbore size creates uncertainty for cement volume calculations, and a poor cement job could intensify the chance for problems in well completion and production operations such as perforation and sand control. In general, instabilities create and intensify problems.

1.1. THEORY OF MECHANICAL WELLBORE FAILURE

Assuming a circular wellbore with impermeable wall, shear and tensile failures happen when in situ stresses exceed rock compressive strength and tensile strength. Breakout or onset of shear failure initiates when the maximum differential stress occurs at the borehole wall (Babcock, 1978). Breakout will cause symmetric elongation or enlargement of the borehole (Figure 1-1). Small breakouts are not a source for any operational concerns. However, wellbore mechanical collapse due to intensive breakouts or wellbore shear failure can trigger instabilities. Practically, the onset of borehole breakout is considered as lower bound of mud weight window or minimum required drilling fluid density. The minimum required drilling fluid density might be higher or lower than formation pore pressure, depending on in situ stresses, and also rock mechanical properties. The minimum required drilling fluid density is controlled by borehole shear failure only if the onset of breakout is above the formation pore pressure. Wellbore tensile failure happens when drilling fluid hydrostatic pressure exceeds the formation tensile strength (Brudy et al., 1999) (Figure 1-1). The fracture initiation pressure is considered as higher mud weight window or maximum drilling fluid density.

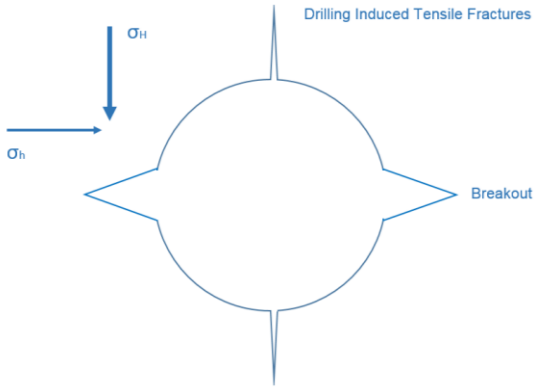

Figure 1-1. Borehole breakout and drilling induced tensile fracture at the wall of a vertical hole with anisotropic horizontal stresses

1.2. CHEMICAL-MECHANICAL SHEAR FAILURE

The assumption of impermeable wellbore wall often might not be valid especially for shales (Chenevert, 1970). Time-dependent drilling fluid invasion in shales causes wellbore instabilities (Chenevert, 1970 & 1989; Hale et al., 1993; Ballard et al., 1994; Bol et al., 1994; Van Oort et al., 1996; Horsrud and Bostrom, 1998). Fluid invasion in shales is believed to be a physiochemical process mainly due to hydraulic potential drive and chemical potential drive (Van Oort et al., 1996; Karaborni et al., 1996). The Darcy flow of water is driven by hydraulic potential gradients (pressure imbalance), and diffusion of solutes are driven by chemical potential gradients (chemical imbalance) between the drilling fluid and the shales' pore fluid. Increase of near wellbore pore pressure reduces the effective stresses causing wellbore failure. Reduction of near wellbore rock strength, increase of hydration stress in pore space, and shales swelling or wellbore size shrinkage are other main consequences of shale hydration. The shale hydration causes differential micro-strains and weakens the cohesive bonds between clay platelets which results in strength reduction (Fam and Dusseault, 1998). (Hale et al., 1993; Ghassemi et al., 2001; Mody et al., 2002). Invaded drilling fluid increases pore pressure since shales have a low permeability and cannot dissipate excess pore pressure (Chenevert, 1970 & 1989; Van Oort et al., 1996; Horsrud and Bostrom, 1998).

There are different theories that have been developed to described the shales swelling process, such as hydraulic pressure balance, capillary suction (surface hydration), and osmosis pressure (Forsans and Schmitt, 1994; Van Oort et al., 1996; Karaborni et al., 1996). However, shales swelling phenomena is not well-understood and there is no agreement as to which mechanism is dominant in the shale hydration. Surface hydration

happens through the bonding of water molecules to oxygen atoms on the surface of the clay's silicate layers, and ionic hydration is caused by formation of hydration shells around exchangeable cations in the clay crystal (Chenevert, 1970 & 1989). Flow of water from a dilute solution to a more concentrated solution through a semi-permeable membrane is called osmosis (Chenevert, 1970, 1989). When the water activity (chemical potential) in the bulk fluid is higher than the water activity of the shale formation, a net flux of ions would flow out and a net flux of water would flow into the shale formation (Marine and Fritz, 1981; Mody et al., 2002). A presence of a semi-permeable membrane is essential for osmosis to occur; the membrane allows only solvent molecules to pass through while restricting solutes and other unwanted particles (Van Oort et al., 1994). However, Ballard et al. (1992) investigated water transport through shale and concluded that shales do not act as semi-permeable membranes as described by Chenevert (1970 & 1989) and that ions can freely diffuse through them. Bol et al. (1992) came to the same conclusion after running a series of experiments. Shales do not act as an ideal semi-permeable membrane; it is well-established that ions do move through shales (e.g. Steiger, 1982; Denis et al., 1991; Ballard et al., 1994; Horsrud et al., 1998). Membrane efficiency was defined as a measure of how well shales can prevent ion movement (Horsrud et al., 1998). Low clay content shales are normally fractured and therefore do not act as a barrier to water and ion movement (Ewy and Stankovich, 2000). While osmotic backflow strengthens shales through pore pressure and water content reduction, ionic diffusion can weaken shales (Marine and Fritz, 1981; Ghassemi et al., 2001). Ion transfer into shales has a negative impact on strength by inducing tensile stresses (Ghassemi et al., 2001). Potassium ion fits more easily into the clay mineral crystal lattice than the sodium ion, which is the dominant native ion in shales

(Ghassemi et al., 2001). When the formation is chemically inert, the fluid invasion is controlled only by the difference between the wellbore pressure and the formation pore pressure (Bol et al., 1994; Ballard et al., 1994). Mody and Hale (1993) believed hydraulic flow is due to pressure difference between the wellbore and formation is dominant in poorly consolidated (more permeable) shales.

1.3. FLUID LOSSES

Fluid losses happen when drilling fluid penetrates natural or pre-existing fractures or when drilling fluid density exceeds the formation fracture gradient– this is often called a drilling-induced fracture. Figure 1-2 shows different scenarios of wellbore pressure leading to fluid losses (Alsaba et al., 2014). To prevent fluid loss events, the drilling fluid density should be kept below the fracture breakdown pressure for intact rock and also below the fracture re-opening pressure for naturally fractured formations. Fluid losses might happen due to drilling practices such as insufficient hole cleaning. Fluid losses may initiate from hole collapse and can be triggered by insufficient cleaning. Borehole pack-off while back-reaming may also lead to fluid losses (Fjear et al., 2008). It should be noted that significant fluid losses happen when the fracture initiates and also propagates beyond the near well region. Fracture propagation happens when the wellbore pressure exceeds the minimum principal stress and an additional term, depending on the conditions for fracture growth at the tip and fracture leakage to the formation (Nygaard and Salehi, 2011). Therefore, in practical terms, the well pressure should not exceed the fracture closure pressure or minimum principal horizontal stress (usually minimum horizontal stress) (Fjear et al., 2008; Nygaard and Salehi, 2011). Moreover, critical stress states in fractured shales

could be enhanced by chemical or mechanical effects and result in formation breakdown (Labenski et al., 2003).

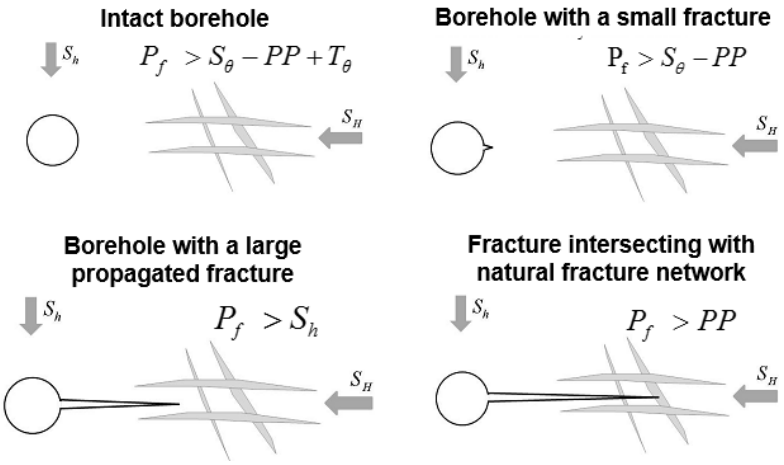

Figure 1-2. Different wellbore pressure conditions for fluid losses (Nygaard and Salehi, 2011)

1.4. WELL INTEGRITY SOLUTIONS

Determining the appropriate minimum required drilling fluid density by rock failure analysis is an essential step to control wellbore instability. To determine wellbore failure stresses, rock strength must be known, an appropriate constitutive model should be selected, and an accurate rock failure criterion must be chosen. Shear rock failure criterion specifies stress conditions at failure. Using of drilling fluid density equal or greater than the estimated borehole breakout will prevent mechanical shear failure of the wellbore (Fjaer et al., 2008). The Kirsch solution for wellbore principal stresses is based on the assumption of impermeable rock and constant pore pressure (Bradley, 1979; Aadnoy and Chenevert, 1987). However, this assumption is not realistic for both low permeable and

high permeable formations and near wellbore pore pressure might change with drilling fluid-rock interaction.

For shales, swelling and pressure transmission through a physiochemical process between wellbore fluid and formation will reduce near wellbore stress and strength (Van Oort et al., 1996; Ghassemi et al., 2011). In order to prevent shales hydration, different drilling fluid systems were designed such as oil-based drilling fluid or water-based drilling fluid systems with different additives (Hale et al., 1993; Van Oort et al., 1996). These solutions could potentially prevent the swelling capability of shales and maintain original pore pressure, water content, and rock strength.

Fluid losses could be mitigated and controlled using lost circulation material (LCM). Preventive LCM treatments widen the mud weight window or, in other words, enhance the fracture gradient (Morita et al., 1990; Van Oort et al., 2011; Mostafavi et al. 2011; Salehi and Nygaard, 2015). The concept of wellbore strengthening can be defined as "a set of techniques used to efficiently plug and seal induced fractures while drilling to deliberately enhance the fracture gradient and widen the operational window" (Salehi and Nygaard, 2012). Enhancement of the fracture gradient could happen by increasing the formation breakdown pressure and fracture re-opening pressure.

1.5. LITERATURE STUDY

The main objective of this section is to review previous studies on wellbore integrity solutions in the following areas: rock failure criteria for wellbore stability analysis, fracture width models for wellbore strengthening applications, drilling fluid

systems for preventing shales swelling, and effects of particle size and size distribution of lost circulation material.

1.5.1. Rock Failure Criteria. Shear rock failure criterion specifies stress conditions at failure. Common rock failure criteria used for wellbore stability analysis are listed in Table 1-1. Rock failure criteria can be classified based on two main characteristics, linearity of the governing equation and the effect of intermediate principal stress. Some rock failure criteria have a linear form, such as Tresca, while other failure criteria have a nonlinear form, such as Drucker-Pager. The second characteristic involves the effect of intermediate principal stress on rock strength. Mohr-Coulomb and Hoek-Brown are examples of rock failure criteria that do not consider the effects of intermediate principal stress. In contrast, rock failure criteria such as Modified Lade and Mogi-Coulomb consider the effect of intermediate principal stress on rock failure. There are numerous rock failure criteria that have been used in wellbore stability analysis to determine the minimum required drilling fluid density, as outlined below, and yet there is no agreement on which failure criterion should be used in practical wellbore stability analysis.

The previous studies on evaluation of rock failure criteria can be divided in two groups. The first group addressed how well the failure criteria can be fitted to triaxial test data. Seven different rock failure criteria were evaluated by Colmenares and Zoback, 2002, based on fitting polyaxial test data, and they concluded that the Modified Lade and the Modified Wiebols-Cook fit best with polyaxial tests. The quantitative comparison of the six rock failure criteria was done by Benz and Schwab, 2008, to determine which criterion gives the best fit with polyaxial test data. The second group of previous studies focused on minimum mud weight predictions for different failure criteria.

Table 1-1. Rock failure criteria

Failure Criteria	Governing Equation	The effect of intermediate principal stress (σ_2)
Mohr-Coulomb (MC) (Jaeger et al., 2007)	$\sigma_1 = q\sigma_3 + C_0$ $q = \frac{1+\sin\phi}{1-\sin\phi}$, $C_0 = \frac{2c\cos\phi}{1-\sin\phi}$	No
Mogi-Coulomb (MG) (Al-Ajmi and Zimmerman, 2005)	$\tau_{oct} = a + b\sigma_{m,2}$ $a = \frac{2\sqrt{2}}{3}\frac{C_0}{q+1}$, $b = \frac{2\sqrt{2}}{3}\frac{q-1}{q+1}$	Yes
Tresca (TR) (Fjaer et al., 2008)	$\frac{(\sigma_1-\sigma_3)}{2} = c = \tau_{max}$, $\frac{C_0}{2} = c$	No
Von Mises (VM) (Jaeger et al., 2007)	$\sqrt{J_2} = \sqrt{\frac{(\sigma_1-\sigma_3)^2+(\sigma_2-\sigma_3)^2+(\sigma_1-\sigma_3)}{6}} = \frac{C_0}{3}$	Yes
Ins. Drucker-Prager (IDP) (Veeken et al., 1989)	$\sqrt{J_2} = k + \alpha J_1$ $\alpha = \frac{3\sin\phi}{\sqrt{9+3\sin\phi^2}}$, $k = \frac{3C_0\cos\phi}{2\sqrt{q}\sqrt{9+3\sin\phi^2}}$	Yes
Cir. Drucker-Prager (CDP) (Zhou, 1994)	$\sqrt{J_2} = k + \alpha J_1$ $\alpha = \frac{\sqrt{3}(q-1)}{(2+q)}$, $k = \frac{\sqrt{3}C_0}{2+q}$	Yes
Hoek-Brown (HB) (Hoek and Brown, 1980)	$\sigma_1 = \sigma_3 + \sqrt{mC_0\,\sigma_3 + s{C_0}^2}$	No
Modified Lade (ML) (Ewy, 1999)	$\frac{{I_1}^3}{I_3} = \eta_1 + 27$ $S = \frac{c}{\tan\phi}$, $\eta = \frac{4\tan^2\phi(9-7\sin\phi)}{(1-\sin\phi)}$	Yes
Modified Wiebols-Cook (MWC) (Zhou, 1994)	$\sqrt{J_2} = A + BJ_1 + C{J_1}^2$ $C = \frac{\sqrt{27}}{2C_1+(q-1)\sigma_3-C_0}\left(\frac{C_1+(q-1)\sigma_3-C_0}{2C_1+(2q-1)\sigma_3-C_0} - \frac{q-1}{q+2}\right)$ $C_1 = (1+0.6\,\mu)C_0$, $B = \frac{\sqrt{3}(q-1)}{q+2} - \frac{C}{3}[2C_0+(q+2)\sigma_3]$ $A = \frac{C_0}{\sqrt{3}} - \frac{C_0}{3}B - \frac{{C_0}^2}{9}C$	Yes
Griffith (GR) (Griffith, 1921)	$(\sigma_1-\sigma_3)^2 = 8T_0(\sigma_1+\sigma_3)$ $\sigma_3 = -T_0$ if $\sigma_1 + 3\sigma_3 < 0$, $T_0 = \frac{C_0}{8}$	No
Modified Griffith (MGR) (McClintock and Walsh, 1962)	$\sigma_1\left[\sqrt{\mu^2+1}-\mu\right] - \sigma_3\left[\sqrt{\mu^2+1}+\mu\right] = 4T_0$ $\frac{C_0}{T_0} = \frac{4}{\sqrt{\mu^2+1}-\mu}$	No
Murrell (MR) (Murrell, 1962)	$(\sigma_1-\sigma_3)^2 + (\sigma_1-\sigma_2)^2 + (\sigma_2-\sigma_3)^2 = 24T_0(\sigma_1+\sigma_2+\sigma_3)$ $T_0 = \frac{C_0}{12}$	Yes
Stassi D'Alia (SD) (Stassi D'Alia, 1967)	$(\sigma_1-\sigma_3)^2 + (\sigma_1-\sigma_2)^2 + (\sigma_2-\sigma_3)^2 =$ $2(C_0-T_0)(\sigma_1+\sigma_2+\sigma_3) + 2C_0T_0$	Yes

McLean and Addis (1990) compared Mohr-Coulomb and different forms of Drucker-Prager to predict the minimum required mud weight. Their results showed that criteria can predict realistic results in one situation but give unrealistic results for other conditions. The Mohr-Coulomb failure criterion was recommended for wellbore stability analysis because it yielded more realistic results compared with the different forms of Drucker-Prager (Mclean and Addis, 1990). The Modified-Lade failure criterion developed by Ewy (1999) included the intermediate principal stress and provided better fit with polyaxial compressive strength results compared to Mohr-Coulomb and Drucker-Prager. Nawrocki (2010) estimated borehole breakout pressure based on evaluation of four rock failure criteria and the Modified Lade criterion was recommended. Some of the previous studies evaluated failure criteria both in fitting polyaxial test data and in estimating the minimum required drilling fluid density. Al Ajmi and Zimmerman developed (2006 ,2005) Coulomb-the linear form of Mogicriterion and compared that with the Mohr-Coulomb failure criterion. They proposed the use of Mogi-Coulomb over Mohr-Coulomb with regard to fitting polyaxial test data as well as predicting the borehole breakout pressure. Three rock failure criteria were compared by Yi et al. (2005) based on minimum drilling fluid density estimation, and it was concluded that the failure criterion which best fits the polyaxial test data can better describe rock failure, therefore providing more reliable results for the minimum required drilling fluid density. Based on their results, no specific failure criterion can consistently estimate higher or lower minimum drilling fluid density compared with the other failure criteria (Yi et al., 2005). Corresponding parameters of five failure criteria were determined by Zhang et al. (2010) using triaxial test data, where Mogi-Coulomb and Hoek-Brown criteria were recommended for wellbore stability analysis.

1.5.2. Review of Fracture Width Models for Wellbore Strengthening. Estimation of the fracture width could be an important design parameter for LCM treatment design (Alberty and McLean, 2004). The efficiency of strengthening treatments and enhancing the fracture gradient might change with particle sizes compared to fracture sizes (Tehrani et al., 2007; Van Oort et al., 2011). Previous parametric studies have been focused on the estimation of the fracture width of an induced symmetric fracture around the wellbore. Assuming perfect sealing of the wellbore pressure by plugging the fracture, Morita et al. (Morita et al., 1996; Morita and Fuh, 2012) developed a plain strain analytical model to estimate the fracture width. Alberty and McLean (2004) presented a model for the fracture width as a function of the fracture length based on a linear, two-dimensional solution of a symmetric wellbore fracture. The estimated fracture width was used to calculate the volume of the fracture and to select the particle sizes (Alberty and McLean, 2004). Considering a slit-like crack with three possible pressurized regions, Deeg and Wang (2004) developed an analytical solution for the fracture width and the stress intensity factor along the fracture (Deeg and Wang, 2004). Wang et al. (2008) modified Deeg and Wang's (2004) model by simplifying it into two pressurized regions, including the pressure behind and in front of the fracture. Deformable, viscous, and cohesive (DVC system) LCM was recommended for efficient sealing of a fracture that would increase the hoop stresses around the borehole (Wang et al., 2008). Finite element analysis conducted by Guo et al. (2011) investigated the aperture of symmetric fractures around the wellbore. A closed-form analytical solution was developed for crack mouth opening displacement (CMOD) based on the linear elastic fracture mechanics and the finite element results (Guo et al., 2011). Comparing the results of the closed-form solution with the finite element analysis

shows that the analytical model results are close to the finite element results for a certain range of wellbore size to the fracture length ratio and in-situ horizontal stresses ratio (Guo et al., 2011). A semi-analytical workflow was developed by Shahri et al. (2015) based on the exact solution of a dislocation-based fracture model, which was provided earlier (Carbonell and Detournay, 1995). Common fracture width models used for wellbore strengthening applications are listed in Table 1-2.

Table 1-2. Fracture width models

Model	Fracture Width Solution
Hillerborg et al. 1976	$w_C = \frac{2\sqrt{2}L(p_f - \sigma_h)}{\sqrt{\sqrt{(p_f - \sigma_h)^4 + \frac{E^2\sigma_h{}^2}{\pi^2(1-\upsilon^2)^2}} - (p_f - \sigma_h)^2}}$
Carbonell and Detournay, 1995	$w_C = \frac{\pi(L)}{2m}\frac{4(1-\upsilon^2)}{\mathrm{E}}\sum_{i=0}^{m} h(t_k)$
Alberty and McLean, 2004	$w_C = \frac{4(1-\upsilon^2)}{\mathrm{E}}(p_w - \sigma_H)\sqrt{(L + r_w)^2 - x^2}$
Wang et al. 2008	$w_C = \frac{8(1-\nu^2)L}{\pi E}\frac{\frac{\pi}{2}\sqrt{1-\left(\frac{r_w}{L}\right)^2}(p_0 - \sigma_h) + (p_w - p_0)}{(2n-1)(2n+1)} \times \left\{\left(\sqrt{1-\left(\frac{r_w}{L}\right)^2}\sin^{-1}\frac{r_w}{L} + \sum_{n=1}^{\infty}\sin\left(2n\sin^{-1}\left(\frac{r_w}{L}\right)\right)\right)\left(2\sqrt{1-\left(\frac{r_w}{L}\right)^2}\cos\left(2n\sin^{-1}\left(\frac{r_w}{L}\right)\right) + \frac{r_w\sin\left(2n\sin^{-1}\left(\frac{r_w}{L}\right)\right)}{Ln}\right)\right\}$
Morita and Fuh, 2012	$w_C = \frac{4(1-\upsilon^2)}{E}L(\sigma_h - p_f)$

1.5.3. Evaluation of LCM Particle Size and Distribution. Sealing fractures using LCM prevents further transferring of drilling fluid pressure to the fracture and fracture propagation (Fuh et al., 1992). The efficiency of strengthening treatments and enhancing the fracture gradient might change with particle sizes compared to fracture sizes (Tehrani et al., 2007; Van Oort et al., 2011). Experimental LCM performance studies have focused

on reducing fluid loss (Savari et al., 2013) or increasing the fracture sealing pressure (i.e., fracture re-opening pressure) (Hettema et al., 2007; Tehrani et al., 2007; Kaageson-Loe et al., 2009; Van Oort et al., 2011; Mostafavi et al., 2011). Fluid loss reduction is studied in high pressure high temperature (HPHT) filter press and plug particle apparatus (PPA) tests (Savari et al., 2013). Creating a seal in fractures, causing an increased sealing pressure, has been experimentally studied on both permeable and impermeable fractures (Hettema et al., 2007; Tehrani et al., 2007; Van Oort et al., 2011). A broader distribution of particle sizes was recommended by Hettema et al. (2007) to get better fracture sealing efficiency (i.e., increased re-opening pressure) of drilling-induced or natural fractures based on the results of a permeable fracture test. The proposed procedure for wellbore strengthening fluid design by Tehrani et al. (2007) focused on the importance of particle sizes in bridging fracture aperture. According to Van Oort et al. (2011), smaller sized particles and narrow particle size distribution (well-sorted) gives a better fracture sealing efficiency. The results of the impermeable fracture tests showed that the particle size distribution should be a function of the type of formation to be strengthened (Van Oort et al., 2011). Using slotted discs with different fracture apertures and fracture tips was one of the other methods used to evaluate LCM performance (Alsaba et al, 2014). Based on the results using different LCM blends with a high pressure LCM testing apparatus, Alsaba et al. (2014) observed that blends with a wide range of particle sizes exhibited the lowest fluid loss. Large scale fracturing experiments suggested large and uniform particle size of LCMs for better sealing efficiency (Morita et al., 1990 and 1992). Based on fracturing experiments, Aadnoy and Belayneh (2004) concluded that coarser particles should be used for bridging the fracture mouth while smaller particles should prevent fluid loss through the bridge. According to

fracturing experiments on shale cores using a block test set up with 5-inch rock cubes, Guo et al. (2014) suggested the particle size distribution and the size of lost circulation materials should be selected based on the fracture aperture. There are other studies that theoretically investigated the effect of LCM particle sizes (Alberty and McLean, 2004; Dupriest, 2005; Salehi and Nygaard, 2015). The importance of the particle size distribution in improving sealing efficiency was emphasized by Alberty and McLean (2004) without specifically addressing how to select the size distribution. According to Dupriest (2005), LCM particle sizes are relatively unimportant since any pill will develop into an immobile mass; however, particle sizes smaller than 100 microns should be used to block pore throats to stop matrix seepage and not as a LCM for minimizing fluid losses. Salehi and Nygaard (2015) indicated that the design of particle sizes in wellbore strengthening pills is a function of the fracture width, while the effect of shearing at the bit face on particle size degradation should be considered.

1.5.4. Fluid Invasion Prevention in Shales. In order to prevent and control drilling fluid invasion into shales, a proper drilling fluid should be designed (Hale et al., 1993; Ballard et al., 1994; Bol et al., 1994; Van Oort et al., 1996; Horsud and Bostrom, 1998). One of the primary solutions is using oil-based fluid instead of water-based fluid (Hale et al., 1993; Ballard et al., 1994; Bol et al., 1994; Van Oort et al., 1996). Oil-based fluid acts as a semi-permeable membrane and creates high capillary pressure, so clay hydration would be significantly mitigated compared to water-based fluid (Ballard et al., 1994; Bol et al., 1994). However, oil-based fluids are expensive, have environmental footprints, and can change wettability of reservoirs under overburden shales (Ballard and Dawe, 1988; Van Oort et al., 1994). An alternative solution for preventing fluid invasion in shales is

putting different additives such as salts to water-based drilling fluid systems (Sherwood and Baily, 1994; Hale et al., 1994). The purpose of using additives is to block pore throats and control factors such as ionic exchange, the chemical potential of drilling fluid, and the hydraulic flow of fluid into shales (Hale et al., 1993; Van Oort et al., 1996). Effectiveness of these additives depends on shale properties since the chemical potential of shales changes with the chemical composition of formation (Schmitt et al., 1994). Moreover, ionic concentration is not uniform throughout the pore space and high cationic concentration on the particles would lead to surface charges (Karaborni et al., 1996; van Olphen, 1977). Thus, the effectiveness of drilling fluid additives for preventing and controlling swelling pressures will be changed for different shales. Furthermore, drilling fluid additives for controlling clay hydration have advantages and disadvantages; for example, one might decrease osmosis potential but accelerate ionic exchange (Ghassemi et al., 2001). Also, isolation of the membrane on the wellbore wall is difficult due to shales' low permeability and low filtration rate. Hydrodynamic forces of the drilling fluid will wear any solid deposition on the wellbore wall. Drilling fluid additives cannot completely prevent swelling in shales; there will always be a residual repulsion between the platelets due to hydration of the clay surfaces and interference between hydrated ions and water molecules (Karaborni et al., 1996).

1.5.4.1. Drilling fluid additives for controlling shales swelling. Potassium chloride (KCl) is a well-known and common solution for controlling fluid invasion in shales (Hale et al., 1993; Bol et al., 1994, Van Oort et al., 1996). Potassium chloride reduces the chemical potential of drilling fluid and controls osmosis potential for shales swelling. High concentration of KCl salt induces high osmotic backflow out of the shale. However,

ionic diffusion can trigger swelling through reactions between ions and the shale matrix (Ghaseemi et al., 2001). Potassium chloride solution cannot prevent ionic exchange and filtrate invasion. Ionic exchange in clay replaces (interlayer space) repulsive ions such as K+ and the swelling pressure may increase, leading to shale instability (Ghaseemi et al., 2001). KCl solutions, even at high saturation levels, cannot plug pore throats. Thus, the flow of fluid into shales will be extended by the hydraulic potential (Van Oort et al., 1996). Also, environmental legislation prohibits the use of KCl in several geographic locations around the world due to environmental sensitivity to potassium (e.g., offshore in the Gulf of Mexico) or to chlorides (ODCU, 2012). There are other types of salts that prevent shales from swelling. Using of sodium chloride (NaCl) has certain advantages compared to potassium chloride. Sodium chloride solution has lower water activity and osmosis potential compared to potassium chloride solution (Chenevert, and Pernot, 1998). Also, the viscosity of saturated sodium chloride is higher than a potassium chloride solution, which might decrease hydraulic potential to some extent (Chenevert, and Pernot, 1998). However, ionic exchange is higher for sodium chloride compared to potassium chloride (Ghassemi et al., 2001).

Polymers have been used as alternatives for salty solutions such as potassium chloride (Beihoffer et al., 1990; Retz et al., 1991). Polymers groups adsorbed onto clay fabrics could resolve the ionic exchange such as K+ ions for potassium chloride (Himes et al., 1991). Polymers with low molecular weight can enter the pore system and penetrate the clay fabric. The significant bulk size of polymers prevents drilling fluid from entering shales and also effectively blocks pore throats (Himes et al., 1991). However, polymers cannot control chemical potential and osmosis flow of fluid in shales. Potassium formate

(KCOOH) is another additive recommended for shale drilling (van Oort et al., 1996). Field experience indicated the positive effect of potassium formate in controlling shales swelling with other salts (Howard, 1995), and yet using salts will accelerate ionic exchange. Saccharides (sugars) are another form of additives used to control shales hydration; they have a low molecular weight and are environmentally friendly (Chenevert, 1989; Reid et al., 1993; Downs et al., 1993; Van Oort et al., 1996). The low molecular weight concentrations of saccharides result in a high viscosity solution which reduces the hydraulic potential of water flow in shales. Solutions of saccharides may decompose from biological organisms, and this could affect properties of fluid for preventing clay hydration (Chenevert, 1989; Reid et al., 1993; Downs et al., 1993).

Application of silicates for controlling shales swelling has been highlighted in the past 20 years (Van Oort et al., 1996; Ding et al., 1996; Ward and Williamson, 1996; Van Oort et al., 2003). Silicates used in the form of sodium and potassium silicates in drilling fluid systems are known to be environmentally friendly and inexpensive. They can control clay hydration and shales swelling in different ways. Invaded solubles in shales can react with ions in the pore fluid (e.g. Ca2+ and Mg2+) to form insoluble precipitates and silicate gel (Van Oort et al., 1996). The gelled and precipitated silicates will act as a barrier and prevent any pressure penetration. Also, a highly efficient osmotic membrane composed of silicates can mitigate the hydraulic flow of water. However, silicates cannot restrict diffusive/osmotic flow of water. Thus, they would be effective when they are combined with salts in drilling fluid systems.

Using of nano particles (i.e 10^{-9} m) to develop a high performance drilling fluid for shales has been addressed in recent years (Sensoy et al., 2009, Cai et al., 2012, Sharma et

al., 2012, Hoelscher et al., 2012, Young and Friedheim, 2013, Contreras et al., 2014, Guo et al., 2015). These studies are either focused on the effect nano particles as shale inhibitor additive or their effect on wellbore strengthening and increasing the sealing efficiency of fracture. Type of nano particles, range of particles sizes, weight percentage of particles in drilling fluid, type of base fluid, and type and properties of shale used in the experimental analysis are major differences in these studies. All previous studies agreed on positive impact of nano particles used in water-based drilling fluid for mitigating fluid invasion in shales, however, there is a lot difference in their analysis, including type, particles weight percentage, and size range of nano particles. Also, small and narrow size range of nano particles (in order of few nanometer) might reduce fluid invasion by blocking pores but it would not have any impact in controlling hydraulic drive of fluid through micro fractures which are common in shales.

1.5.4.2. Experimental evaluation of drilling fluid additives for shales. There are different kinds of experiments to evaluate the effectiveness of drilling additives for controlling shales swelling. Shale-fluid interaction has been analyzed in these different ways: weight, volume, pressure, and rock surface hardness index (Steiger, 1993; Van Oort et al. 1996; Guo et al., 2015). Indentation tests, scratch tests, swelling tests, pressure penetration tests, and hydraulic fracturing tests are the main categories of experiments to evaluate the effectiveness of drilling fluid additives for controlling swelling in shales (Guo et al., 2015). Also, some tests are designed to evaluate the effect of drilling fluid additives on chemical potentials or hydraulic potentials of clay hydration (Steiger and Leung, 1991; Chenevert and Osisanya, 1992; Salisbury et al., 1991; Mese, 1995, Santos et al., 1997). However, the most common experiment is the pressure penetration test (PPT) (Steiger,

1993; Van Oort et al. 1996; Guo et al., 2015). Basically, PPT measures the amount of pressure transmitted to the shale samples. Disk-shape shale samples are exposed to fluid on top with constant or dynamic pressure and also constant fluid pressure on the bottom as confining pressure (Steiger, 1993; Van Oort et al. 1996; Guo et al., 2015). One of the challenges with shales experiments is keeping the in situ water content. Different interaction of shale-fluid will be observed if in situ water content is altered (Santos et al., 1996). Thus, in order to get reliable results, in situ water content should be preserved.

1.5.5. Literature Review Discussion. The review reveals that a few failure criteria, including Stassi D'Alia, have not been considered (Colmenares and Zoback, 2002; Benz and Schwab, 2008; Mclean and Addis, 1990; Ewy, 1999; Nawrocki, 2010; Al Ajmi and Zimmerman, 2005 and 2006; Yi et al., 2005; Zhang et al., 2010). Some of the previous studies were focused only on quantitative comparison or determination of the best-fitting parameters for the different rock failure criteria based on data from triaxial test results (Colmenares and Zoback, 2002; Benz and Schwab, 2008). Also, in some previous studies, hypothetical data sets were used for the stress data, rock mechanical properties, and well depth, which caused results to be unrealistic in some cases (Nawrocki, 2010; Yi et al., 2005; Zhang et al., 2010). For example, true vertical well depths of 12,000 m or 28,000 m were chosen for analysis and, therefore, the results were not directly applicable to the stability of wells for petroleum exploitation (Zhang et al., 2010). Furthermore, quantitative comparisons have been previously studied on selected failure criteria, but few evaluations of the failure criteria were based on typical petroleum related situations. Finally, estimated shear failure by different rock criteria were not compared with the actual field case shear failure.

The reviewed fracture width models (Hillerborg et al., 1976; Carbonell and Detournay, 1995; Alberty and McLean, 2004; Wang et al., 2008; Morita and Fuh, 2012) have the fracture width primarily as a function of the fracture length, in addition to rock properties, wellbore pressure, fluid pressure within the fracture, and in-situ stresses. One of the main limitations of the reviewed analytical models is the length of fracture being used as an input parameter, which reflects the impracticality of measuring fracture length in the field. Also, the model by Morita and Fuh (2012) is based on the fixed fracture length (approximately 6 inches), which might not be realistic. Another simplification of the current models is assuming constant fluid pressure within the fracture, since the pressure beyond the plugging material might decrease gradually for both permeable and impermeable formations. The fracture shape of drilling-induced fractures or natural fractures might not necessarily be a line crack, and the fracture width also might change along the fracture.

Laboratory evaluation of LCMs results (Savari et al., 2013; Hettema et al., 2007; Tehrani et al., 2007; Kaageson-Loe et al., 2009; Van Oort et al., 2011; Mostafavi et al., 2011; Alsaba et al, 2014; Morita et al., 1990 and 1992; Aadnoy and Belayneh, 2004; Guo et al., 2014; Alberty and McLean, 2004; Dupriest, 2005; Salehi and Nygaard, 2015) showed that the particle size distribution is a critical parameter to effectively seal fractures, shown as reduced fluid losses, increased fracture breakdown or re-opening pressure. However, there are still limited published results on how the particle size distribution could affect the performance of different LCMs. The majority of tests conducted (Savari et al., 2013; Hettema et al., 2007; Tehrani et al., 2007; Kaageson-Loe et al., 2009; Van Oort et al., 2011; Mostafavi et al., 2011; Alsaba et al, 2014) have been with slotted/tapered discs,

which do not simulate the process of inducing and propagation of fractures while drilling. The previous hydraulic fracturing experiments (Morita et al., 1990 and 1992; Aadnoy and Belayneh, 2004; Guo et al., 2014) show adding LCM increases the fracture gradient, and yet no agreement has been achieved on how LCM strength, particle size, and size distribution affect the fracture sealing efficiency (i.e., strengthening).

Previous evaluation of drilling fluid additives for controlling shales swelling using pressure penetration tests (Salisbury et al., 1991; Chenevert and Osisanya, 1992; Steiger, 1993; Mese, 1995; Van Oort et al. 1996; Santos et al., 1997; Sensoy et al., 2009; Cai et al., 2012; Sharma et al., 2012; Hoelscher et al., 2012; Young and Friedheim, 2013; Contreras et al., 2014; Guo et al., 2015) shows positive and negative sides of additives. Some of the additives such as polymers are good for controlling hydraulic potential, but they cannot control ionic exchange and chemical potential. Application of nano particles in water-based drilling fluid system to control fluid invasion in shales is fairly new approach. Positive effect of nano particles for mitigating fluid invasion into shales has been concluded in recent studies, however, there is a lot differences in their analysis, including type, weight percentage of particles in drilling fluid, and size range of nano particles. Also, small and narrow size range of nano particles (in order of few nanometers) might reduce fluid invasion by blocking pores but it would not have any impact in controlling hydraulic drive through micro fractures which are common in shales.

1.6. RESEARCH OBJECTIVES

According to the literature review, there is no common agreement as to what failure criteria need to be used for wellbore stability analysis. Also, there is no published study on

comparison of estimated borehole breakouts by different criteria with actual field-reported shear failure. Different fracture width models have been introduced, but they have not been evaluated by experimental analysis. The importance of LCM particle size and particle size distribution has been introduced for enhancing the wellbore fracture gradient; however, no agreement has been achieved on how LCM particle size and size distribution affect the fracture sealing efficiency (i.e., strengthening). Application of nano particles for controlling fluid invasion into shales is a new approach and finding an efficient way of combining nano particles in water-based drilling fluid is still under investigation. Also, there is a lot differences in recent studies on performance of nano particles for inhibiting shale including type, weight percentage of particles in fluid, and size range of nano particles.

To overcome the identified gaps in the literature, the main objective of this dissertation is to improve wellbore integrity by controlling mechanical shear failure, enhancing the fracture gradient of the wellbore using LCMs, and preventing swelling in shales and time-dependent wellbore instabilities. To reach the main objective of this dissertation, the following research sub-objectives were planned:

1. Compare the estimated borehole breakout by different failure criteria with field-reported shear failure.
2. Investigate the effect of rock strength variations and strength anisotropy on estimated borehole breakout by different criteria.
3. Analyze the fracture width models for realistic estimation of fracture behavior.
4. Perform laboratory evaluation of previously recommended LCM blends using hydraulic fracturing experiment.

5. Characterize LCM particle size and particle size distribution effects on enhancing the fracture gradient.
6. Experimentally evaluate using fine grained Coal Combustion Residuals for controlling fluid invasion into shales.

The first two paper “Comparison of Rock Failure Criteria in Predicting Borehole Shear Failure” and “Effect of Rock Strength Variation on the Estimated Borehole Breakout Using Shear Failure Criteria” addressed the first two objectives. The third paper “Analysis of Analytical Fracture Models for Wellbore Strengthening Applications, an Experimental Approach” addressed the third and fourth objectives. The fourth paper “Can Particle Size Distribution of Lost Circulation Materials Affect the Fracture Gradient?” addressed the fifth objectives. Last objective has been addressed in the fifth paper “Experimental Evaluation on Using Fine Grained Coal Combustion Residuals for Controlling Fluid Invasion in Shales”.

PAPER

I. COMPARISON OF ROCK FAILURE CRITERIA IN PREDICTING BOREHOLE SHEAR FAILURE

Reza Rahimi, Runar Nygaard

Department of Geosciences and Geological and Petroleum Engineering,

Missouri University of Science and Technology, Rolla, MO, United States

ABSTRACT

Selection of the appropriate rock failure criteria is one of the key steps in determining minimum required mud weight in wellbore stability analysis. Numerous failure criteria have been used for rock failure analysis but there is no common agreement of which failure criterion to select. In this paper, thirteen failure criteria used in predicting borehole shear failure were evaluated for four field cases. In a comparison of the results with actual field failure cases, Tresca, Von Mises, and Inscribed Drucker-Prager overestimated the rock breakout and predicted the highest required minimum required mud weight for all cases. Also the results of these criteria are significantly higher than the actual borehole shear failure. Circumscribed Drucker-Prager underestimated the rock breakout and predicted the lowest bound of the minimum required mud weight in most cases which is mainly less than actual onset of borehole breakout. The minimum required mud weights determined by Modified Lade, Modified Wiebols-Cook and Mogi-Coulomb is above, but close to, the onset of breakout based on the field reported failure cases. This means that

using of any of these three criteria in wellbore stability analysis could be a safe approach. Furthermore, Modified Lade, Modified Wiebols-Cook and Mogi-Coulomb provided similar results for all studied cases, so these failure criteria may be used interchangeably.

1. INTRODUCTION

Determining the appropriate minimum required mud weight by rock failure analysis is an essential step to control wellbore instability. To determine wellbore failure stresses, rock strength must be known, an appropriate constitutive model should be selected, and an accurate rock failure criterion must be chosen. There are numerous rock failure criteria that have been used in wellbore stability analysis to determine the minimum required mud weight, as outlined below, but there is no agreement on which failure criterion should be used in practical wellbore stability analysis.

The previous studies on evaluation of rock failure criteria can be divided in two groups. First the group addressed how well the failure criteria can be fitted to triaxial test data. Seven different rock failure criteria were evaluated by Colmenares and Zoback [1] based on fitting polyaxial test data, and they concluded that the Modified Lade and the Modified Wiebols-Cook fit best with polyaxial tests. The quantitative comparison of the six rock failure criteria was done by Benz and Schwab [2] to determine which criterion gives the best fit with polyaxial test data. The second group of previous studies focused on minimum mud weight prediction for different failure criteria. Mclean and Addis [3] compared Mohr-Coulomb and different forms of Drucker-Prager to predict the minimum required mud weight. Results showed that a criterion can predict a realistic result in one situation but give unrealistic results for other conditions. The Mohr-Coulomb failure criterion was recommended for wellbore stability analysis because of the more realistic results compared with the different forms of Drucker-Prager [3]. The Modified-Lade failure criterion was developed by Ewy [4] and the advantages of this new criterion over Mohr-Coulomb and Drucker-Prager was presented. The borehole breakout pressure was

predicted by Nawrocki [5] based on evaluation of four rock failure criteria and the Modified Lades criterion was recommended. Some of the previous studies evaluated failure criteria both in fitting polyaxial test data and estimation of the minimum required mud weight. Al Ajmi and Zimmerman [6, 7] developed the linear form of Mogi-Coulomb and compared that with the Mohr-Coulomb failure criterion. They proposed the use of Mogi-Coulomb over Mohr-Coulomb with regard to fitting polyaxial test data as well as prediction of the borehole breakout pressure. Three rock failure criteria were compared by Yi et al. [8] based on minimum mud weight estimation, and it was concluded that the failure criterion which best fits the polyaxial test data can better describe rock failure, and therefore provide more reliable results for the minimum required mud weight. Based on their results, no specific failure criterion can consistently estimate higher or lower minimum mud weight compared with the other failure criteria [8]. Corresponding parameters of five failure criteria were determined by Zhang et al. [9] using triaxial test data, where Mogi-Coulomb and Hoek-Brown criteria were recommended for wellbore stability analysis.

The review reveals that a few failure criteria, including Stassi d'Alia, have not been considered [1-9]. Some of the previous studies were only focused on quantitative comparison or determination of the best fitting parameters for the different rock failure criteria based on triaxial test results data [1, 2] . Also, in some previous studies, hypothetical data sets were used for the stress data, rock mechanical properties, and well depth which caused results to be unrealistic in some cases [5, 8 and 9] and. For example, true vertical well depths of 12,000 m or 28,000 m, were chosen for analysis and therefore, the results were not directly applicable to the stability of wells for petroleum exploitation [9]. Furthermore, quantitative comparisons have been previously studied on selected

failure criteria, but few evaluations of the failure criteria were based on typical petroleum related situations. Finally, estimated shear failure by different rock criteria were not compared with the actual field case shear failure. Rahimi and Nygaard [10] addressed the first three challenges by statistical comparison of the result of different rock failure criteria for different lithology using the field data set from Rulison field in western Colorado [11]. They investigated similarities and differences of rock failure criteria for prediction of the minimum required mud weight under different rock lithology and stress data.

This paper is focused on the last shortcoming of previous studies which is the lack of comparison between the estimated borehole shear failure under compressive stresses by different criteria and actual field reported shear failure. Thirteen of the most common rock failure criteria were evaluated based on prediction of borehole failure using the data set from four field cases. The results of failure criteria were compared with actual field case shear failure in order to investigate using which of these failure criteria could be a safe approach in wellbore stability analysis. There are many different factors which affect stability of borehole including anisotropic rock properties, weakness planes, chemically induced plasticity, time dependent behavior, but the purpose of this study was to evaluate the rock failure criteria based on the classical shear failure in a linear poro-elastic material using the Kirsch's equations which gives the maximum differential stress concentration on the borehole wall.

2. ROCK FAILURE CRITERIA

Shear rock failure criterion specifies stress conditions at failure. Common rock failure criteria can be classified based on two main characteristics - linearity of the governing equation and considering the effect of intermediate principal stress. One group of the rock failure criteria have a linear form, such as Tresca, while other failure criteria have a nonlinear form, such as the Drucker-Pager. The second characteristic involves considering the effect of intermediate principal stress on rock strength. Mohr-Coulomb and Hoek-Brown are examples of rock failure criteria that do not consider the effects of intermediate principal stress. In contrast, rock failure criteria such as Modified Lade and Mogi-Coulomb consider the effect of intermediate principal stress on rock failure. Table 2-1 shows the characteristics of all rock failure criteria used in this paper and the Appendix describes the different rock criteria and the common names used throughout the paper. Uniaxial compressive strength (UCS) and internal angle of friction are two intrinsic rock properties that were used in this study as base parameters for evaluation of failure criteria. The Kirsch's solution [12, 13] was used to determine the in situ stresses at the borehole wall for an impermeable formation. Borehole breakouts during drilling operation are a sort of rock shear failure. In this study, classical shear failure as result of concentration of differential stress at the borehole wall was considered.

Table 2-1. Rock Failure Criteria

Failure Criteria	Governing Equation	The effect of intermediate principal stress (σ_2)
Mohr-Coulomb (MC) [13]	$\sigma_1 = q\sigma_3 + C_0$ $q = \frac{1+\sin\phi}{1-\sin\phi}$, $C_0 = \frac{2c\cos\phi}{1-\sin\phi}$	No
Mogi-Coulomb (MG) [6]	$\tau_{oct} = a + b\sigma_{m,2}$ $a = \frac{2\sqrt{2}}{3}\frac{C_0}{q+1}$, $b = \frac{2\sqrt{2}}{3}\frac{q-1}{q+1}$	Yes
Tresca (TR) [12]	$\frac{(\sigma_1-\sigma_3)}{2} = c = \tau_{max}$, $\frac{C_0}{2} = c$	No
Von Mises (VM) [13]	$\sqrt{J_2} = \sqrt{\frac{(\sigma_1-\sigma_3)^2+(\sigma_2-\sigma_3)^2+(\sigma_1-\sigma_3)}{6}} = \frac{C_0}{3}$	Yes
Ins. Drucker-Prager (IDP) [14, 15]	$\sqrt{J_2} = k + \alpha J_1$ $\alpha = \frac{3\sin\phi}{\sqrt{9+3\sin\phi^2}}$, $k = \frac{3C_0\cos\phi}{2\sqrt{q}\sqrt{9+3\sin\phi^2}}$	Yes
Cir. Drucker-Prager (CDP) [14, 16]	$\sqrt{J_2} = k + \alpha J_1$ $\alpha = \frac{\sqrt{3}(q-1)}{(2+q)}$, $k = \frac{\sqrt{3}C_0}{2+q}$	Yes
Hoek-Brown (HB) [17]	$\sigma_1 = \sigma_3 + \sqrt{mC_0\,\sigma_3 + s{C_0}^2}$	No
Modified Lade (ML) [4, 18]	$\frac{{I_1}^3}{I_3} = \eta_1 + 27$ $S = \frac{c}{\tan\phi}$, $\eta = \frac{4\tan^2\phi(9-7\sin\phi)}{(1-\sin\phi)}$	Yes
Modified Wiebols-Cook (MWC) [16,19]	$\sqrt{J_2} = A + BJ_1 + C{J_1}^2$ $C = \frac{\sqrt{27}}{2C_1+(q-1)\sigma_3-C_0}\left(\frac{C_1+(q-1)\sigma_3-C_0}{2C_1+(2q-1)\sigma_3-C_0} - \frac{q-1}{q+2}\right)$ $C_1 = (1+0.6\,\mu)C_0$, $B = \frac{\sqrt{3}(q-1)}{q+2} - \frac{C}{3}[2C_0 + (q+2)\sigma_3]$ $A = \frac{C_0}{\sqrt{3}} - \frac{C_0}{3}B - \frac{{C_0}^2}{9}C$	Yes
Griffith (GR) [12, 20]	$(\sigma_1-\sigma_3)^2 = 8T_0(\sigma_1+\sigma_3)$ $\sigma_3 = -T_0$ if $\sigma_1 + 3\sigma_3 < 0$, $T_0 = \frac{C_0}{8}$	No
Modified Griffith (MGR) [21, 22]	$\sigma_1\left[\sqrt{\mu^2+1}-\mu\right] - \sigma_3\left[\sqrt{\mu^2+1}+\mu\right] = 4T_0$ $\frac{C_0}{T_0} = \frac{4}{\sqrt{\mu^2+1}-\mu}$	No
Murrell (MR) [23]	$(\sigma_1-\sigma_3)^2 + (\sigma_1-\sigma_2)^2 + (\sigma_2-\sigma_3)^2 = 24T_0(\sigma_1+\sigma_2+\sigma_3)$ $T_0 = \frac{C_0}{12}$	Yes
Stassi d'Alia (SD) [24]	$(\sigma_1-\sigma_3)^2 + (\sigma_1-\sigma_2)^2 + (\sigma_2-\sigma_3)^2 =$ $2(C_0-T_0)(\sigma_1+\sigma_2+\sigma_3) + 2C_0T_0$	Yes

3. STATISTICAL ANALYSIS OF ROCK FAILURE CRITERIA

In order to address the shortcomings of previous studies, statistical comparison of rock failure criteria was done using the field data set from Rulison field in Western Colorado (Table 3-1) to investigate the effect of variation of rock mechanical properties and stresses on the result of failure criteria for the minimum required mud weight. Detailed description of the data and the methodology can be found in [10]. In short, three lithologies were studied in a normal faulted stress regime. The results of the statistical analysis are presented using the percentage difference method and TRIZ table of contradictions [14]. Each failure criteria onset of breakout result is compared to all other failure criteria and the percentage differences are calculated. Each table cell represents the percentage difference between the two failure criteria results corresponding to the row and column header. A percentage difference interval of [0%-5%) is highlighted by the orange color and indicates similar results. Yellow is the lower intermediate range [5%-15%), blue is the upper intermediate range [15%-30%). The part of the contradiction tables highlighted by the red color shows the largest differences [30%->). The vertical axis shows the results for vertical boreholes while the horizontal axis shows the results for the horizontal borehole.

3.1. ANALYSIS OF RESULTS

The results of minimum required mud weight by different rock failure criteria for each specific scenario have been presented in a plot of minimum mud weight vs. wellbore inclination (Figure 3-1, Figure 3-3, Figure 3-5 and Figure 3-7). The statistical comparisons of the results using the percentage difference method were presented through the table of contradictions (Figure 3-2, Figure 3-4, Figure 3-6, and Figure 3-8). As described earlier,

similarities and differences of the results by rock failure criteria investigated are highlighted by color codes which stand for different percentage difference interval.

Table 3-1. Rock mechanical properties and stresses data, Rulison field [11]

Strength Level	Shale			Sandstone			Siltstone		
	ϕ (°)	UCS (MPa)	v	ϕ (°)	UCS (MPa)	v	ϕ (°)	UCS (MPa)	v
Weak	22	6	0.1	40	11	0.21	50	15	0.14
Medium	15	9	0.23	33	16	0.15	35	30	0.2
Hard	7	17	0.15	33	24	0.2	8	37	0.18
Stresses data, Well RWF 332-21									
Depth (m)	σ_H (g/cc)		σ_H (g/cc)		σ_V (g/cc)		p_0 (g/cc)		
1500	1.51		2.27		2.52		1.02		
2000	1.75		2.3		2.53		1.4		
2500	2		2.5		2.5		1.6		

According to the results, the variation of rock mechanical properties can significantly change the result of minimum required mud weight by some of the failure criteria. For instance, Circumscribed Drucker-Prager usually predicts the lower bounds for the minimum required mud weight (Figure 3-1 and Figure 3-5) but its results are in the middle range for shale with low internal angle of friction (Φ: 7º) (Figure 3-3 and Figure 3-7). In the same case for shale, higher UCS (in the order of 17 MPa) caused different failure criteria to be in the lower boundary of results. This difference was clearly shown in table of contradictions where the largest difference (red color) moved from the corner of the contradiction table (Figure 3-2 and Figure 3-6) to the center of contradiction tables (Figure

3-4 and Figure 3-8). A greater tensile strength derived by increased UCS (17 MPa) is the main reason why Murrell, Stassi d'Alia, and Modified Griffith criteria are the lower bound of the results (Figure 3-3 and Figure 3-4, Figure 3-7, and Figure 3-8). The estimated minimum required mud weight results of Murrell, Stassi d'Alia, Modified Griffith and Hoek-Brown criteria are more sensitive to changing of rock mechanical properties compared to the other criteria. Also, for siltstone with very high internal angle of friction (Φ: 50º), the results of Circumscribed Drucker-Prager as the lowest boundary of results, has a significant difference of (in the order of 100% to 300%) compared with the other failure criteria (Figure 3-5 and Figure 3-6). Tresca and Von Mises gave the highest estimated mud weight in most cases (Figure 3-1-Figure 3-6), but Inscribed Drucker-Prager represented the highest estimated mud weight for high UCS siltstone (37 MPa) with low internal angle of friction (Figure 3-7). The corresponding contradiction table (Figure 3-8) shows this difference as the highest percentage difference for both vertical and horizontal borehole belongs to the Inscribed Drucker-Prager criterion. Modified Lade, Modified Wiebols-Cook and Mogi-Coulomb provided similar results for the three cases studied, so these failure criteria may be used interchangeably without altering the results (Figure 3-1, Figure 3-3, Figure 3-5, and Figure 3-7). These similarities can be seen in the contradiction tables (Figure 3-2, Figure 3-4, Figure 3-6, and Figure 3-8) by the orange color when these failure criteria were compared.

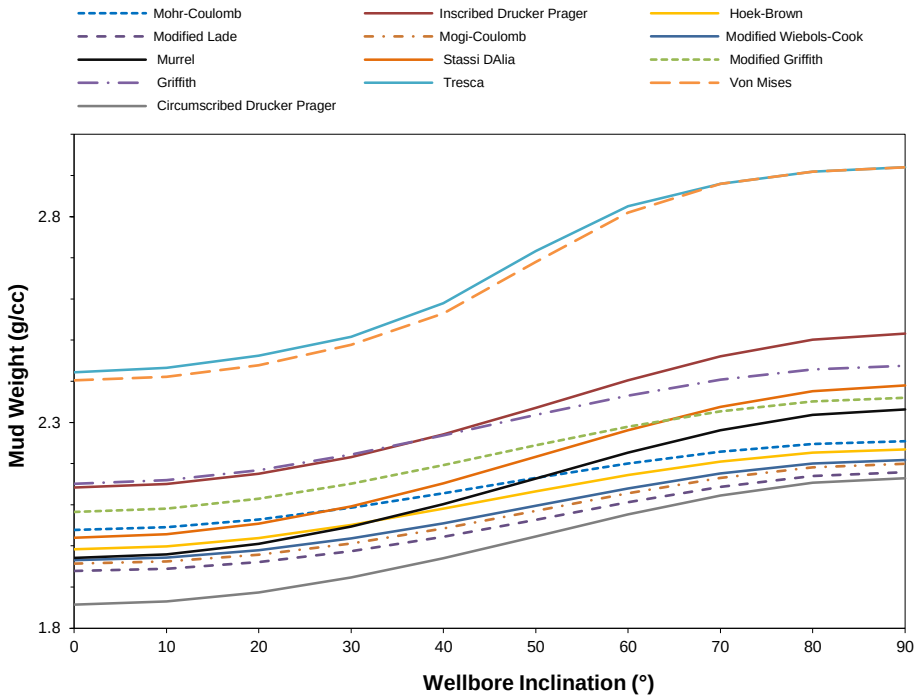

Figure 3-1. Minimum mud weight vs wellbore inclination by different failure criteria for shale (UCS: 6 MPa, Φ: 22°, at 2000 m depth and azimuth of 0°)

Horizontal Borehole

Vertical Borehole	CDP	ML	MG	MWC	MR	HB	SD	MC	MGR	IDP	GR	VM	TR
CDP		1	3	4	11	6	15	7	14	23	19	51	51
ML	-6		1	2	9	4	13	6	12	21	17	49	49
MG	-8	-1		1	8	3	12	4	11	19	15	47	47
MWC	-8	-2	-1		7	2	11	3	10	19	14	46	46
MR	-10	-3	-2	-1		-5	3	-4	3	11	7	36	36
HB	-11	-4	-3	-2	-1		9	1	8	16	12	43	43
SD	-14	-7	-6	-5	-4	-2		-7	-1	7	3	32	32
MC	-14	-8	-6	-6	-4	-3	-1		6	15	11	41	41
MGR	-18	-12	-10	-9	-8	-7	-4	-4		8	4	33	33
IDP	-23	-16	-15	-14	-12	-11	-8	-8	-4		-4	23	23
GR	-24	-17	-15	-14	-13	-12	-9	-8	-5	-1		27	27
VM	-44	-36	-34	-33	-32	-30	-27	-26	-22	-17	-16		0
TR	-46	-38	-36	-35	-33	-32	-29	-28	-24	-19	-18	-1	

Figure 3-2. Comparison of results by different failure criteria for shale (UCS: 6 MPa, Φ: 22°)

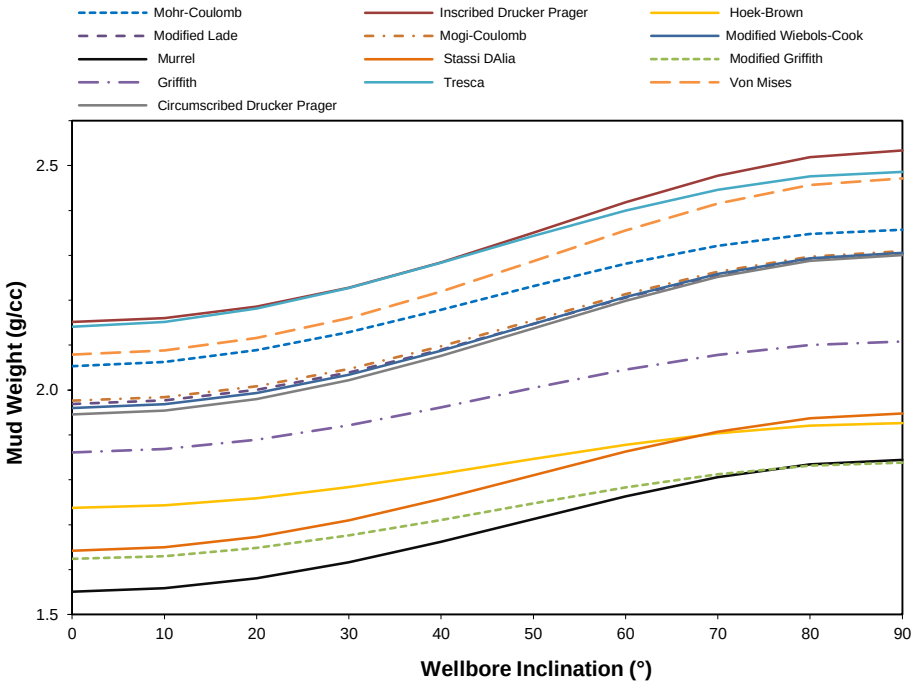

Figure 3-3. Minimum mud weight vs wellbore inclination by different failure criteria for shale (UCS: 17 MPa, Φ: 7°, at 2000 m depth and azimuth of 0°)

Horizontal Borehole

Vertical Borehole	CDP	ML	MG	MWC	MR	HB	SD	MC	MGR	IDP	GR	VM	TR
CDP		0	0	0	-19	-16	-15	3	-19	11	-8	8	9
ML	-1		0	0	-19	-16	-15	3	-19	10	-8	8	9
MG	-2	0		0	-20	-16	-15	2	-20	10	-8	8	8
MWC	-1	0	1		-19	-16	-15	2	-19	10	-8	8	9
MR	20	21	21	20		4	6	27	0	37	14	34	35
HB	13	14	14	14	-8		1	22	-4	31	9	28	29
SD	15	16	17	16	-6	2		20	-5	30	8	27	28
MC	-6	-4	-4	-5	-32	-22	-25		-21	8	-10	5	6
MGR	16	17	17	16	-5	3	1	20		37	14	34	35
IDP	-11	-10	-9	-10	-38	-28	-31	-5	-32		-16	-2	-1
GR	4	5	5	5	-20	-11	-13	9	-14	13		17	18
VM	-8	-6	-6	-7	-34	-24	-27	-2	-28	3	-12		1
TR	-11	-9	-9	-10	-38	-27	-31	-5	-31	0	-15	-3	

Figure 3-4. Comparison of results by different failure criteria for shale (UCS: 17 MPa, Φ: 7º)

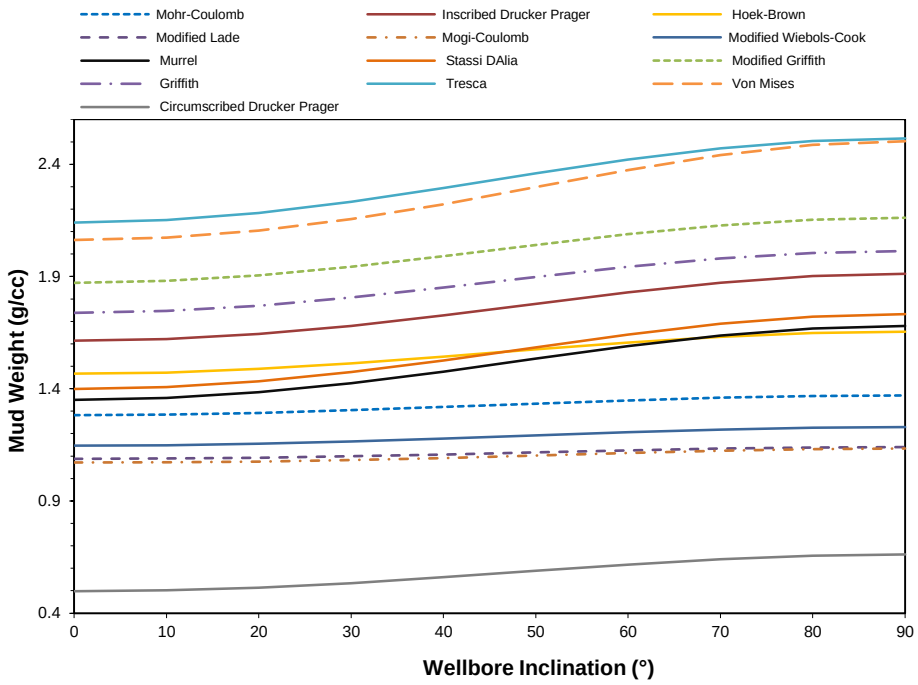

Figure 3-5. Minimum mud weight vs wellbore inclination by different failure criteria for siltstone (UCS: 15 MPa, Φ: 50°, at 1500 m depth and azimuth of 0°)

Horizontal Borehole

Vertical Borehole	CDP	ML	MG	MWC	MR	HB	SD	MC	MGR	IDP	GR	VM	TR
CDP		72	71	85	152	149	160	106	225	188	203	276	278
ML	-118		-1	8	47	45	52	20	89	68	76	119	120
MG	-115	1		8	48	46	53	21	90	68	77	120	121
MWC	-129	-5	-7		37	35	41	12	76	56	64	103	104
MR	-170	-24	-26	-18		-1	3	-18	29	14	20	49	50
HB	-193	-35	-37	-28	-9		5	-17	31	16	22	51	52
SD	-180	-28	-30	-22	-4	5		-21	25	10	16	44	45
MC	-157	-18	-20	-12	5	12	8		58	39	47	82	83
MGR	-274	-72	-74	-63	-39	-28	-34	-46		-11	-7	16	16
IDP	-223	-48	-51	-41	-20	-10	-15	-26	14		5	31	31
GR	-248	-60	-62	-52	-29	-18	-24	-35	7	-8		24	25
VM	-312	-90	-92	-80	-53	-41	-48	-61	-10	-28	-19		0
TR	-328	-97	-99	-87	-58	-46	-53	-67	-14	-33	-23	-4	

Figure 3-6. Comparison of results by different failure criteria for siltstone (UCS: 15 MPa, Φ: 50º)

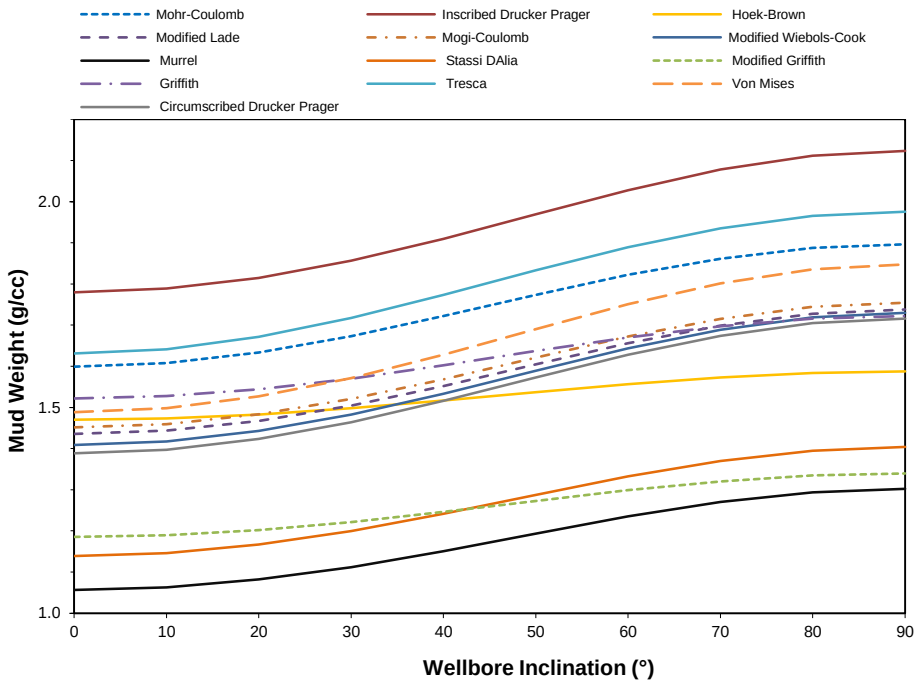

Figure 3-7. Minimum mud weight vs wellbore inclination by different failure criteria for siltstone (UCS: 37 MPa, Φ: 8º, at 2000 m depth and azimuth of 0°)

Horizontal Borehole

Vertical Borehole	CDP	ML	MG	MWC	MR	HB	SD	MC	MGR	IDP	GR	VM	TR
CDP		1	2	1	-24	-7	-18	11	-22	24	0	8	15
ML	-3		1	0	-25	-9	-19	9	-23	22	-1	6	14
MG	-5	-1		-1	-26	-10	-20	8	-24	21	-2	5	13
MWC	-1	2	3		-25	-8	-19	10	-23	23	0	7	14
MR	24	26	27	25		22	8	46	3	63	32	42	52
HB	-6	-2	-1	-4	-39		-12	19	-16	34	8	16	24
SD	18	21	22	19	-8	23		35	-5	51	23	32	41
MC	-15	-11	-10	-14	-51	-9	-40		-29	12	-9	-3	4
MGR	15	17	18	16	-12	19	-4	26		58	29	38	47
IDP	-28	-24	-23	-26	-69	-21	-56	-11	-50		-19	-13	-7
GR	-10	-6	-5	-8	-44	-4	-34	5	-28	14		7	15
VM	-7	-4	-3	-6	-41	-1	-31	7	-26	16	2		7
TR	-17	-14	-12	-16	-54	-11	-43	-2	-38	8	-7	-10	

Figure 3-8. Comparison of results by different failure criteria for siltstone (UCS: 37 MPa, Φ: 8º)

4. FIELD CASE EVALUATION

In this section, rock failure criteria were evaluated based on the prediction of borehole shear failure for four field cases.

4.1. TULLICH FIELD, NORTH SEA

Wellbore instability while drilling wells in the Tullich field of the North Sea resulted in significant nonproductive time and cost overruns [15]. Major instability concern was drilling of the horizontal section in the 100 ft thick Balder B2, reservoir zone with interbedded claystone layers in the predominant sandstone layer. A geomechanical model was developed to determine stresses and rock strength properties. The stress regime is identified to be a normal faulting regime [15] and the analysis of the image log proved that the maximum horizontal stress orientation was between 40º to 60º in the reservoir. Table 4-1 shows the summary of rock strength properties and stress data for the Balder B2 zone. In the previously drilled well 9/23a-29Z, packoffs resulting in mud loss were reported while drilling the reservoir interval with 10.95 lb/gal of oil based mud [15]. Although final side track (9/23a-T2W) was successfully drilled through the horizontal section of reservoir zone using 10.8 lb/gal oil based mud, based on the shape and size of cavings, the borehole encountered minor breakouts close to onset of shear failure [15].

The calculated minimum required mud weight (onset of breakout) for the different failure criteria using the Tullich field data is shown in Figure 4-1. Circumscribed Drucker-Prager criterion underestimated the rock breakout and the result of minimum required mud weight is less than the field reported mud weight. The result of the Murrell is less than field reported failure because of higher tensile strength derived from high compressive strength

(UCS: 13.4 MPa). Tresca, Von Mises, Inscribed Drucker-Prager predicted minimum required mud weights between 0.4 to 0.55 g/cc higher than the field reported mud weight. The estimated minimum required mud weight by Modified Lade, Modified Wiebols-Cook and Mogi-Coulomb is above but close to the field reported mud weight as an onset of breakout.

Table 4-1. Field cases data

		Rock Mechanical Properties				Stresses Data				Drilling Data	Drilling Events
Field	Lithology	Depth (m)	UCS (MPa)	Φ (^{0})	ν	σ_h (g/cc)	σ_H (g/cc)	σ_v (g/cc)	P_P (g/cc)		
Tullich, North Sea Well 9/23a-T2	Claystone Sandstone	1753	13.4	24.3	0.26	1.5	1.9	2	1	Inclination: 90^0 Azimuth: (214^0) Mud Weight: 1.31 g/cc	BE- Pack-off- Mud Loss
Oseberg, North Sea Well B-35	Claystone	2525	15.4	14	0.25	1.82	1.82	2	1.15	Inclination: 78 ^{0} MW: 1.54 g/cc	Tight hole
Oseberg, North Sea Well B-30T4	Claystone	2525	15.4	14	0.25	1.82	1.82	2	1.15	Inclination: 70 ^{0} MW: 1.47 g/cc	Section lost
Goodwyn, Australia Well No.8	Shale	2830	7	35	0.3	1.7	2.2	2.4	1.1	Vertical Well Mud Weight: 1.15 g/cc	Reaming, More than 10% of BE
NWS, Australia Well A-1	Shale	1100	7	27.1	0.3	1.8	2.4	2.3	1.05	Inclination: 61.5^0 Azimuth: 10^0 Mud Weight: 1.25 g/cc	Details of instabilities were not reported.
NWS, Australia Well B-5- A	Shale	1513	8.4	26.7	0.3	1.73	2.16	2.3	1.05	Inclination: 78^0 Azimuth: 86.5^0 Mud Weight: 1.15 g/cc	Details of instabilities were not reported.
NWS, Australia Well B-5- B	Shale	1513	18	34.6	0.2	1.73	2.16	2.3	1.05	Inclination: 78^0 Azimuth: 86.5^0 Mud Weight: 1.15 g/cc	Details of instabilities were not reported.

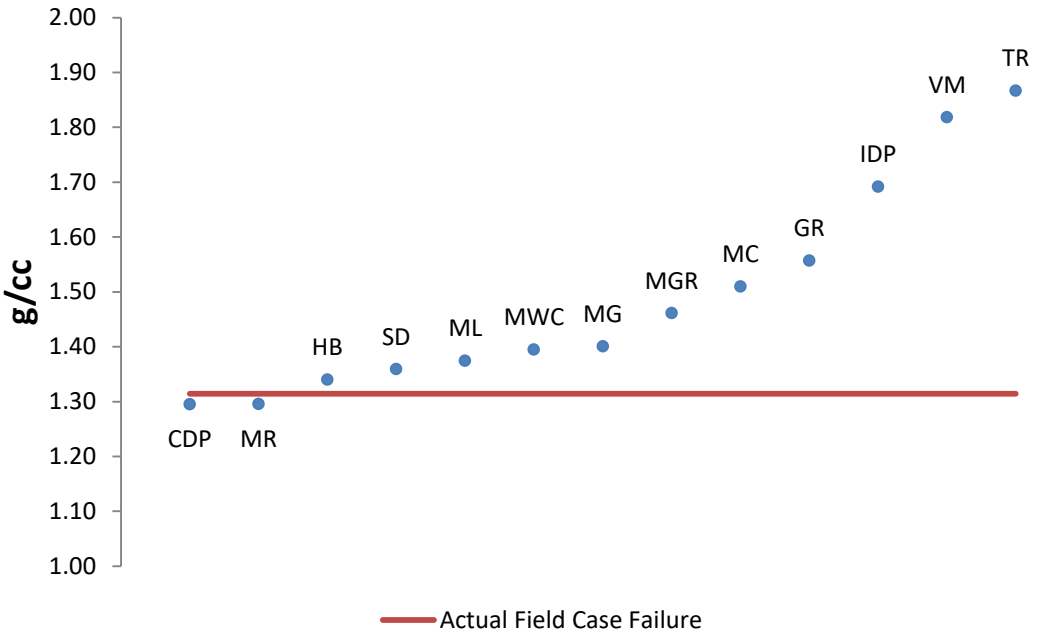

Figure 4-1. Comparison of the estimated minimum mud weight by different failure criteria and actual field failure case, Tullich Field, North Sea

4.2. OSEBERG FIELD, NORTH SEA

Borehole stability problems occurred within the Draupne shale formation in couple of highly inclined wells in the Oseberg field, Norwegian sector of the North Sea [16]. 71% of total drilling time for well 30/9-B-30X was downtime related to wellbore instability. Numerous pack-off, lost circulation, twist-off and stuck pipe events were experienced while drilling. Tight-hole and pack-off were frequently seen in all side tracks of well B-30. Rock mechanical properties were determined by triaxial test results on core sample of the Drapune shale formation. The stress regime was reported as normal faulting and due to the lack of strong evidence of anisotropy, horizontal stresses were assumed to be isotropic [16]. Rock mechanical properties and stress data for this case are given in Table 4-1. Two wells were evaluated for the rock shear failure prediction. Well B-30/T4 intermediate section

was lost due to severe instability in the Draupne shale formation. Well B-35 experienced tight-hole and pack-offs through the same formation. Although, the caliper log for mentioned wells is not available, it was reported that well B-30/T4 experienced complete failure which corresponds with well B-35 which experienced moderate failure (less than 10% of borehole enlargement) which is considered as a lower bound of onset of failure at 1.54 g/cc mud weight.

According to the result for well B-35 (Figure 4-2), Murrell, Stassi d'Alia, Hoek-Brown, and Modified Griffith estimated the lower bound of minimum required mud weight which is between 0.15 to 0.2 g/cc lower than field reported mud weight. The main reason is the effect of higher magnitude of tensile strength derived from high compressive strength (UCS: 15.4 MPa). Tresca, Von Mises, and Inscribed Drucker-Prager estimated the higher bound of the results which is 0.2 g/cc higher than the field reported mud weight. The estimated minimum required mud weight by Circumscribed Drucker-Prager criterion is lower but close to the actual field reported failure (Figure 4-2). The results of Modified Lade, Modified Wiebols-Cook, and Mogi-Coulomb are close to the actual field reported mud weight as an onset of breakout. In case of well B-30/T4, severe borehole failure was encountered and this finally resulted in section loss. Based on the results for well B-30/T4 (Figure 4-2), Murrell, Stassi d'Alia, Hoek-Brown, and Modified Griffith estimated the lower bound of minimum required mud weight, same as well B-35, which is due to the effect of the higher tensile strength derived from higher compressive strength (UCS). Tresca, Inscribed Drucker-Prager, and Von Mises estimated the higher bound of the results which is 0.24 to 0.28 g/cc higher than the field reported mud weight. The result of Circumscribed Drucker-Prager is lower but very close to the field reported failure (Figure

4-2). The results of Modified Lade, Modified Wiebols-Cook, and Mogi-Coulomb for well B-30/T4 show higher difference (0.1 g/cc) with field reported mud weight compared to the result of same criteria for well B-35 which experienced minor instabilities. It could be concluded based on our results that a higher mud weight could reduce borehole instability problems. It was reported in the post wellbore analysis of the Oseberg field [16], the Draupne shale was more stable in sidetracks wells drilled with higher mud density which is in agreement with the result of this analysis.

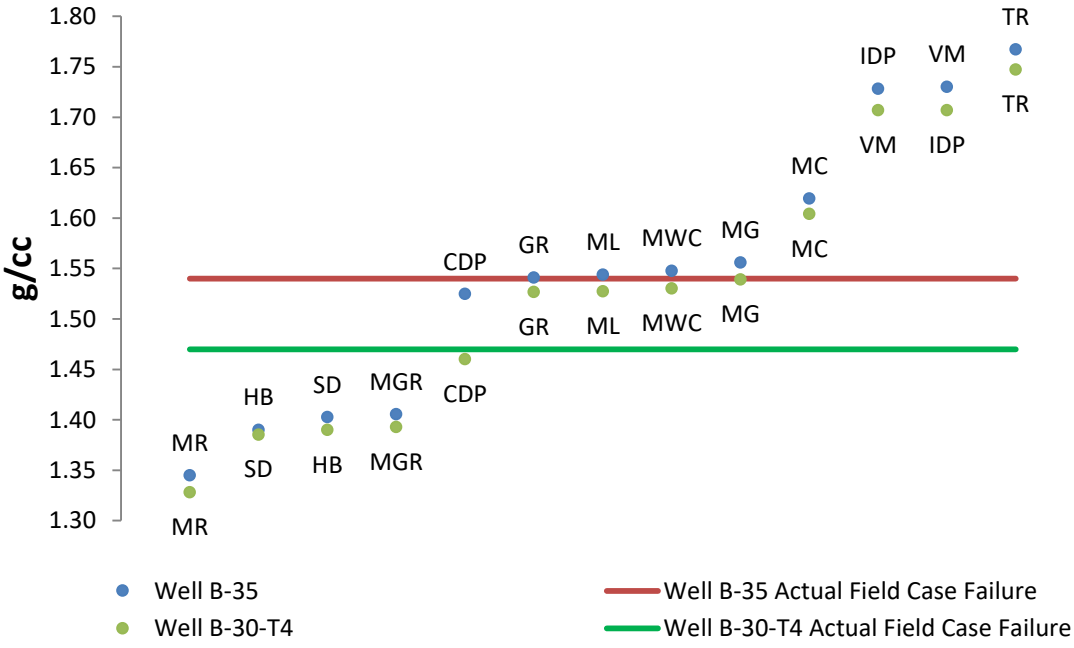

Figure 4-2. Comparison of the estimated minimum mud weight by different failure criteria and actual field failure case, Oseberg Field, North Sea

4.3. GOODWYN FIELD, AUSTRALIA

Shale instability while drilling highly inclined wells was a major challenge toward the development of Goodwyn field in the North West Shelf of Australia [17]. The rock

mechanical properties and stress data for Goodwyn field is given in Table 4-1. Log correlations were used to derive the rock strength properties. Stresses were found to be under a normal faulting regime [17]. The well Goodwyn-8 was chosen for evaluation of failure criteria in prediction of borehole shear failure. Goodwyn-8 is a vertical well which mainly experienced instabilities through the shale of Haycock, Windalia and Muderong formations. Although several instabilities like tight-hole and reaming problems was reported in well Goodwyn-8 and the borehole enlargement of 10% observed [17], the well was successfully drilled to target depth. It means that reported instabilities in well Goodwyn-8 are probably close to onset of shear failure as minor breakouts.

Based on the results for Goodwyn-8 (Figure 4-3), the estimated results of minimum required mud weight by all failure criteria are higher than the field reported mud weight. This is mainly related to the severe level of borehole failure for Goodwyn-8 which was experienced hole enlargement and tight-hole and reaming problems at certain depth. In this situation, the estimated result by Circumscribed Drucker-Prager is slightly higher (0.06 g/cc) than field case failure while the results of other rock failure criteria show higher difference. Tresca and Von Mises represented the highest bond of the results for minimum required mud weight which is significantly higher (1.3 g/cc) than field reported mud weight (Figure 4-3). Modified Lade, Modified Wiebols-Cook, and Mogi-Coulomb Criteria estimated very similar results for the minimum required mud weight in the lower medium bound of the results which are higher (between 0.32 to 0.39 g/cc) than field reported failure (Figure 4-3). Based on the drilling data and results of this analysis, predicted minimum required mud weight by these three criteria could potentially be a safe approach for controlling the shale instability in Haycock, Windalia and Muderong formations.

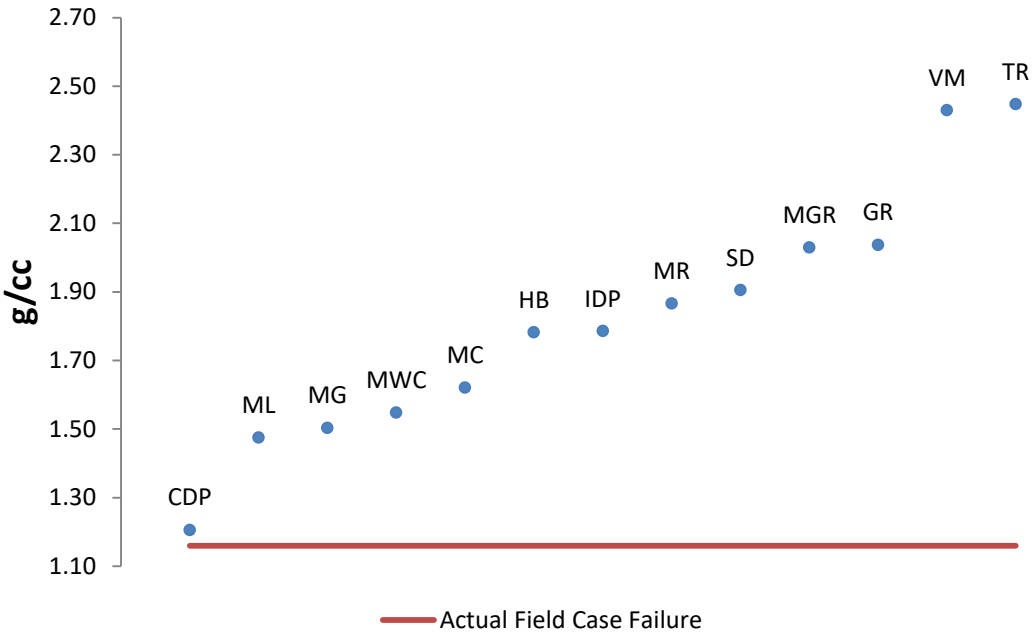

Figure 4-3. Comparison of the estimated minimum mud weight by different failure criteria and actual field failure case, Well B-30-T4, Goodwyn Field, Australia

4.4. NORTHWEST SHELF, AUSTRALIA

Frequent wellbore instability resulting in drilling delay and extensive nonproductive time was one of the main obstacles of increasing the oil and gas production in the Northwest Shelf of Australia [18]. The fields A and B were considered for the evaluation of rock failure criteria in prediction of borehole shear failure since the complete data set of rock mechanical properties and stresses data were available [18]. Stresses for field A appeared to be in boundary between normal and strike slip faulting regime. Due to high inclination of planned wells, it was found that drilling in direction of the minor horizontal stress would be the optimum trajectory. The stress regime for field B found to be a normal faulting regime and the rock mechanical properties determined to be diverse through the target zone [18]. Due to difference in rock strength level, failure criteria were

evaluated for both higher and lower bound of rock mechanical properties in field B. Based on the reported drilling events [18], well A-1 experienced minor instabilities which could be considered as onset of failure at 1.25 g/cc mud weight. Well B-4 experienced higher level of instabilities compared to well A-1 and the insufficient mud weight (1.13 to 1.15 g/cc) was reported to be the main reason [18].

According to the result for well A-1 (Figure 4-4), Circumscribed Drucker-Prager estimated the lowest bound of the results for the minimum required mud weight which is 0.15 g/cc higher than the field reported mud weight. Tresca and Von Mises criteria estimated the higher bound of the results which has significant difference (1 g/cc) with the field reported mud weight. Modified Lade, Modified Wiebols-Cook, and Mogi-Coulomb criteria estimated very similar results for the minimum required mud weight in lower medium bound of results which is 0.25 g/cc higher than the field reported failure (Figure 4-4). The result of this analysis suggests that higher mud weight could potentially prevent borehole instability problem for Well A-1. As it was mentioned, due to diverse rock mechanical properties of target formation in field B, both higher and lower bounds were considered for the analysis. Based on the results for Well B-4 using the lower bound of rock mechanical properties (Figure 4-4), Hoek-Brown and Circumscribed Drucker-Prager represented the lower bound of minimum required mud weight which both are 0.35 g/cc higher than the field reported mud weight. The Modified Lade, Modified Wiebols-Cook, and Mogi-Coulomb criteria estimated very similar results which are slightly higher than the results of Hoek-Brown and Circumscribed Drucker-Prager. Higher bound of the results for minimum required mud weight was represented by the Tresca, Von Mises and Inscribed Drucker-Prager criteria which are 1.15 g/cc higher than the field reported failure (Figure

4-4). In this case, the estimated results by all failure criteria show a considerable difference with the field reported mud weight. This means that using higher mud weight will potentially control borehole instabilities (Figure 4-4). Based on the results for the well B-4 using the higher bound of rock mechanical properties (Figure 4-4), the estimated minimum required mud weight by Circumscribed Drucker-Prager is less than the field reported mud weight despite the use of the same criterion for well B-4 using lower bound of rock mechanical properties.

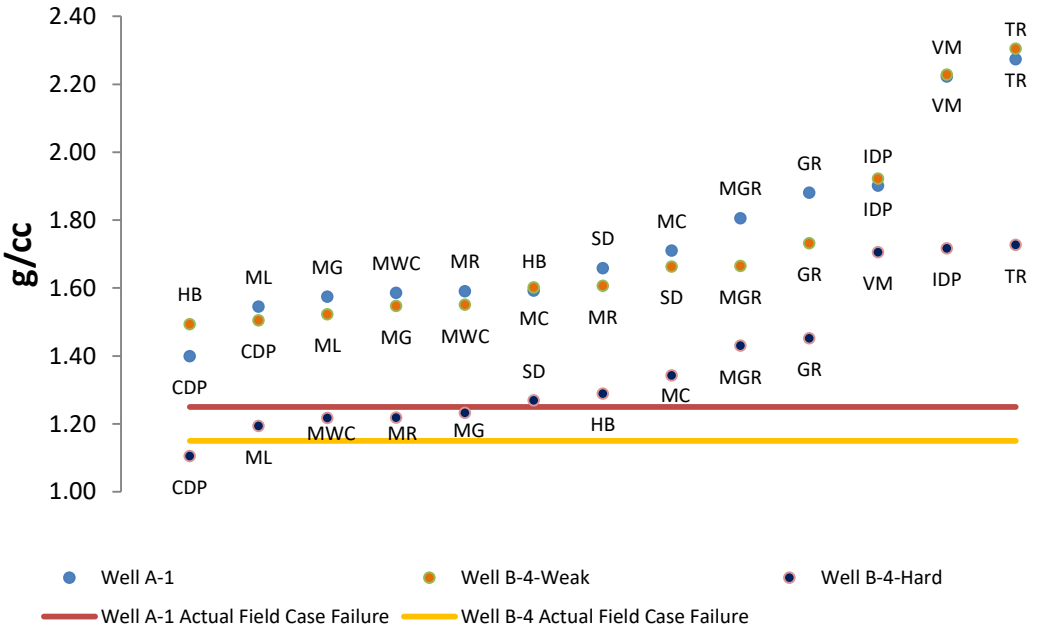

Figure 4-4. Comparison of the estimated minimum mud weight by different failure criteria and actual field failure case, Northwest Shelf, Australia

Tresca, Inscribed Drucker-Prager, and Von Mises criteria estimated the higher bound of results of the minimum required mud weight which is 0.6 g/cc higher than the field reported failure. The results of Modified Lade, Modified Wiebols-Cook, and Mogi-

Coulomb Criteria are similar in the lower bound of medium range which is higher than the field reported mud weight (Figure 4-4). It could be concluded that the estimated results by these three failure criteria could potentially improve borehole instabilities for well B-4.

5. DISCUSSION

A criterion for minor breakout as an onset of shear failure is a breakout width of less than 60 degrees [19]. However, the field determination of the onset of shear failure can be inferred based on recorded drilling events with the lack of caliper logs. For the Tullich field, the estimated results by Modified Lade, Modified Wiebols-Cook, Mogi-Coulomb and Stassi d'Alia criteria are higher but close to the field reported mud weight as an onset of breakout (Figure 4-1). The level of failure for well 9/23a-T2W was limited to minor borehole breakouts as per caving observed on the surface while drilling horizontal section in reservoir using 1.3 g/cc oil based mud. This means that increasing mud weight to the level which was estimated by these four failure criteria could potentially control borehole instabilities. In the case of the Oseberg field, two wells with different levels of failure were considered. According to the results for the well B-35 which experienced the tight hole (Figure 4-2), Modified Lade, Modified Wiebols-Cook, and Mogi-Coulomb estimated minimum mud weight which is slightly higher than the field reported mud weight. Considering the level of failure, the result of Mogi-Coulomb could be a safe approach in drilling of the wellbore. For the well B-30T4 which was experienced higher level of failure (Lost section), the result of Griffith, Modified Lade, Modified Wiebols-Cook, and Mogi-Coulomb are similar and higher than the field reported failure (Figure 4-2). Increasing mud weight to the level which was predicted by these four criteria could potentially prevent borehole instability problems. Analysis of results for well Goodwyn-8 shows that using the estimated minimum required mud weight by Modified Lade, Modified Wiebols-Cook, and Mogi-Coulomb could potentially prevent borehole instability (Figure 4-3). For Field A in Northwest Shelf of Australia, the level of failure for Well A-1 was limited to minor

instabilities [18]. Since the estimated minimum required mud weight by all criteria are higher than actual field failure case (Figure 4-4), the fact of increasing mud weight would improve the borehole stability. Based on the analysis of previous cases, using the results of Modified Lade, Modified Wiebols-Cook, and Mogi-Coulomb will be recommended. Considering the results of well B-5 using the lower bound of mechanical properties (Figure 4-4), all failure criteria estimated minimum required mud weight higher than the field reported mud weight. Since the well B-5 experienced severe failure, increasing mud weight would definitely contribute in controlling borehole instabilities. Based on the analysis of previous cases, using the results of Modified Lade, Modified Wiebols-Cook, and Mogi-Coulomb will be recommended. For the well B-5 using higher bound of the mechanical properties, the estimated result of minimum required mud weight by Circumscribed Drucker-Prager is lower than the field reported mud weight (Figure 4-4). The results of Modified Lade, Modified Wiebols-Cook, and Mogi-Coulomb criteria are similar and above the field reported mud weight. Although, using the highest bound of the rock mechanical properties is a conservative approach, the results of all criteria except Circumscribed Drucker-Prager are still above the field used mud weight. Therefore, higher mud will definitely be recommended to prevent borehole instabilities. Figure 5-1 shows the comparison of failure criteria based on the prediction of borehole shear failure for all studied cases. The results of different failure criteria ranked from the lowest to the highest for each field case. Circumscribed Drucker-Prager estimated the lowest bound of the results in almost all of studied cases which is mainly lower than actual field failure cases. Tresca, Von Mises and Inscribed Drucker-Prager criteria estimated the higher bound of the results for all field cases (Figure 5-1). The results of Modified Lade, Modified Wiebols-Cook, and

Mogi-Coulomb are always above but close to the field reported mud weight. This means that these failure criteria do not underestimate the breakout of rock to give an unsafe prediction of minimum required mud weight less than actual failure cases and also they do not overestimate the breakout of rock to predict conservative minimum required mud weigh as Tresca, Von Mises and Inscribed Drucker-Prager.

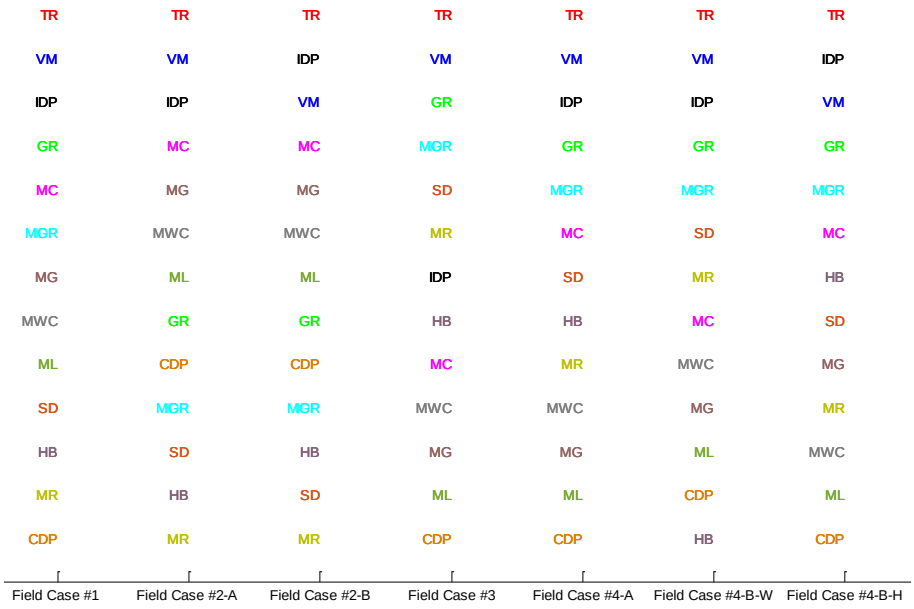

Figure 5-1. Relative ranking of the estimated minimum required mud weight by different failure criteria for all field cases

6. CONCLUSIONS

In this paper, thirteen rock failure criteria were statistically compared and then evaluated based on the prediction of borehole shear failure for four field cases. Based on the results of statistical analysis, Tresca, Von Mises and Inscribed Drucker-Prager always estimate a higher bound of result for the minimum required mud weight. Circumscribed Drucker-Prager estimates a lower bound of results except for formations with low frictional angle. The estimated minimum required mud weight results of Murrell, Stassi d'Alia, Modified Griffith and Hoek-Brown criteria are more sensitive to changing of rock mechanical properties compared to the other criteria. Modified Lade, Modified Wiebols-Cook and Mogi-Coulomb provided similar results, so these failure criteria may be used interchangeably. According to the results of field cases, Tresca, Von Mises, and Inscribed Drucker-Prager overestimate the breakout of rock and over predict the minimum required mud weight; therefore, they are too conservative for wellbore stability analysis. Circumscribed Drucker-Prager underestimates the breakout of rock and under predicts the minimum required mud weight, so using this criterion is an unsafe approach in wellbore stability analysis. Due to sensitivity of Murrell, Stassi d'Alia, Modified Griffith and Hoek-Brown to variation of rock mechanical properties, using these criteria is not recommended. Using of Mohr-Coulomb is not suggested because of overestimating rock breakout and a conservative prediction of the minimum required mud weight .The results of Modified Lade, Modified Wiebols-Cook, and Mogi-Coulomb criteria are always close to the field reported onset of failure. Hence, using these three failure criteria is recommended and could potentially prevent borehole instability.

REFERENCES

[1] Colmenares LB, Zoback MD. A statistical evaluation of intact rock failure criteria constrained by polyaxial test data for five different rocks. Int J of Rock Mech Min Sci 2002; 39: 695–729.

[2] Benz T, Schwab R. A quantitative comparison of six rock failure criteria. Int J of Rock Mech Min Sci 2008; 45(7): 1176–1186.

[3] McLean MR, Addis MA. Wellbore Stability Analysis: A review of current methods of analysis and their field application. In: Proceedings of the IADC/SPE Drilling Conference, Houston, Texas, February 27- March 2, 1990. SPE 19941.

[4] Ewy RT. Wellbore-stability predictions by use of a Modified Lade criterion. SPE Drill & Complet 1999; 14(2): 85–91. SPE-56862.

[5] Nawrocki PA. Critical wellbore pressures using different rock failure criteria. In: Proceedings of ISRM International Symposium and 6th Asian Rock Mechanics Symposium, New Delhi, India, October 23–27, 2010.

[6] Al-Ajmi AM, Zimmerman RW. Relation between the Mogi and the Coulomb failure criteria. Int J of Rock Mech Min Sci 2005; 42(3): 431–439.

[7] Al-Ajmi AM, Zimmerman RW. Stability analysis of deviated boreholes using the Mogi-Coulomb failure criterion, with applications to some North Sea and Indonesian reservoirs. In: Proceedings of the IADC/SPE Asia Pacific Drilling Technology Conference and Exhibition, Bangkok, Thailand, November 13-15, 2006. SPE 104035. 3

[8] Yi X, Ong SH, Russel JE. Improving borehole stability analysis by quantifying the effects of intermediate principal stress using polyaxial rock strength test data. In: Proceedings of the 40th U.S. Symposium on Rock Mechanics (USRMS), Anchorage, Alaska, June 25–29, 2005.

[9] Zhang L, Cao P, Radha KC. Evaluation of rock strength criteria for wellbore stability analysis. Int J of Rock Mech Min Sci 2010; 47(8): 1304–1316.

[10] Rahimi R, Nygaard R. What difference does selection of rock failure criteria make in wellbore stability analysis? In: Proceedings of the 48th US Rock Mechanics / Geomechanics Symposium, Minneapolis, Minnesota, June 1-4, 2014.

[11] Higgings SM. Geomechanical modeling as a reservoir characterization tool at Rulison field, Piceance basin, Colorado. Golden CO USA, Colorado School of Mine, MS thesis, 2006.

[12] Bradley WB. Failure of inclined borehole. Energy Resources Technology 1979; 101(4):232-239.

[13] Aadnoy BS, Chenevert ME. Stability of highly inclined boreholes. J SPE Drill Eng 1987; 2(4): 364-374.

[14] Hipple J. The Ideal Result. 1rd ed. Springer New York; 2012.

[15] Russel KA, Ayan C, Hart NJ, Rodriguez JM, Scholey H, Sugden C, Davidson JK. Predicting and preventing wellbore instability: Tullich field development, North Sea. SPE Drill & Complet 2006; 14(1): 12-22.

[16] Okland D, Cook JM. Bedding-related borehole instability in high-angle wells. In: Proceedings of the SPE/ISRM Rock Mechanics in Petroleum Engineering, Trondheim, July 8-10, 1998. SPE 47285.

[17] Tan CP, Willoughby DR. A pragmatic approach to managing wellbore instability in extended reach wells in the Goodwyn field. In: Proceedings of the SPE Annual Technical Conference and Exhibition, Houston, Texas, October 3-6, 1999. SPE 56565.

[18] Chen X, Tan CP., Haberfield CM. A comprehensive practical approach for wellbore instability management. In: Proceedings of the SPE International Oil and Gas Conference and Exhibition, Beijing, China, October 3-6, 1998. SPE 48898.

[19] Zoback MD. Reservoir geomechanics. 1rd ed. Cambridge. Cambridge University Press; 2007.

[20] Jaeger JC, Cook NGW, Zimmerman RW. Fundamentals of rock mechanics. 4rd ed. Oxford. Blackwell Publishing; 2007.

[21] Mogi, K. Fracture and flow under high triaxial compression. J Geophys Res 1971; 76(5): 1255–1269.

[22] Fjaer E, Holt RM, Horsrud P, Raaen AM, Risnes R. Petroleum related rock mechanics. 2rd ed. Oxford. Elsevier; 2008.

[23] Drucker DC, Prager W. Soil mechanics and plastic analysis of limit design. J. Quar App Math 1952; 10: 157–165.

[24] Veeken CAM, Walters JV, Kenter CJ, Davies DR. Use of plasticity models for predicting borehole stability. In: Proceedings of the ISRM International Symposium, Pau, France, August 30-September 2, 1989.

[25] Zhou S. A program to model the initial shape and extent of borehole breakout. J Comput and Geosci 1994; 20(7-8): 1143–1160.

[26] Hoek E, Brown ET. Empirical strength criterion for rock masses. J Geotech Eng 1980; 106(9): 1013–1035.

[27] Lade PV. Elasto-plastic stress-strain theory for cohesionless soil with curved yield surfaces. J Sol Struc 1977; 13(11): 1019–1035.

[28] Wiebols GA, Cook NGW. An energy criterion for the strength of rock in polyaxial compression. Int J of Rock Mech Min Sci 1968; 5(6): 529–549.

[29] Griffith AA. The phenomena of rupture and flow in solids. J Phil Trans Roy Soc Lon 1921; Res. 221: 163–198.

[30] Brace WF. An extension of the Griffith theory of fracture to rocks. J Geophys Res 1960; 65(10): 3477-3480.

[31] McClintock FA, Walsh JB. Friction on Griffith cracks under pressure. In: Proceedings of the 4th U.S. National Congress of Applied Mechanics, Berkeley, California, 1962.

[32] Murrell SAF. A criterion for brittle fracture of rocks and concrete under triaxial stress and the effect of pore pressure on the criterion. In: Proceedings of 5th symposium on Rock Mechanics, Minneapolis, Minnesota, 1962.

[33] Stassi D'Alia F. Flow and fracture of materials according to a new limiting condition of yielding. Mechanica 1967; 2(3): 178–195.

II. EFFECT OF ROCK STRENGTH VARIATION ON THE ESTIMATED BOREHOLE BREAKOUT USING SHEAR FAILURE CRITERIA

Reza Rahimi, Runar Nygaard

Department of Geosciences and Geological and Petroleum Engineering,

Missouri University of Science and Technology, Rolla, MO, United States

ABSTRACT

One of the primary goals of wellbore stability analysis is the estimation of the shear failure onset or borehole breakout. Estimation of borehole shear failure requires selecting an appropriate failure criterion. Numerous failure criteria have been used for rock failure analysis, but there is no common agreement of which criterion to select for wellbore stability analysis. In general, rock failure criteria mainly depend on rock mechanical properties and in situ stresses. This paper investigates the effect of rock strength variation and strength anisotropy on the estimated borehole shear failure using thirteen different criteria. A rock strength database was created from different US unconventional shale plays. Rock failure criteria were ranked based on the estimated borehole breakout for different shales. According to the results for different levels of rock strength, there are some failure criteria that are highly responsive to variation in rock mechanical properties. Circumscribed Drucker-Prager, Modified Griffith, and Inscribed Drucker-Prager criteria have shown great response to the change in the internal angle of friction. Murrell, Stassi

D’Alia, Hoek-Brown, and Griffith are sensitive to variation of UCS. Mogi-Coulomb, Modified Wiebols-Cook, Modified Lade, and Mohr-Coulomb failure criteria did not show any significant response to the variation of rock mechanical properties and strength anisotropy.

1. INTRODUCTION

Costly consequences of borehole breakouts are common in drilling. To prevent this, a geomechanical model should be developed to determine the borehole breakout or onset of shear failure to be used as a lower bound of drilling fluid density (i.e., minimum required mud weight). The previous evaluations of rock failure criteria [1-9] are either focused on fitting ployaxial test data [1, 2] or comparison of rock failure criteria which was not necessarily based on data related to realistic petroleum exploitation [5, 8, and 9]. Previous studies did not address a comparison of rock failure criteria with actual field-reported shear failure or a sensitivity analysis of input parameters such as rock mechanical properties and in situ stresses on the estimated breakout. Rahimi and Nygaard [10] addressed the first topic by comparing rock failure criteria in predicting borehole shear failure for four different field cases. According to their results, the minimum required drilling fluid density determined by Modified Lade, Modified Wiebols-Cook and Mogi-Coulomb is higher, but close to, the onset of breakout based on the field-reported failure cases [10]. The sensitivity of rock failure criteria to rock mechanical properties was observed in a previous study [11] that investigated the similarities and the differences between failure criteria in predicting of the minimum required drilling fluid density under different rock lithology and stresses data. However, analysis by [11] was limited to data from only one field and had a limited range of rock strength. None of previous studies on the evaluation of failure criteria considered the effect of strength anisotropy. To better understand the effect of rock strength and strength anisotropy on the estimated minimum required drilling fluid density by different failure criteria, more analysis is required based on a broader rock strength database.

This paper analyzes the effect of rock strength variation and strength anisotropy on the estimated borehole shear failure under compressive stresses by various criteria, with a focus on US main unconventional shale plays.

2. ROCK FAILURE CRITERIA

Shear rock failure criteria specify stress conditions at failure. The shear failure is the most common failure mode besides tensile and pore collapse failure [12]. Common rock failure criteria can be classified based on two main characteristics: linearity of the governing equation and the effect of intermediate principal stress. One group of the rock failure criteria has a linear form, such as Tresca, while other failure criteria have a nonlinear form, such as the Drucker-Pager. The second characteristic involves considering the effect of intermediate principal stress on rock strength. Mohr-Coulomb and Hoek-Brown are examples of rock failure criteria that do not consider the effects of intermediate principal stress. In contrast, rock failure criteria such as Modified Lade and Mogi-Coulomb consider the effect of intermediate principal stress. Table 2-1 lists all rock failure criteria used in this paper.

Table 2-1. Rock failure criteria

Failure Criteria	Governing Equation	The effect of intermediate principal stress (σ_2)
Mohr-Coulomb (MC) [13]	$\sigma_1 = q\sigma_3 + C_0$ $q = \frac{1+\sin\phi}{1-\sin\phi}$, $C_0 = \frac{2c\cos\phi}{1-\sin\phi}$	No
Mogi-Coulomb (MG) [6]	$\tau_{oct} = a + b\sigma_{m,2}$ $a = \frac{2\sqrt{2}}{3}\frac{C_0}{q+1}$, $b = \frac{2\sqrt{2}}{3}\frac{q-1}{q+1}$	Yes
Tresca (TR) [12]	$\frac{(\sigma_1-\sigma_3)}{2} = c = \tau_{max}$, $\frac{C_0}{2} = c$	No
Von Mises (VM) [13]	$\sqrt{J_2} = \sqrt{\frac{(\sigma_1-\sigma_3)^2+(\sigma_2-\sigma_3)^2+(\sigma_1-\sigma_3)}{6}} = \frac{C_0}{3}$	Yes
Ins. Drucker-Prager (IDP) [14, 15]	$\sqrt{J_2} = k + \alpha J_1$ $\alpha = \frac{3\sin\phi}{\sqrt{9+3\sin\phi^2}}$, $k = \frac{3C_0\cos\phi}{2\sqrt{q}\sqrt{9+3\sin\phi^2}}$	Yes
Cir. Drucker-Prager (CDP) [14, 16]	$\sqrt{J_2} = k + \alpha J_1$ $\alpha = \frac{\sqrt{3}(q-1)}{(2+q)}$, $k = \frac{\sqrt{3}C_0}{2+q}$	Yes
Hoek-Brown (HB) [17]	$\sigma_1 = \sigma_3 + \sqrt{mC_0\,\sigma_3 + s{C_0}^2}$	No
Modified Lade (ML) [4, 18]	$\frac{{I_1}^3}{I_3} = \eta_1 + 27$ $S = \frac{c}{\tan\phi}$, $\eta = \frac{4\tan^2\phi(9-7\sin\phi)}{(1-\sin\phi)}$	Yes
Modified Wiebols-Cook (MWC) [16,19]	$\sqrt{J_2} = A + BJ_1 + C{J_1}^2$ $C = \frac{\sqrt{27}}{2C_1+(q-1)\sigma_3-C_0}\left(\frac{C_1+(q-1)\sigma_3-C_0}{2C_1+(2q-1)\sigma_3-C_0} - \frac{q-1}{q+2}\right)$ $C_1 = (1+0.6\,\mu)C_0$, $B = \frac{\sqrt{3}(q-1)}{q+2} - \frac{C}{3}[2C_0 + (q+2)\sigma_3]$ $A = \frac{C_0}{\sqrt{3}} - \frac{C_0}{3}B - \frac{{C_0}^2}{9}C$	Yes
Griffith (GR) [12, 20]	$(\sigma_1-\sigma_3)^2 = 8T_0(\sigma_1+\sigma_3)$ $\sigma_3 = -T_0$ if $\sigma_1 + 3\sigma_3 < 0$, $T_0 = \frac{C_0}{8}$	No
Modified Griffith (MGR) [21, 22]	$\sigma_1\left[\sqrt{\mu^2+1}-\mu\right] - \sigma_3\left[\sqrt{\mu^2+1}+\mu\right] = 4T_0$ $\frac{C_0}{T_0} = \frac{4}{\sqrt{\mu^2+1}-\mu}$	No
Murrell (MR) [23]	$(\sigma_1-\sigma_3)^2 + (\sigma_1-\sigma_2)^2 + (\sigma_2-\sigma_3)^2 = 24T_0(\sigma_1+\sigma_2+\sigma_3)$ $T_0 = \frac{C_0}{12}$	Yes
Stassi d'Alia (SD) [24]	$(\sigma_1-\sigma_3)^2 + (\sigma_1-\sigma_2)^2 + (\sigma_2-\sigma_3)^2 =$ $2(C_0-T_0)(\sigma_1+\sigma_2+\sigma_3) + 2C_0T_0$	Yes

3. ROCK STRENGTH

The stress level at which a rock fails is commonly called the strength of the rock [12]. Contributing factors of intact rock strength can be classified in three major groups: type of rock composition, type of grains bonding, and mechanical quality of bonding between grains [25]. Internal rock structure such as lamination, schistosity, and anisotropy also having a key influence on rock strength properties [25]. Rock strength can be defined as tensile strength, compressive strength, and shear strength. The uniaxial compressive strength and frictional angle are key inputs for geomechanical analysis of wellbore instability. Uniaxial compressive strength (UCS) is the most used practical property to classify the rock strength. UCS is a function of rock structure, rock composition, time, loading, temperature, and confining pressure [26, 27, and 28]. There are large varieties of rock composition and structures that cause very diverse mechanical properties. Classification of different rocks based on the compressive strength has been rarely addressed. Uniaxial compressive strength of major rock types was reported based on a laboratory testing by Vutukuri et al. [29]. Carmichael [30] classified the rock strength into five different groups based on UCS magnitude. A rock with UCS higher than 220 MPa is classified as a very high-strength rock and a rock with UCS less than 28 MPa is classified as a very low-strength rock [30]. The range and average of uniaxial compressive strength for typical rock types was reported by John and DeGraff [31]. The rock strength data from laboratory testing was gathered for different lithology in United States by Goodman [32] in order to find a general trend for rock strength. Locker [33] compiled close to 1900 exiting data pairs to find the range of typical rock strength for common rock lithology. Despite all

reported efforts for classifying rock strength, the rock strength is quite diverse even for a certain lithology or type of rock.

3.1. US UNCONVENTIONAL SHALE PLAYS

The experimental analysis of the elastic properties of main US shale plays showed a wide range of rock strength properties and significant anisotropy [34]. In this study, a series of US unconventional rock strength data was gathered (Table 3-1) to compare rock failure criteria in estimating borehole breakout. These mechanical properties are either log correlated parameters or derived based on rock mechanical testing of core samples. Laboratory measurements of dry rock specimens might not be very accurate because the fluid in pore space could affect rock properties in different ways [35]. Pore fluid can reduce the rock strength due to reduction of surface energy, stress corrosion, capillary pressure, or chemical effects [35]. Previous experiments [36] showed the strength of silicate-rich rock can be reduced by 30% for saturated rocks. Also, laboratory experiments are typically performed on high quality core samples, while in situ rocks normally have macroscopic fractures and joints, resulting in potentially higher UCS than the actual in situ strength [35]. Because the geophysical log provides continuous reading, the characterization of variation in rock properties variation is more plausible. Also, many different correlations for rock mechanical properties based on sonic velocity readings from a large database have been investigated and a reasonable consistency was found [37]. As a conservative approach for wellbore stability analysis, strength properties correlated from log data are typically used as a lower bound of rock strength for geomechanical models.

Table 3-1. Rock strength data for main US unconventional play

Rock Type	UCS (MPa)	Frictional Angle (°)	Poisson's ratio	Method
Taylor Shale [38]	3	26	0.2	Core Testing
Clagget Shale [38]	4	26	0.2	Core Testing
Bearpaw Shale [38]	5	14	0.2	Core Testing
Pierre Shale [37]	6	21	0.39	Seismic Correlation
Piceance Basin Shale I [10]	6	22	0.1	Core Testing
Pierre Shale I [37]	10.7	23	0.35-0.37	Seismic Correlation
Piceance Basin Shale II [10]	17	7	0.15	Core Testing
Pierre Shale III [37]	22.00	23	0.22	Seismic Correlation
Antrim Shale [37]	22.00	23	0.22	Seismic Correlation
El Paso Shale [12]	26	21	0.1	Core Testing
New Albany Shale [37]	29.00	23	0.18	Seismic Correlation
Marcellus Shale [37]	29.00	23	0.18	Seismic Correlation
Haynsville Shale [37]	32.00	23	0.17	Seismic Correlation
Eagle Ford Shale [37]	38.00	23	0.14	Seismic Correlation
Barnett Shale [37]	43	24	0.13	Seismic Correlation
Woodford Shale [37]	43	24	0.13	Seismic Correlation
Monterey Shale [37]	60	24	0.09	Seismic Correlation
Piceance Basin Shale III [37]	67.4	28	0.275	Core Testing
Muddy Shale [30]	99	14.4	0.2	Core Testing
El Paso Shale I [30]	112	21.4	0.26	Core Testing
Haynesville Shale I [34]	110	19	0.25	Core Testing
Fort Johnson Shale [34]	125	28	0.25	Core Testing
Barnett Shale I [34]	150	34	0.25	Core Testing
Shale Eagle Ford I [34]	160	19	0.25	Core Testing
Shale Eagle Ford II [34]	170	25	0.25	Core Testing
Shale Haynesville II [34]	180	25	0.25	Core Testing
Shale Barnett II [34]	230	40	0.2	Core Testing

4. ANISOTROPY

Previous studies found that strength changes with orientation of the principal stress with respect to the laminated layer or bedding plane in anisotropic rocks [40-46]. [40] experimentally investigated the failure mechanism of rocks with planar anisotropy. The slip between layers was found to be the controlling mechanism of shear fracture when the bedding angle was inclined at 45 to 60° of maximum principal stress direction. Flow within layers or slip across layer boundaries was suggested as a potential mechanism of failure at greater inclination than 60° [40]. [41] investigated the mechanical anisotropy of three laminated rocks by triaxial testing of specimens. According to their results, the studied rocks showed 40% reduction in rock strength at bedding inclination of 20 to 30°. They found out that shear strength, tensile strength, frictional angle, and elastic constants of studied laminated rocks would vary with bedding direction [41]. [42] experimentally investigated the mechanical properties of three anisotropic sedimentary rocks. Based on their observations, shear along the bedding plane, shear across the bedding plane, and plastic flow along the bedding plane are main failure mechanisms for anisotropic rock that depend on orientation and initial stress state. They found that compressive strength, cohesion, and frictional angle would change by the orientation of the anisotropic plane, and an empirical model was developed based on the experimental observation [42]. Anisotropic elastic response, plastic deformation and failure behavior of Tournemire shale was investigated using triaxial compression testing by [43]. According to their findings, Tournemire shale exhibits large anisotropic plastic deformations and nonlinear elastic behavior. Also, anisotropic failure behavior of shale was affected by confining pressure and loading orientation [43]. [44] conducted a series of tests on Pierre shale, including the

Brazilian test and drained and undrained triaxial tests in order to investigate the mechanical properties. They found that the bedding plane orientation has a significant effect on mechanical properties with 12% maximum reduction in tensile strength and 6% maximum reduction in compressive strength. Uniaxial and consolidated drained triaxial tests were performed on Moncos shale to evaluate the plane of patchy weakness anisotropic model compared to Griffith crack and plane of weakness models [45]. Post failure analysis of core samples revealed that bedding planes may behave as weak planes, which tend to fail before intrinsic failure depending on orientation of applied stress. The effect of bedding plane orientation on compressive strength was studied using uniaxial testing results and the minimum strength was observed at bedding inclination of 60° where post failure analysis of core samples showed sliding on the lamination plane [46]. All previous studies on anisotropic properties of shales agreed on the effect of bedding plane orientation on compressive strength and frictional angle. Also, the majority of these experimental studies showed identical compressive strength at bedding plane orientation of 0 and 90° [40-46]. Figure 4-1 shows anisotropic compressive strength data gathered from literature.

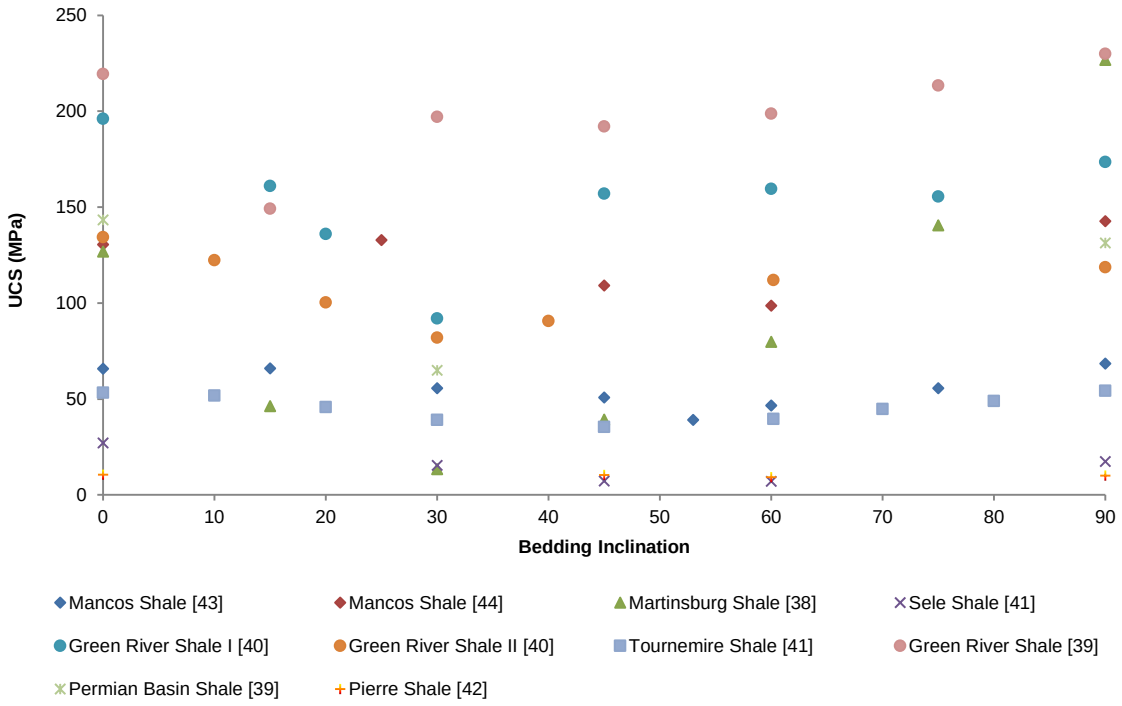

Figure 4-1. Compressive strength at different bedding inclination

5. METHODOLOGY

Rock strength data from main US unconventional shale plays were gathered and sorted based on UCS (Table 3-1). The anisotropy data set was collected from limited published studies (Figure 4-1). UCS and the internal angle of friction are two intrinsic rock properties that were used in this study as base parameters for the evaluation of failure criteria. Rock mechanical data (Table 3-1) was used to estimate the minimum required drilling fluid density that is an onset of shear failure (borehole breakout). A normal faulting regime was assumed for the analysis, where the vertical stress was 1 psi/ft, the maximum horizontal stress was 0.8 psi/ft, the minimum horizontal stress was 0.7 psi/ft, and the pore pressure was 0.43 psi/ft for a 1500 meter deep well. The in situ stresses were determined using the Kirsch solution for an impermeable formation [47, 48]. Thirteen of the most common rock failure criteria were compared based on the prediction of borehole breakout using the rock strength database. The estimated borehole breakouts by various failure criteria for each type of shale were ranked and compared with other shales at various well inclinations. Also, rock failure criteria were evaluated based on the effect of strength anisotropy at various bedding inclinations. The results were interpreted to identify the rock failure criteria that are more responsive to the variation of the rock mechanical properties UCS and internal angle of friction. Borehole breakouts during drilling operation are a sort of rock shear failure. In this study, classical shear failure was considered as result of concentration of differential stress at the borehole wall.

6. RESULTS

Figure 6-1 is a plot of the drilling fluid density versus wellbore inclination that shows the minimum estimated drilling fluid density by different failure criteria for Clagget shale. Figure 6-2 shows a comparison of the estimated minimum required drilling fluid density by different failure criteria for two different shales at three wellbore inclinations, where criteria are ranked from the lowest to the highest estimated drilling fluid density for each shale. According to the results for the Clagget shale (Figure 6-1), Tresca and Von Mises criteria estimated the higher bound of results and Circumscribed Drucker-Prager estimated the lower bound. The difference between the lowest and the highest estimated minimum required drilling fluid density was about 1 g/cc (Figure 6-1). By comparing the order of failure criteria in estimating the minimum required drilling fluid density for the Clagget shale with the Bearpaw shale (Figure 6-2), a difference in the rank of the shear failure criteria is observed.

The Clagget shale and the Bearpaw shale have a comparable compressive strength but the frictional angle is lower for the Bearpaw (14°) compared to the Clagget shale (26°) (Table 3-1). In this case, the estimated minimum drilling fluid densities by Circumscribed Drucker-Prager criterion are not in the lower bound of results as they are for the Clagget shale (Figure 6-2). Instead, the estimated fluid densities by Modified Griffith, Murrell, Stassi D'Alia and Hoek-Brown are in the lower bound (Figure 6-2). The Piceance Basin shale I has a similar frictional angle compared to the Clagget shale but higher compressive strength (6 MPa) (Table 3-1). The minimum estimated drilling fluid density using Hoek-Brown criterion approached the lower bound and is the lowest for wellbore inclination of 60 and 90° compared to the results for Clagget shale (Figure 6-3).

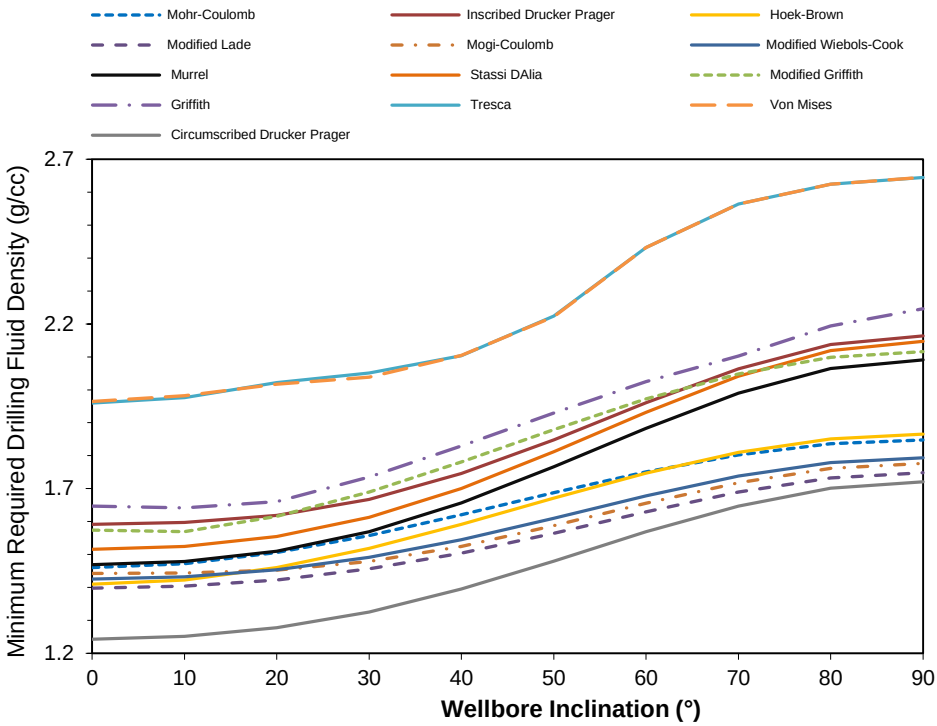

Figure 6-1. Drilling fluid density vs inclination for Clagget shale

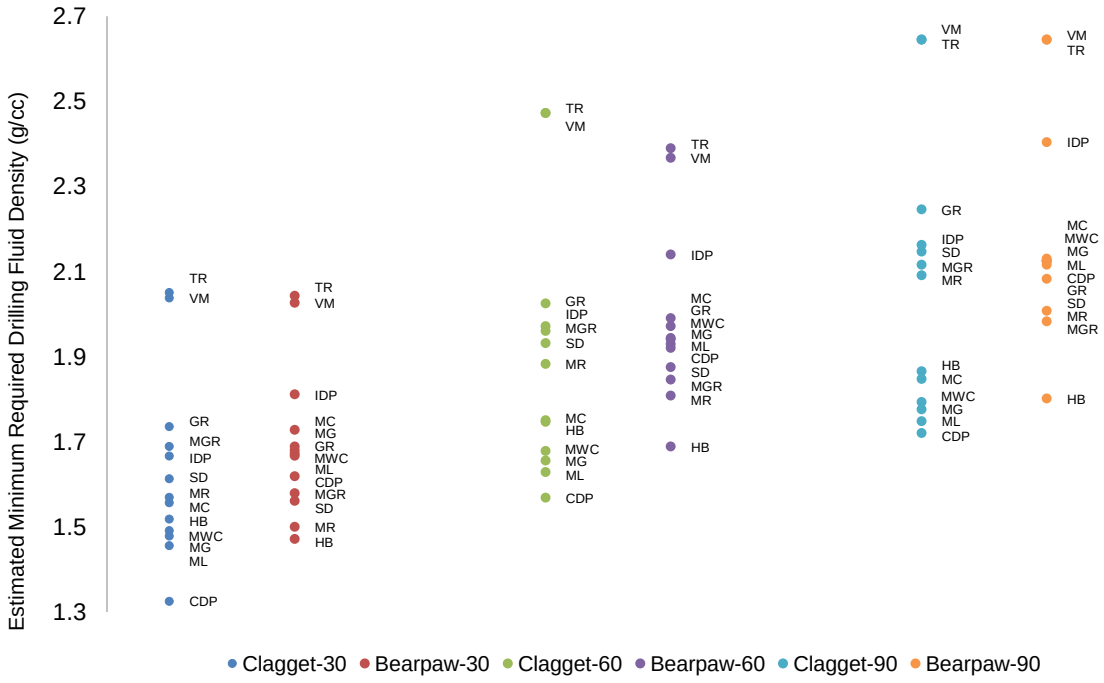

Figure 6-2. Comparison of estimated required drilling fluid density by failure criteria for Clagget and Bearpaw shale at different wellbore inclination

Tresca and Von Mises criteria represented the higher bound of the estimated drilling fluid density for Clagget, Bearpaw, and Piceance Basin I shales (Figures 6-1 to 6-3). The Pierre shale II has a higher compressive strength (10.7 MPa) compared to the Piceance Basin shale I (6 MPa) but they have a comparable internal angle of friction (Table 3-1). The failure criteria on the higher bound (Tresca and Von Mises) are the same for both Pierre shale II and the Piceance Basin shale I (Figure 6-4). However, different failure criterion (Murrell) is approaching the lower bound of the estimated drilling fluid density for the Pierre shale II (Figure 6-4). For the wellbore inclination of 30°, the Murrell replaced the Circumscribed Drucker-Prager at the lower bound the results (Figure 6-4). The Piceance Basin shale II has a higher compressive strength (17 MPa) compared to the Pierre shale II (10.7 MPa) but a lower internal angle of friction (7°) (Table 3-1).

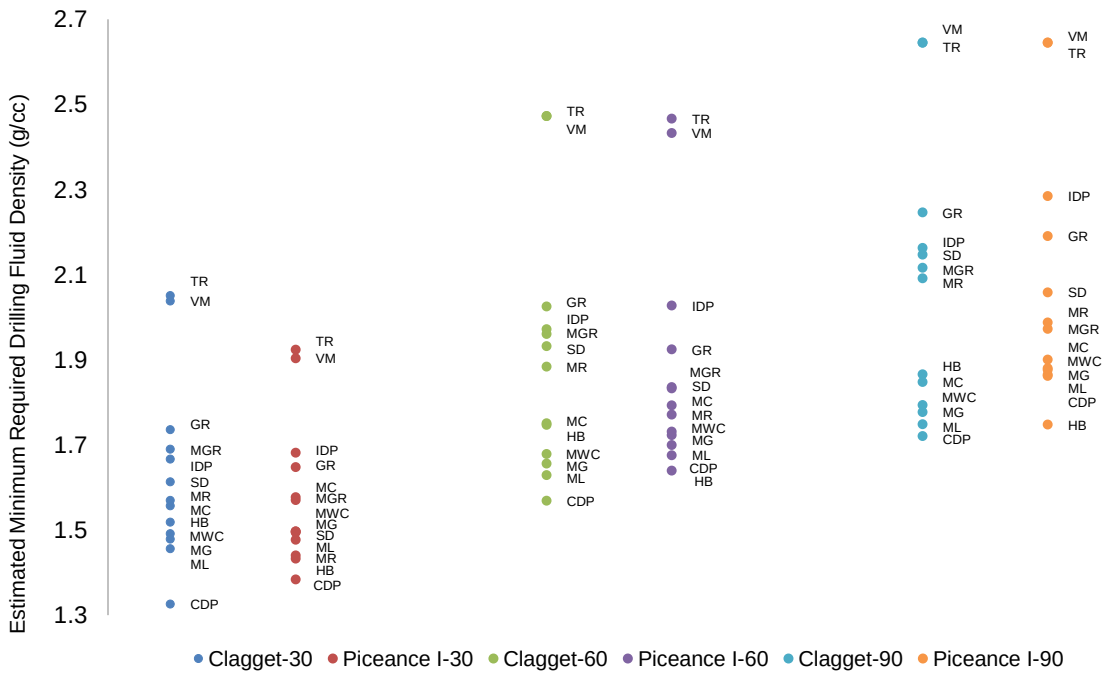

Figure 6-3. Comparison of estimated required drilling fluid density by failure criteria for Clagget and Piceance basin I shale at different wellbore inclination

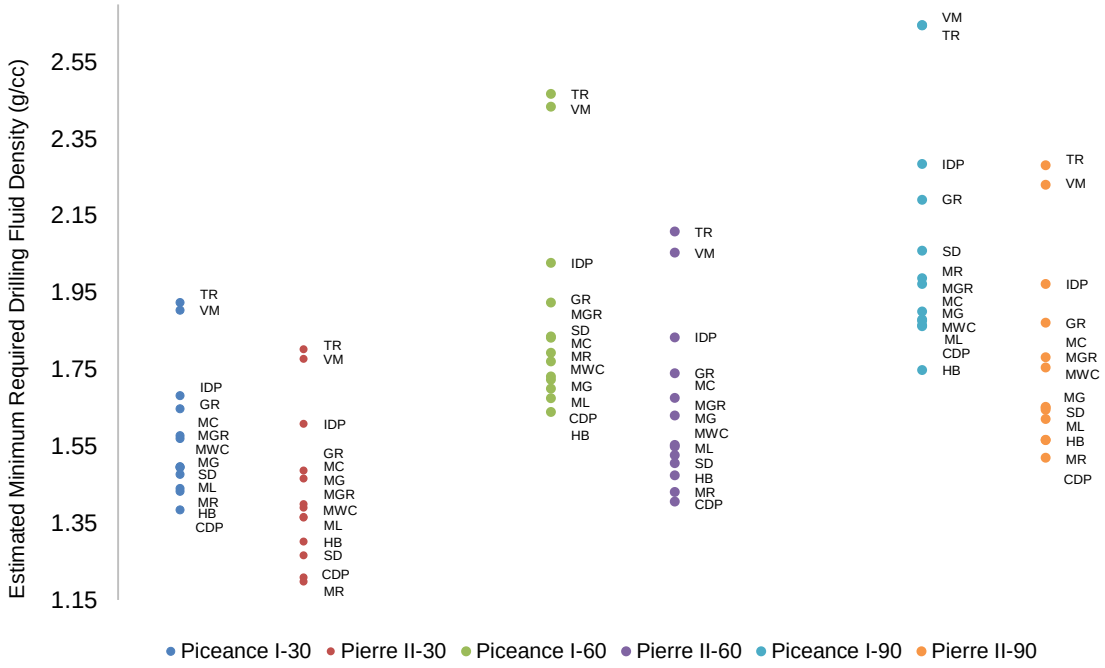

Figure 6-4. Comparison of estimated required drilling fluid density by failure criteria for Piceance basin I and Pierre II shale at different wellbore inclination

The Inscribed Drucker-Prager criterion replaced the Tresca and Von Mises criteria in the highest bound of the estimated drilling fluid density (Figure 6-5). The rank of the Modified Griffith and Circumscribed Drucker-Prager criteria for the Piceance Basin shale II experienced major change compared to the Pierre shale II but in an opposite way (Figure 6-5). The predicted drilling fluid density by Modified Griffith approached the lower bound, while the Circumscribed Drucker-Prager represented the middle range of the estimated drilling fluid density (Figure 6-5). The Murrell criterion represented the lowest bound for the Piceance Basin shale II at the wellbore inclination of 30 and 60° while the lowest for the 90° wellbore inclination was represented by Modified Griffith criterion (Figure 6-5). The Antrim shale has a higher compressive strength (22 MPa) and higher internal angle of friction (23°) compared to the Piceance Basin shale II (Table 3-1). The estimated drilling fluid density by Circumscribed Drucker-Prager criterion approached the lower range of the

results compared to the results of the same criterion for the Piceance Basin shale II, which was in the middle range (Figure 6-6). The higher bound of estimated drilling fluid density represented by the Inscribed Drucker-Prager criterion while it is replaced by Tresca for highly deviated and horizontal wellbores (Figure 6-6). The results of Modified Griffith criterion approached the middle range of the results for the Antrim shale compared to the results of the same criterion for the Piceance II shale (Figure 6-6).The same order of failure criteria in estimating the minimum required drilling fluid density was observed for all other stronger shales listed in Table 3-1, including El Paso, New Albany, Marcellus, Haynsville, Eagle Ford, Barnett, and Woodford shales (Figure 6-7). Figures 6-8 through 6-10 represent the effect of strength anisotropy on the estimated minimum required drilling fluid density for three different shales (Pierre, Mancos, and Tournemire) for a horizontal wellbore.

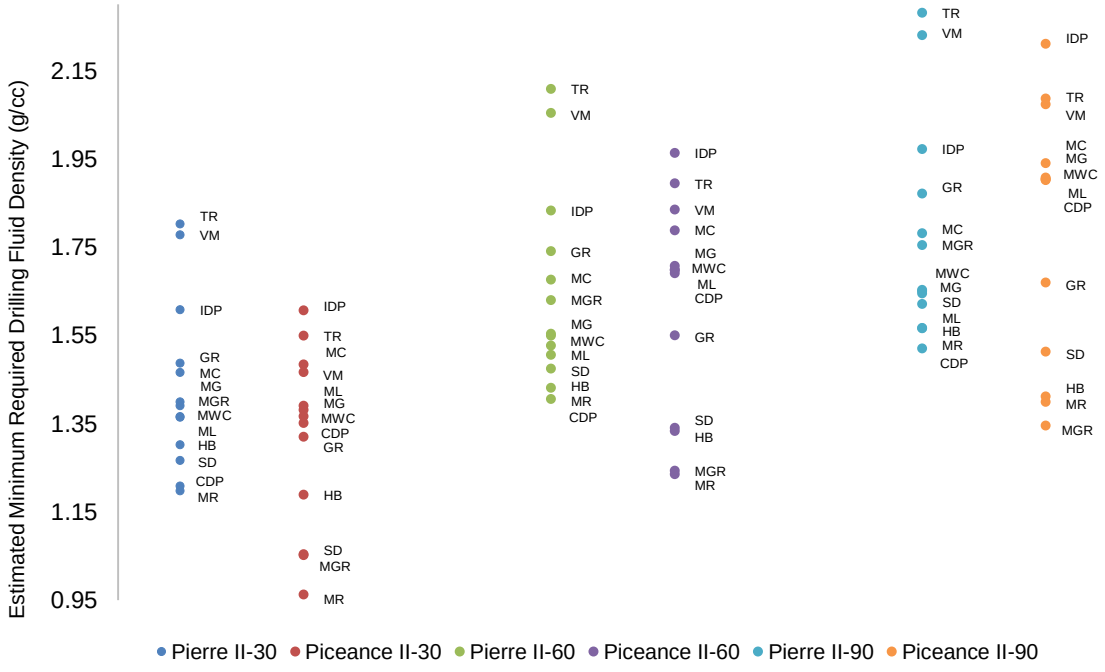

Figure 6-5. Comparison of estimated required drilling fluid density by failure criteria for Pierre II and Piceance basin II shale at different wellbore inclination

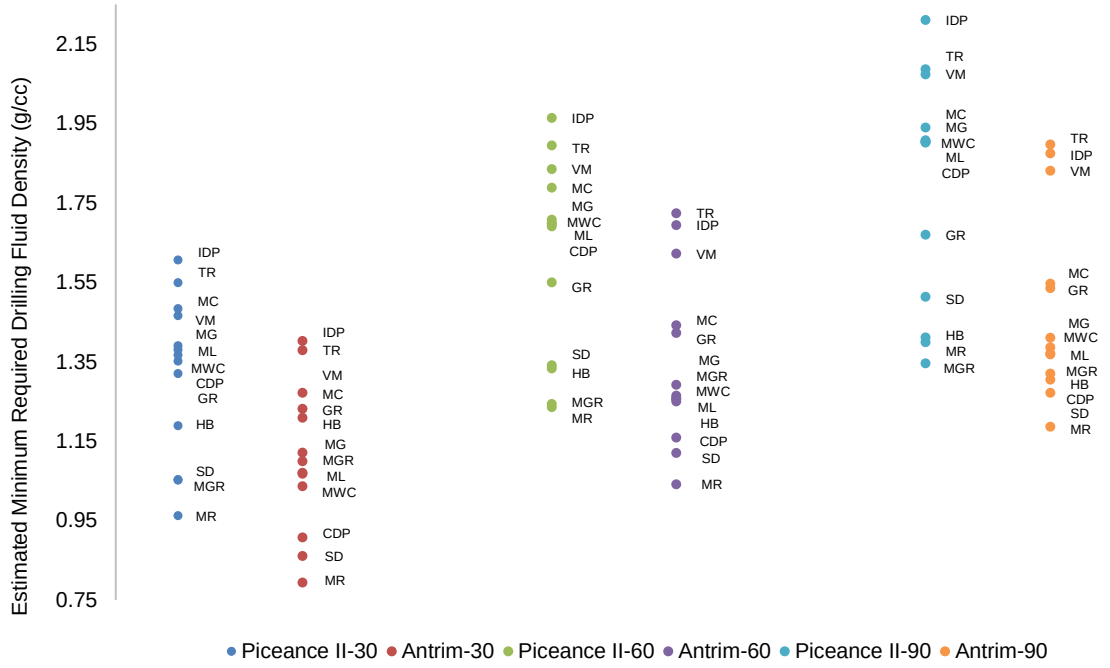

Figure 6-6. Comparison of estimated required drilling fluid density by failure criteria for Piceance basin II and Antrim shale at different wellbore inclination

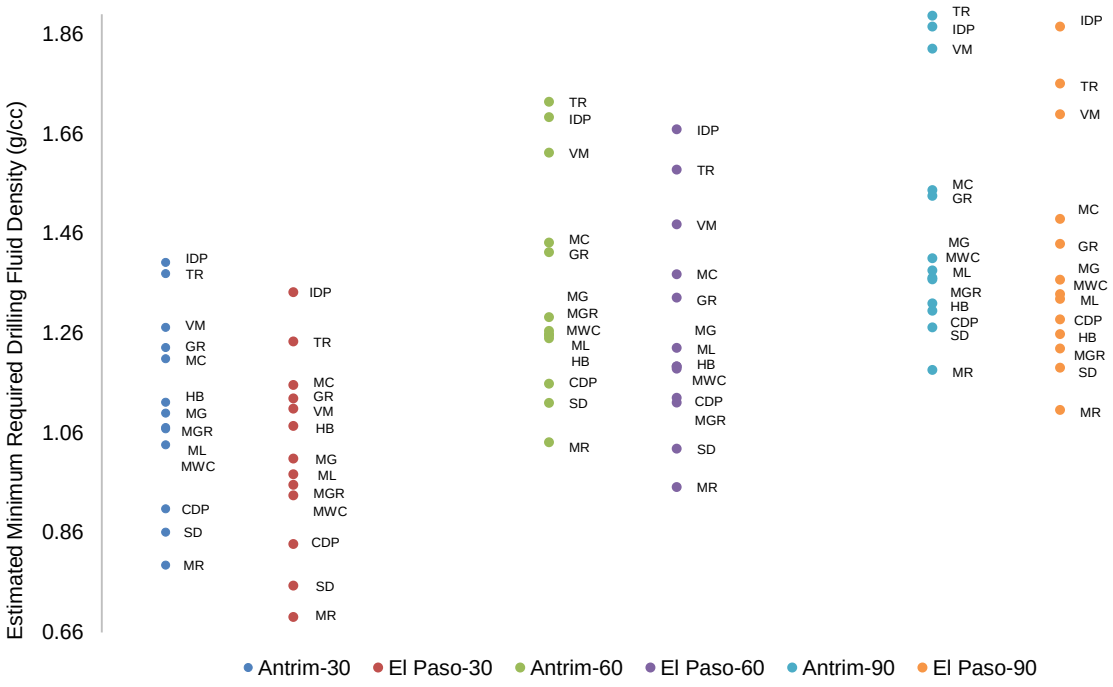

Figure 6-7. Comparison of estimated required drilling fluid density by failure criteria Antrim and El Paso shale at different wellbore inclination

The color code of each data series represents the bedding inclinations with respect to drilling axis in a horizontal wellbore where four data points for each shale were selected based on availability of anisotropy data. The estimated intervals of minimum drilling fluid density with sorted order of criteria are shown vertically, corresponding to each bedding inclination. According to the results for Pierre shale, the main difference in range of estimated drilling fluid density and order of criteria was observed for 60° of bedding inclination, where the lowest strength anisotropy was reported (12 % lower than compressive strength at 0° of bedding inclination) (Figure 6-9). The Hoek-Brown criterion replaced Circumscribed Drucker-Prager at the lower bound of results and Murrell criterion replaced Modified Wiebols-Cook in the middle range for the 60° of bedding inclination (Figure 6-8).

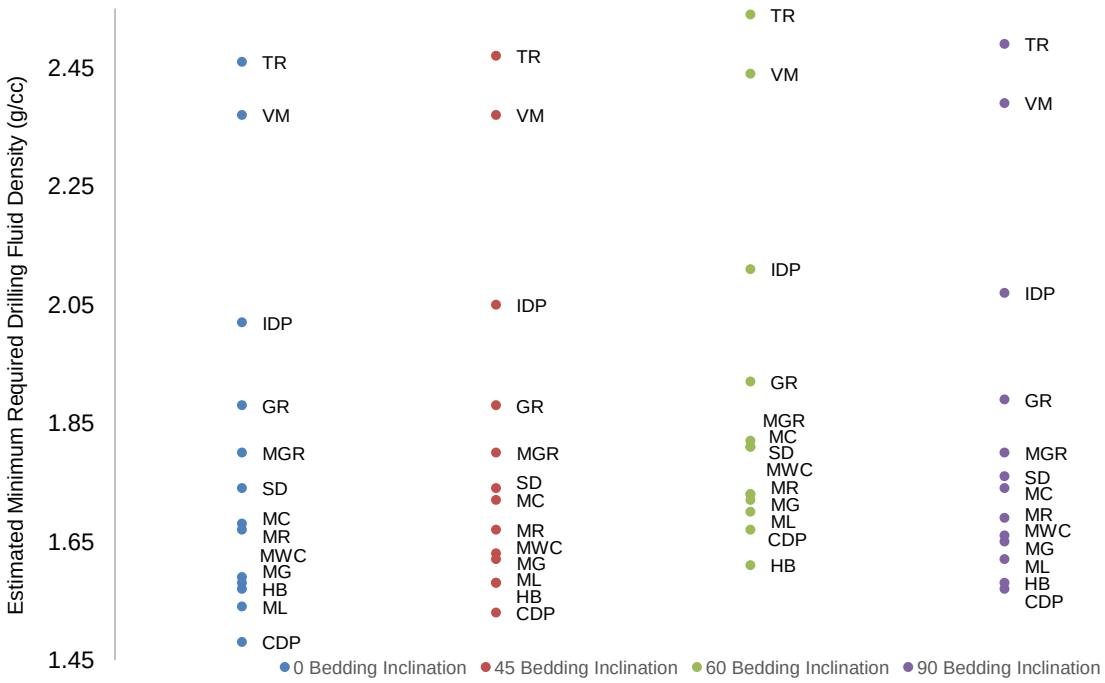

Figure 6-8. Range of estimated minimum required drilling fluid density by different criteria at different bedding inclination for Pierre shale

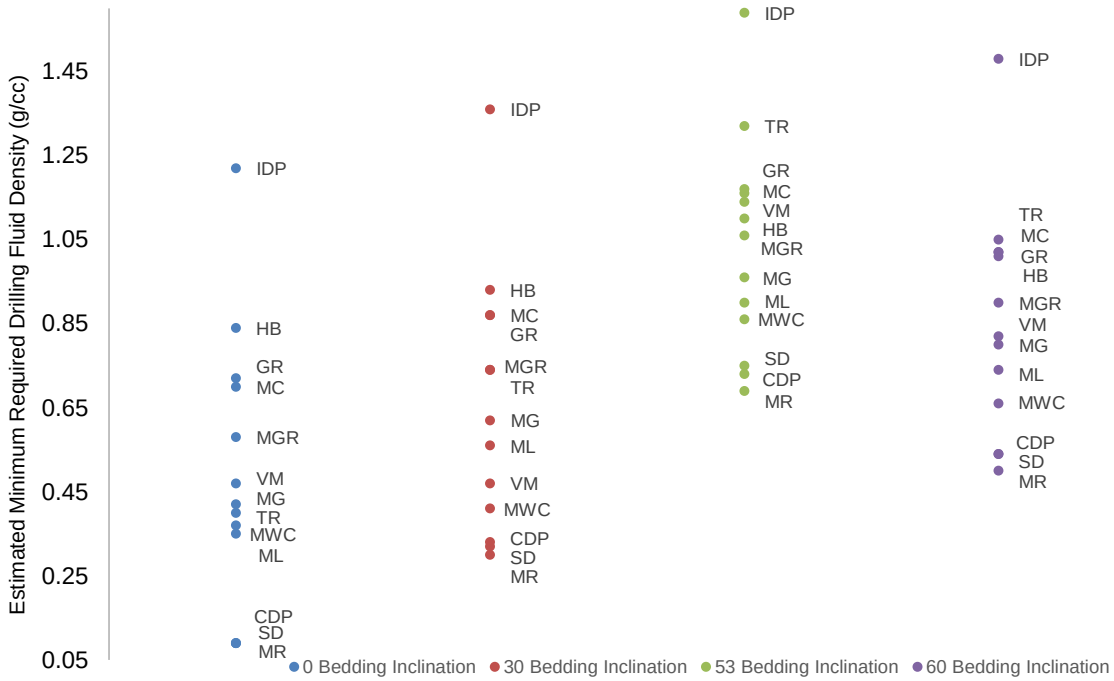

Figure 6-9. Range of estimated minimum required drilling fluid density by different criteria at different bedding inclination for Mancos shale

Higher range of drilling fluid density was also estimated for 60° of inclination since the strength anisotropy was maximum (12% strength reduction) (Figure 6-8). A higher and lower bound of results did not change for four bedding inclinations of Mancos shale where the higher bound and the lower bound of the results were represented by the Inscribed Drucker-Prager criterion the Murrell criterion respectively (Figure 6-9). A higher range of drilling fluid density was also estimated for 53° of bedding inclination because strength anisotropy was maximum (32% strength reduction) (Figure 6-9). Major difference in the order of criteria was also observed for bedding inclination of 53 degree where Tresca and Von Mises approached the higher bound of results (Figure 6-9). Maximum strength anisotropy for Tournemire shale was reported at 45° of bedding inclination where higher range of minimum required drilling fluid density resulted and main difference in order of criteria was observed (Figure 6-10). The results of Von Mises criterion ranked higher for

the 45 degree of bedding inclination compared to the 0° of bedding inclination, which was a major observation for the Tournemire shale. The Inscribed Drucker-Prager and Murrell criteria represented higher and lower bound of the results for all four bedding inclinations of Tournemire shale (Figure 6-10).

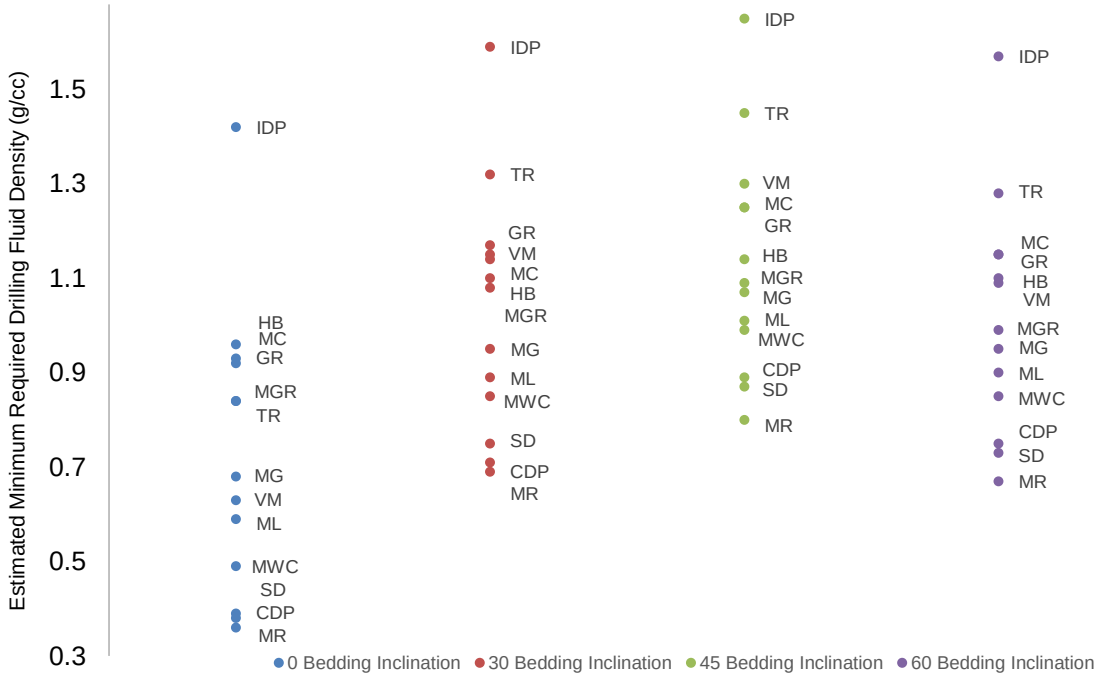

Figure 6-10. Range of estimated minimum required drilling fluid density by different criteria at different bedding inclination for Tournemire shale

7. DISCUSSION

According to a comparison of estimated drilling fluid density by different failure criteria for Bearpaw and Clagget shale (Figure 6-1), Circumscribed Drucker-Prager, Murrell, Stassi D'Alia, Hoek-Brown and Modified Griffith criteria responded to the change in UCS and frictional angle more than the other criteria. The Bearpaw shale has higher compressive strength compared to the Clagget shale, however it has a lower internal angle of friction (14°) (Table 3-1). Looking at the governing equation (Table 2-1) for the Circumscribed Drucker-Prager criterion, the decrease in the internal angle of friction might be the main reason in this change which seems to be the same for the Modified Griffith (Figure 6-1). However, for Murrell, Stassi D'Alia and Hoek-Brown increasing UCS caused their rank to change (Figure 6-1) because the UCS has a dominant effect in the governing equation for these three criteria (Table 2-1). A difference in the rank of criteria was observed for Piceance Basin shale I compared to Bearpaw shale (Figure 6-2). The Piceance Basin shale I has a higher compressive strength compared to the Clagget shale; however, the internal angle of friction was the same for the both shales (Table 3-1). The order of those failure criteria which are responsive to variation of frictional angle, Circumscribed Drucker-Prager and Modified Griffith did not change for Piceance Basin shale I even though to the change was observed in the results for Bearpaw shale (Figure 6-3). Murrell, Stassi D'Alia, and Hoek-Brown criteria, which are responsive to variation of UCS, showed the ranking change from Clagget shale to Piceance Basin shale I (Figure 6-3). Pierre shale II has a higher compressive strength compared to the Piceance Basin shale I (Table 3-1), though they have a similar internal angle of friction. This difference in UCS between Pierre shale II and Piceance Basin shale I (4.7 MPa) is more than the difference between Piceance

Basin shale I and Clagget shale (2 MPa). The ranking of those failure criteria (Circumscribed Drucker-Prager and Modified Griffith) that are responsive to the variation of frictional angle, did not change for Pierre shale II (Figure 6-4). Failure criteria that are more sensitive to the variation of the UCS (Murrell, Stassi D'Alia and Hoek-Brown) showed more significant change in the estimated drilling fluid density ranking for Pierre shale II compared to Piceance Basin shale I (Figure 6-4). The results of these three criteria are very close to the lower bound for Pierre shale II (Figure 6-4). The ranking of the estimated drilling fluid density using the different criteria shows a different trend from Pierre shale II to Piceance Basin shale II (Figure 6-5). Piceance Basin shale II has a higher UCS (About 8 MPa) than Pierre shale II and a lower internal angle of friction (7°) (Table 3-1). The effect of increasing UCS on failure criteria in the lower bound is more than what was observed for the Pierre shale II (Figure 6-5). A different failure criterion represents the higher bound for Piceance Basin shale II, Inscribed Drucker-Prager (Figure 6-5). Looking at the governing equation for Inscribed Drucker-Prager, the effect of the internal angle of friction variable is more than UCS (Table 2-1). The rank of Griffith and Modified Griffith criteria changed for Piceance Basin shale II compared to the Pierre shale II (Figure 6-5). This ranking change of Griffith criterion is due to higher UCS (17 MPa) because the tensile component in the governing equation of Griffith criterion is directly derived from a constant ratio with UCS (Table 2-1). However, for the Modified Griffith this ranking change is a combination of different UCS and the internal angle of friction because the tensile component in the governing equation is related to the UCS with a ratio as a function of the internal angle of friction (Table 2-1). Antrim shale has higher UCS (22 MPa) compared to the Piceance Basin shale II (17 MPa), and also a higher internal angle of

friction (23°). The order of Circumscribed Drucker-Prager changed to a lower rank for Antrim shale because the criterion's governing equation is more responsive to change in the internal angle of friction (Figure 6-6). Murrell, Stassi D'Alia, Modified Griffith, and Hoek-Brown criteria are dominated the lower bound of the results due to higher UCS (Figure 6-6). El Paso shale has higher UCS (26 MPa) compared to Antrim shale but comparable internal angle of friction (Table 3-1). Comparing the results for Antrim and El Paso shales (Figure 6-7), similar order of criteria was observed. There are some failure criteria that were not relatively influenced by the variation of UCS and the internal angle of friction such as Mogi-Coulomb, Modified Wiebols-Cook, Modified Lade, and Mohr-Coulomb (Figures 6-2 to 6-7). As it was observed in studied cases, variation of rock strength can significantly affect the estimated minimum required drilling fluid density by some failure criteria depending on the governing equation of criteria and how the constant parameters in the governing equations are derived from rock mechanical properties (UCS and internal angle of friction).

8. CONCLUSIONS

In this paper, the effect of rock strength variation and strength anisotropy on predicting borehole shear failure by thirteen different rock failure criteria was investigated. A dataset of rock mechanical properties of various shale plays was gathered and sorted based on the UCS as a common indication of rock strength. Anisotropy data set was collected based on limited published studies. Minimum required drilling fluid density was estimated by rock failure criteria using various levels of shales strength. According to the comparison of results for different shales, there are some failure criteria that are highly responsive to the variation in rock mechanical properties. Circumscribed Drucker-Prager, Modified Griffith, and Inscribed Drucker-Prager have shown great response to the change in the internal angle of friction. Murrell, Stassi D'Alia, Hoek-Brown, and Griffith are sensitive to variation of UCS. Tresca and Von Mises are responsive to strength anisotropy based on the results for Tournemire and Mancos shales. The combined effect of strength anisotropy level and strength level can affect the order of estimated minimum drilling fluid density by different criteria, especially for weaker shales. Mogi-Coulomb, Modified Wiebols-Cook, and Modified Lade failure criteria did not show any significant response to the variation of rock mechanical properties and strength anisotropy. Also, the accuracy of estimated borehole shear failure by these three criteria has been verified before. Thus, using these three criteria would be recommended for wellbore stability analysis.

REFERENCES

[1] Colmenares LB, Zoback MD. A statistical evaluation of intact rock failure criteria constrained by polyaxial test data for five different rocks. Int J of Rock Mech Min Sci 2002; 39: 695–729.

[2] Benz T, Schwab R. A quantitative comparison of six rock failure criteria. Int J of Rock Mech Min Sci 2008; 45(7): 1176–1186.

[3] McLean MR, Addis MA. Wellbore Stability Analysis: A review of current methods of analysis and their field application. In: Proceedings of the IADC/SPE Drilling Conference, Houston, Texas, February 27- March 2, 1990. SPE 19941.

[4] Ewy RT. Wellbore-stability predictions by use of a Modified Lade criterion. SPE Drill & Complet 1999; 14(2): 85–91. SPE-56862.

[5] Nawrocki PA. Critical wellbore pressures using different rock failure criteria. In: Proceedings of ISRM International Symposium and 6th Asian Rock Mechanics Symposium, New Delhi, India, October 23–27, 2010.

[6] Al-Ajmi AM, Zimmerman RW. Relation between the Mogi and the Coulomb failure criteria. Int J of Rock Mech Min Sci 2005; 42(3): 431–439.

[7] Al-Ajmi AM, Zimmerman RW. Stability analysis of deviated boreholes using the Mogi-Coulomb failure criterion, with applications to some North Sea and Indonesian reservoirs. In: Proceedings of the IADC/SPE Asia Pacific Drilling Technology Conference and Exhibition, Bangkok, Thailand, November 13-15, 2006. SPE 104035.

[8] Yi X, Ong SH, Russel JE. Improving borehole stability analysis by quantifying the effects of intermediate principal stress using polyaxial rock strength test data. In: Proceedings of the 40th U.S. Symposium on Rock Mechanics (USRMS), Anchorage, Alaska, June 25–29, 2005.

[9] Zhang L, Cao P, Radha KC. Evaluation of rock strength criteria for wellbore stability analysis. Int J of Rock Mech Min Sci 2010; 47(8): 1304–1316.

[10] Rahimi R, Nygaard R. Comparison of rock failure criteria in predicting borehole shear failure. Int J of Rock Mech Min Sci 2015; 79: 29–40.

[11] Rahimi R, Nygaard R. What difference does selection of rock failure criteria make in wellbore stability analysis? In: Proceedings of the 48th US Rock Mechanics / Geomechanics Symposium, Minneapolis, Minnesota, June 1-4, 2014.

[12] Fjaer E, Holt RM, Horsrud P, Raaen AM, Risnes R. Petroleum related rock mechanics. 2rd ed. Oxford. Elsevier; 2008.

[13] Jaeger JC, Cook NGW, Zimmerman RW. Fundamentals of rock mechanics. 4rd ed. Oxford. Blackwell Publishing; 2007.

[14] Drucker DC, Prager W. Soil mechanics and plastic analysis of limit design. J. Quar App Math 1952; 10: 157–165.

[15] Veeken CAM, Walters JV, Kenter CJ, Davies DR. Use of plasticity models for predicting borehole stability. In: Proceedings of the ISRM International Symposium, Pau, France, August 30-September 2, 1989.

[16] Zhou S. A program to model the initial shape and extent of borehole breakout. J Comput and Geosci 1994; 20(7-8): 1143–1160.

[17] Hoek E, Brown ET. Empirical strength criterion for rock masses. J Geotech Eng 1980; 106(9): 1013–1035.

[18] Lade PV. Elasto-plastic stress-strain theory for cohesionless soil with curved yield surfaces. J Sol Struc 1977; 13(11): 1019–1035.

[19] Wiebols GA, Cook NGW. An energy criterion for the strength of rock in polyaxial compression. Int J of Rock Mech Min Sci 1968; 5(6): 529–549.

[20] Griffith AA. The phenomena of rupture and flow in solids. J Phil Trans Roy Soc Lon 1921; Res. 221: 163–198.

[21] Brace WF. An extension of the Griffith theory of fracture to rocks. J Geophys Res 1960; 65(10): 3477-3480.

[22] McClintock FA, Walsh JB. Friction on Griffith cracks under pressure. In: Proceedings of the 4th U.S. National Congress of Applied Mechanics, Berkeley, California, 1962.

[23] Murrell SAF. A criterion for brittle fracture of rocks and concrete under triaxial stress and the effect of pore pressure on the criterion. In: Proceedings of 5th symposium on Rock Mechanics, Minneapolis, Minnesota, 1962.

[24] Stassi D'Alia F. Flow and fracture of materials according to a new limiting condition of yielding. Mechanica 1967; 2(3): 178–195.

[25] Schon J. Physical Properties of Rocks. 1st ed. Elsevier; 2011.

[26] Franklin, J.A. and Dusseault, M.B. 1991. Rock engineering applications, McGraw-Hill Ryerson Limited.

[27] Nygård, R., Gutierrez, M., Bratli, R.K. and Høeg, K. 2006. Brittle–ductile transition, shear failure and leakage in shales and mudrocks. Marine and Petroleum Geology, 23(2), pp.201-212.

[28] Bjorlykke, K. 2010. Petroleum Geoscience: From Sedimentary Environments to Rock Physics, Springer.

[29] Vutukuri VS, Lama RD, Saluja SS. Handbook on mechanical properties of rocks. Vol. 4. Testing techniques and results. Trans Tech Publications; 1978.

[30] Carmichael RC. Practical Handbook of Physical Properties of Rocks & Minerals. 1st ed. CRC Press; 1988.

[31] Johnson RB, DeGraff JV. Principles of Engineering Geology. 1st ed. Wiley Press; 1988.

[32] Goodman RE. Introduction to Rock Mechanics. 2nd ed. Wiley Press; 1989.

[33] Lockner DA. Rock failure. J of Rock physics and phase relations: A handbook of physical constants. 1995; 3: 127–147.

[34] Sone H. Mechanical properties of shale gas reservoir rocks and its relation to the in-situ stress variation observed in shale gas reservoirs. Ph. D. thesis, Stanford Univ.

[35] Chandong C, Zoback MD, Khaksar A. Empirical relations between rock strength and physical properties in sedimentary rocks. J of Petroleum Science and Engineering. 2006; 51: 223–237.

[36] Dobereiner L, DeFreitast MH. Geotechnical properties of weak sandstones. Géotechnique. 1986; 36(1): 79-94.

[37] Perry FV, Kelley RE, Dobson PF, Houseworth JE. Regional Geology: A GIS Database for Alternative Host Rocks and Potential Siting Guidelines. U.S. Department of Energy. 2014.

[38] Aristorenas GV. Time-dependent behaviour of tunnels excavated in shale. Ph. D. thesis, Massachusetts Institute of Technology.

[39] Senseny PE, Fossum AF, Pfeifle TW. Non-associative constitutive laws for low porosity rocks. International Journal for Numerical and Analytical Methods in Geomechanics. 1983; 7(1): 101-115.

[40] Donath FA. Experimental study of shear failure in anisotropic rocks. Geological Society of America Bulletin. 1961;72(6):985-9.

[41] Chenevert ME, Gatlin C. Mechanical anisotropies of laminated sedimentary rocks. Society of petroleum engineers journal. 1965; 5(01):67-77.

[42] McLamore RR, Gray KE. The Mechanical Behavior of Anisotropic Sedimentary Rocks. ASME. J. Eng. Ind. 1967;89(1):62-73. doi:10.1115/1.3610013.

[43] Niandou H, Shao JF, Henry JP, Fourmaintraux D. Laboratory investigation of the mechanical behaviour of Tournemire shale. International Journal of Rock Mechanics and Mining Sciences. 1997; 34(1):3-16.

[44] Islam MA, Skalle P. An experimental investigation of shale mechanical properties through drained and undrained test mechanisms. Rock Mechanics and Rock Engineering. 2013; 46(6):1391-413.

[45] Fjær E, Nes OM. Strength anisotropy of Mancos shale. In: Proceedings of 47th US Rock Mechanics/Geomechanics Symposium 2013 Jan 1. American Rock Mechanics Association.

[46] Mokhtari M. Characterization of anisotropy in organic-rich shales: shear and tensile failure, wave velocity, matrix and fracture permeability. PhD Dissertation, Colorado School of Mines, 2015.

[47] Bradley WB. Failure of inclined borehole. Energy Resources Technology 1979; 101(4):232-239.

[48] Aadnoy BS, Chenevert ME. Stability of highly inclined boreholes. J SPE Drill Eng 1987; 2(4): 364-374.

III. ANALYSIS OF ANALYTICAL FRACTURE MODELS FOR WELLBORE STRENGTHENING APPLICATIONS, AN EXPERIMENTAL APPROACH

Reza Rahimi, Mortadha Alsaba, and Runar Nygaard

Department of Geosciences and Geological and Petroleum Engineering,

Missouri University of Science and Technology, Rolla, MO, United States

ABSTRACT

Drilling fluid losses are challenging to prevent or mitigate during drilling. Lost circulation treatments are applied to stop losses using a corrective approach or to hinder losses using a preventive approach, also known as wellbore strengthening. The key factors that must be determined when treating losses are the fracture width and the required particle size. The fracture width is often estimated using analytical fracture models. In this paper, five different fracture width models were analyzed and compared to hydraulic fracturing experiments. The hydraulic experiments were conducted on impermeable concrete cores to investigate the effect of adding lost circulation materials (LCM) to enhance the fracture breakdown pressure and the fracture re-opening pressure. The results showed that adding LCM blends enhanced the breakdown pressure up to 18% and the re-opening pressure up to 210%. The cores that were fractured with fluid-containing solids had a larger fracture width compared to the fractured cores using base fluid. Comparing the measured fracture widths from experiments with analytical models showed a discrepancy in the fracture width estimation for all of the models and the experiments, except for one model.

1. INTRODUCTION

Lost circulation materials have been used widely to treat lost circulation events in the past few decades, and yet improving efficiency of these treatments is an ongoing goal for the drilling industry. Sealing fractures using LCM prevents further transferring of drilling fluid pressure to the fracture and prevents fracture propagation [1]. Estimation of the fracture width could be an important design parameter for LCM treatment design [2]. The efficiency of strengthening treatment and enhancing fracture gradient might change with particle sizes compared to fracture sizes [3, 4]. Models with different limitations and assumptions have been developed for determining the fracture width and the stress intensity factor. Previous parametric studies have been focused on the estimation of the fracture width or re-opening pressure of an induced symmetric fracture around the wellbore. Assuming perfect sealing of the wellbore pressure by plugging the fracture, Morita et al. [5-7] developed a plain strain analytical model to estimate the fracture width [5-7]. Alberty and McLean [2] presented a model for the fracture width as a function of the fracture length based on a linear, two-dimensional solution of a symmetric wellbore fracture. The estimated fracture width was used to calculate the volume of the fracture and select the particle sizes [2]. Considering a slit-like crack with three possible pressurized regions, Deeg and Wang [8] developed an analytical solution for the fracture width and the stress intensity factor along the fracture [8]. Wang et al. [9] modified [8]'s model by simplifying it into two pressurized regions, including the pressure behind and in front of the fracture. Deformable, viscous, and cohesive (DVC system) LCM was recommended for efficient sealing of a fracture that would increase the hoop stresses around the borehole [9]. Finite element analysis conducted by [10] investigated the aperture of symmetric

fractures around a wellbore. A closed-form analytical solution was developed for crack mouth opening displacement (CMOD) based on the linear elastic fracture mechanics and the finite element results [10]. Comparing the results of the closed-form solution with the finite element analysis shows that the analytical model results are close to the finite element results for a certain range of wellbore size to the fracture length ratio and in-situ horizontal stresses ratio. A semi-analytical workflow was developed [11] based on the exact solution of a dislocation-based fracture model, which was provided earlier [12]. The result of the fracture re-opening pressure from [12]'s model was compared to the results of [7]'s model using the same input parameters. The review revealed that none of the previous studies had evaluated analytical fracture models with experimental or field data. Also, all of the analytical models used different assumptions.

The main objective of this paper is to evaluate the fracture width estimate of five analytical fracture models. To reach this objective, three goals have been defined: 1) analyze the effect of different input parameters on the estimated fracture width, including rock properties, in-situ stresses, anisotropy, borehole size and fracture geometry; 2) investigate the effect of adding different LCM for enhancing the fracture breakdown pressure and the fracture re-opening pressure; and 3) compare the estimated fracture widths with the measured fracture width. A sensitivity analysis was investigated for the five analytical fracture models. Then hydraulic fracturing experiments were conducted on impermeable concrete cores using an oil-based drilling fluid with different LCM. The experimental data and mechanical properties of core samples were used to estimate the fracture width. The fracture width was measured under optical microscopy after retrieving the samples from the fracturing apparatus.

2. REVIEW OF WELLBORE STRENGTHENING FRACTURE MODELS

Five analytical models [13, 12, 2, 9, &7] were used to estimate the fracture width (Table 2-1). The models listed in Table 2-1 and used throughout this paper are: Hillerborg et al., Carbonell and Detournay, Alberty and McLean, Wang et al., and Morita and Fuh, respectively. All models assume a symmetric fracture around the wellbore (Figure 2-1). In some models, LCM particles are assumed to plug the mouth of fracture while, in other models, LCM could be located at a distance from the fracture mouth [2]. All of the models are based on the theory of linear elastic fracture mechanics (LEFM). Hillerborg et al. [13] developed an analytical solution for the fracture width estimation where the model stresses are assumed to act across a crack as long as it is narrowly opened [13] (Table 2-1).

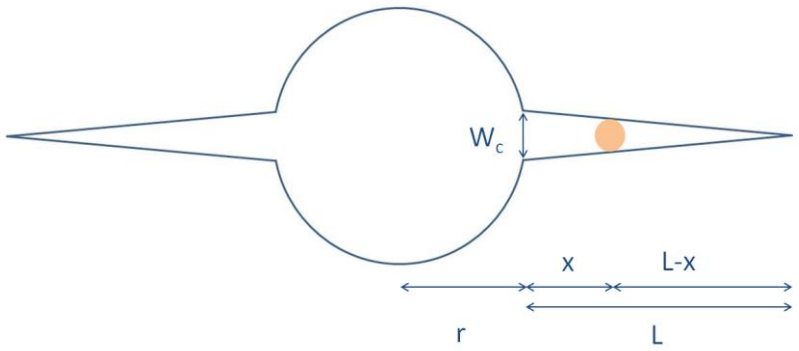

Figure 2-1. Sketch of a symmetric bi-wing fracture around a wellbore. L (Fracture length), r (Wellbore radius), Wc (Fracture width), and x (Plug distance from fracture mouth)

Based on this model, crack propagation decreases when the crack width increases [13]. The model was developed for aggregated materials such as concrete where the fracture width is almost equal to the maximum size of aggregate particles by order of a few

millimeters. Carbonell and Detournay's model is a semi-analytical solution that estimates the fracture propagation pressure using a dislocation-based approach [12]. Their solution was based on the original singular solution of a finite edge dislocation on the boundary of circular wellbore in an infinite elastic plane derived by Warren [14]. Both the stress intensity factor at the tip of fracture and the fracture width could be determined using a Guass-Chebyshev integration formula [15] to address the singular integral of dislocation density function (Table 2-1). Even though the model gives a solution for the fracture width, the fracture length is an input parameter. In addition, the pressure along the fracture is assumed to be constant. Alberty and McLean's model is a modified two-dimensional line crack solution used to compare the results of the fracture width from a finite element model with their analytical model. The original solution was for a small line crack (Continuum Fracture Mechanics). The fracture width could be estimated at any distance from the fracture mouth; however, the estimate is dependent on the fracture length being similar to [12] and [13] models. Wang et al.'s model (Table 2-1) is a semi-analytical solution for the fracture width based on two distinct pressurized regions [9] and was developed by simplifying an earlier model that included three pressurized regions [8]. The crack length is calculated using an analytical solution for the stress intensity factor by comparing the fracture stress intensity factor to the fracture toughness of rock. . Morita and Fuh (Table 2-1) developed a closed-form solution to estimate the fracture width based on a two-dimensional boundary element model [7]. The developed analytical model determines the fracture width as a function of rock properties, in-situ stress, the length of fracture, and the wellbore pressure (Table 2-1); however, the fracture width (plug width) is an input parameter to find the fracture length. The solution for the fracture length is based on linear

elastic fracture mechanics [16]. Since the plugging material might sit somewhere along the fracture, possibly close to the tip of the fracture rather than mouth of the fracture, an alternate closed-form solution was provided. The plug size is considered to be the same as the fracture width and a certain length of fracture (close to 6 inches) is assumed.

Table 2-1. Analytical fracture models
(m and h(t_k) are Chebyshev polynomial properties [15])

Model	Fracture Width Solution
Hillerborg et al. 1976	$w_C = \frac{2\sqrt{2}L(p_f - \sigma_h)}{\sqrt{\sqrt{(p_f - \sigma_h)^4 + \frac{E^2{\sigma_h}^2}{\pi^2(1-v^2)^2}} - (p_f - \sigma_h)^2}}$
Carbonell and Detournay, 1995	$w_C = \frac{\pi(L)}{2m}\frac{4(1-v^2)}{\mathrm{E}}\sum_{i=0}^{m} h(t_k)$
Alberty and McLean, 2004	$w_C = \frac{4(1-v^2)}{\mathrm{E}}(p_w - \sigma_H)\sqrt{(L+r_w)^2 - x^2}$
Wang et al. 2008	$w_C = \frac{8(1-\nu^2)L}{\pi E}\frac{\left\{\frac{\pi}{2}\sqrt{1-\left(\frac{r_w}{L}\right)^2}(p_0-\sigma_h) + (p_w-p_0)\left(\sqrt{1-\left(\frac{r_w}{L}\right)^2}\sin^{-1}\frac{r_w}{L} + \sum_{n=1}^{\infty}\sin\left(2n\sin^{-1}\left(\frac{r_w}{L}\right)\right)A\right)\right\}}{(2n-1)(2n+1)}$ $A = \left(2\sqrt{1-\left(\frac{r_w}{L}\right)^2}\cos\left(2n\sin^{-1}\left(\frac{r_w}{L}\right)\right) + \frac{r_w\sin\left(2n\sin^{-1}\left(\frac{r_w}{L}\right)\right)}{Ln}\right)$
Morita and Fuh, 2012	$w_C = \frac{4(1-v^2)}{E}L(\sigma_h - p_f)$

The models reviewed in this study have the fracture width primarily as a function of the fracture length, in addition to rock properties, wellbore pressure, fluid pressure within the fracture, and in-situ stresses. One of the main limitations of the reviewed analytical models is the length of fracture being used as an input parameter, which reflects the impracticality of measuring fracture length in the field. Also, models [7] and [12] are based on the fixed fracture length (approximately 6 inches.), which might not be realistic.

Another simplification of the current models is assuming constant fluid pressure within the fracture, since the pressure beyond the plugging material might decrease gradually for both permeable and impermeable formations. The fracture shape of drilling induced fractures or natural fractures might not necessarily be a line crack and the fracture width might change along the fracture. To evaluate the assumptions and applicability of the various fracture models on the estimated result of the fracture and the fracture widths, a sensitivity analysis of the input parameters, in conjunction with experimental validation, was required.

3. SENSITIVITY ANALYSIS

The sensitivity analysis investigates which fracture models' input parameters have a significant effect on the fracture width estimation. The sensitivity analysis was performed using a published data set given in Table 3-1 [7]. The input parameters for each model were plotted as dimensionless, scale- normalized with the base case data of Table 3-1 on the horizontal axis and the resulting fracture width on the vertical axis (Figure 3-1).

Table 3-1. Sensitivity analysis input data [7]

Parameter		Value	Unit
Minimum horizontal stress	σ_h	1000	psi
Maximum horizontal stress	σ_H	1000	psi
Young's Modulus	E	10^6	psi
Poisson's ratio	v	0.2	
Fracture length	L	5.21	inches
Wellbore radius	r_w	4.25	inches
Pressure along the fracture	P_f	0	psi
Wellbore Pressure	P_w	3797	psi

Based on the sensitivity analysis for Hillerborg et al.'s model (Figure 3-1.a), increasing the minimum horizontal stress is the dominant effect in decreasing the estimated fracture width, compared to Young's modulus and Poisson's ratio. Increasing the wellbore pressure and the fracture length will increase the estimated fracture width (Figure 3-1.a). Young's modulus has the most impact on the estimated fracture width in Carbonell and Detournay's model (Figure 3-1.b).

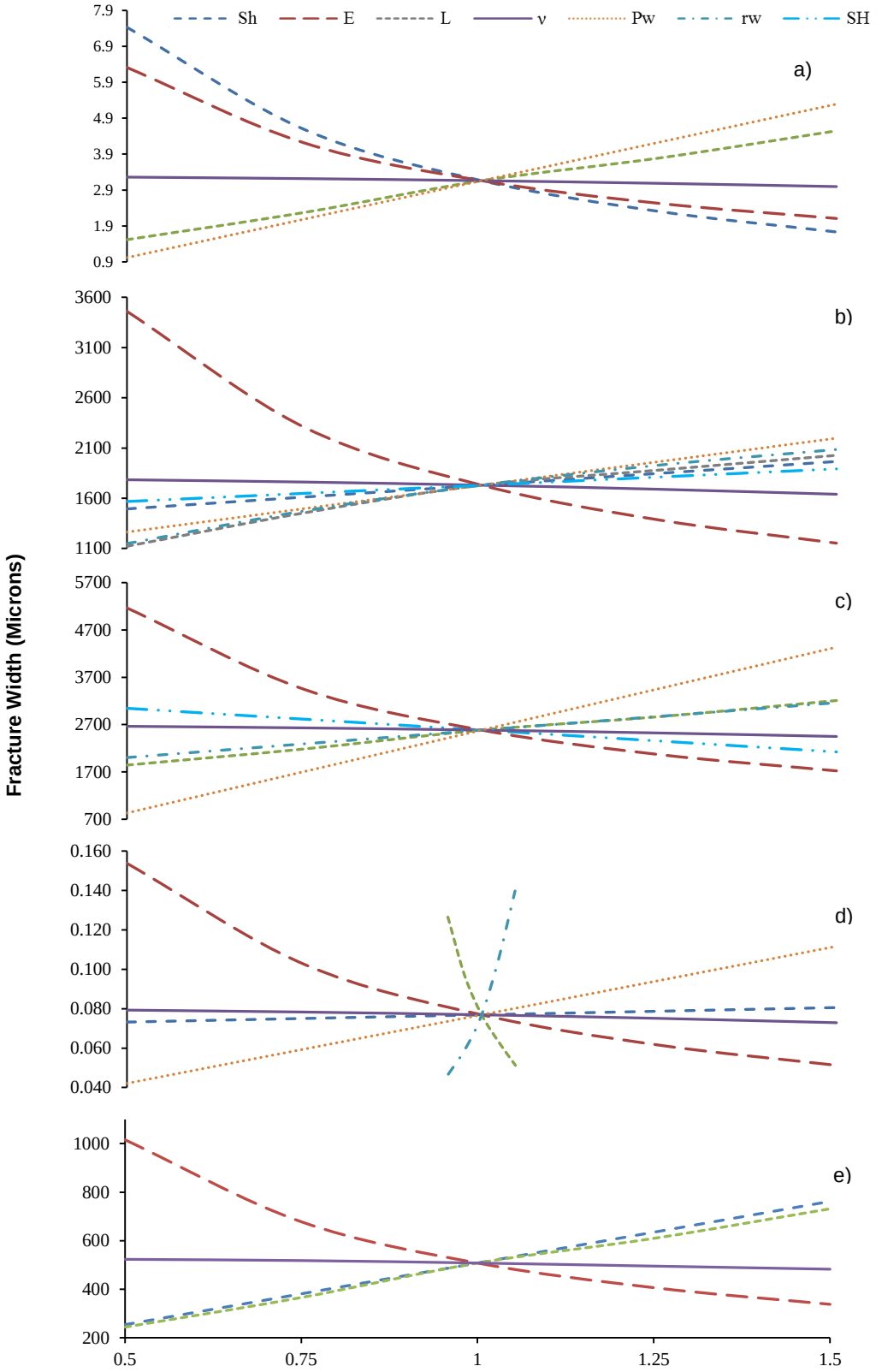

Figure 3-1. Sensitivity analysis of input parameters (Sh, SH, E, Pw, rw) for a) Hillerborg et al. b) Carbonell and Detournay c) Alberty and McLean d) Wang et al. and e) Morita and Fuh models

Increasing Poisson's ratio has the lowest effect on the estimated fracture width. The effect of the minimum horizontal stress is higher than the maximum horizontal stress (Figure 3-1.b). Also, the effect of the minimum horizontal stress is higher than the fracture length and the wellbore radius (Figure 3-1.b). The effects of changing the wellbore radius and the fracture length on the estimated fracture width are comparable. Increasing Young's modulus and Poisson's ratio decreases the estimated fracture width, while increasing horizontal stresses, fracture length and wellbore radius will increase the estimated fracture width (Figure 3-1.b). For Alberty and McLean's model, wellbore pressure is the dominant parameter in the fracture width change compared to the length of fracture and the wellbore radius (Figure 3-1.c). In this model, the pressure along the fracture is assumed to be equal to wellbore pressure. Increasing the maximum horizontal stress, Young's modulus, and Poisson's ratio have a reverse result on the estimated fracture width. Poisson's ratio has the least impact on the estimated fracture width, which is similar to other models' results (Figure 3-1.c). The sensitivity analysis results for Wang et al.'s model compared to the others (Figure 3-1.a to 3-1.d), the fracture length and the wellbore size has been studied for a shorter length compared to other parameters, since the model is defined for only a given fracture length and wellbore radius (Figure 3-1.d). Wang et al. [9] model also gives only a minor change in the fracture width when changing the minimum horizontal stress value. Increasing the wellbore pressure or the minimum horizontal stress increases the estimated fracture width while increasing Young's modulus and Poisson's ratio decreases it. Morita and Fuh's model (Figure 3-1.e) shows that Young's modulus and Poisson's ratio have the highest and lowest effect on the results of estimated fracture width, respectively. Increasing the minimum horizontal stress and the fracture length gives wider fracture width (Figure3-

1.e). As seen in Figure 3-1 for all the fracture models, the effects of Young's modulus and Poisson's ratio are the same, while the minimum horizontal stress and the fracture length show a different effect for the fracture width estimates for each model. Figure 3-2 and 3-3 compare the effect of the minimum horizontal stress and the fracture length on the estimated fracture width for all models. The vertical axis represents the dimensionless scaled value of the fracture width, and the horizontal axis represents the magnitude of the fracture length (Figure 3-2) and the minimum horizontal stress (psi) (Figure 3-3).

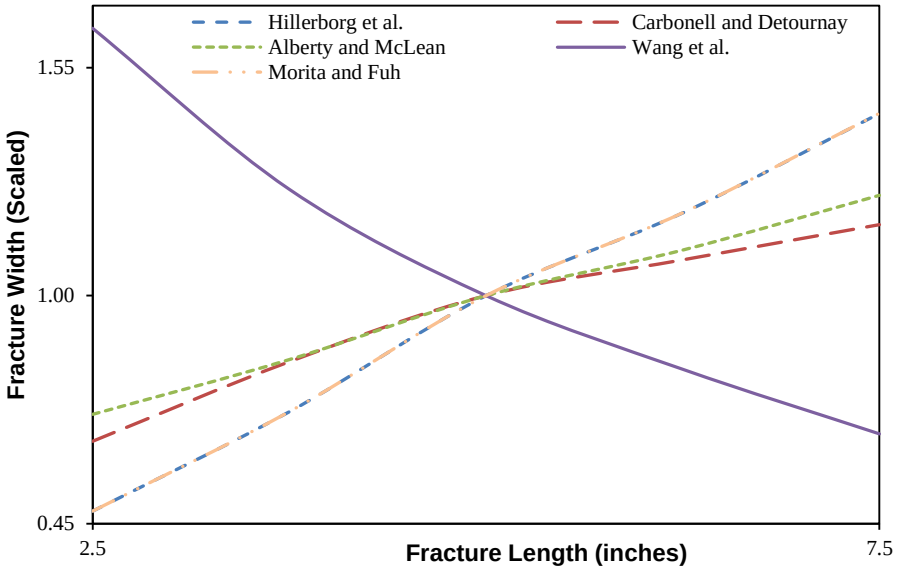

Figure 3-2. Scaled fracture width vs. fracture length for the different fracture models

Comparing the results of the models based on the fracture length (Figure 3-2), Wang et al.'s model is the only one that shows a decreasing trend for the fracture width solution by increasing the fracture length. Morita and Fuh's and Hillerborg et al.'s models demonstrate exactly the same behavior, and the effect of increasing the fracture length to increase the estimated fracture width in these two models is more significant than

Carbonell and Detournay's and Alberty and McLean's models (Figure 3-2). According to the comparison of fracture models based on the minimum horizontal stress (Figure 3-3), the results of Hillerborg et al.'s model was influenced much more than other fracture models by variation of the minimum horizontal stress. The estimated fracture width value decreases by increasing the minimum horizontal stress for Hillerborg et al.'s and Alberty and McLean's model. Variation of the minimum horizontal stress has a minor effect on the estimated results of the fracture width by Carbonell and Detournay's and Wang et al.'s models. The fracture width results of Morita and Fuh's model increased by increasing the minimum horizontal stress (Figure 3-3).

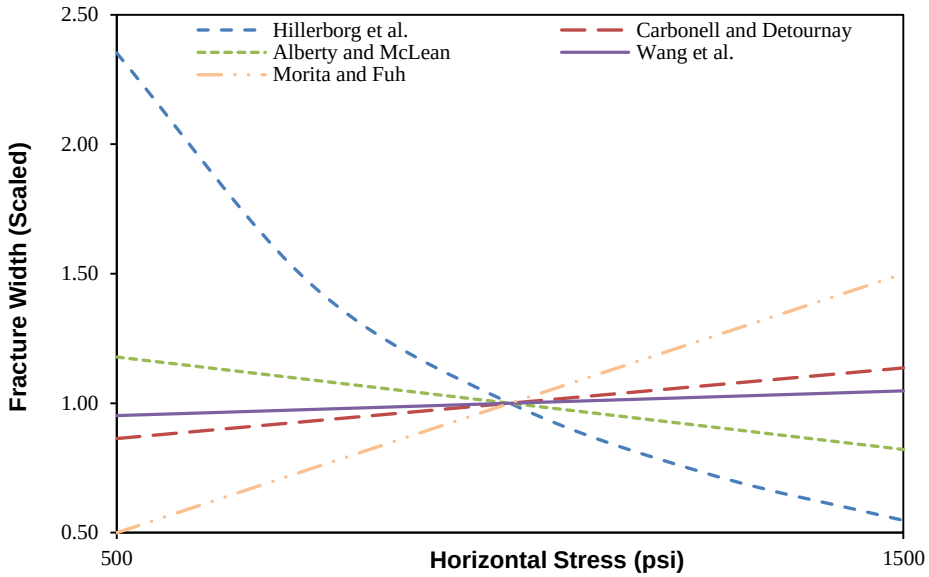

Figure 3-3. Scaled fracture width vs. horizontal stress for the different fracture models

4. EXPERIMENTAL EVALUATION

According to the sensitivity analysis results from the different analytical fracture models, the fracture width estimation will change significantly with the variation of some input parameters. At the same time, there is no agreement among the different models as to the results of the estimated fracture width. For wellbore strengthening applications by means of LCM addition, the accurate estimation of fracture width is a key factor for an efficient strengthening treatment design. So, an experimental analysis was conducted to compare the estimated fracture width from analytical models with experimental data.

4.1. HYDRAULIC FRACTURING EXPERIMENT

Hydraulic fracturing experiments were performed on five concrete cores using five different drilling fluid formulations (OBM). Figure 4-1 shows a schematic drawing of the hydraulic fracturing apparatus. Two pumps are used to apply confining and injection pressure. A hydraulic hand pump is used to apply overburden stress on the core sample, and a metal accumulator is used to inject fluids into the core. Injection pressures were recorded using LabVIEW© software. Cement core samples were prepared using Portland cement (Class H) to simulate impermeable formations. Class H cement was mixed with API recommended water requirements of 38% by weight of cement in a large batch, following standard mixing procedures to ensure the same physical properties of the fractured cores. The cement mixture was poured into 5 7/8-inch (diameter) x 9-inch (height) molds and left to cure for at least 7 days. Mechanical properties of the concrete samples and testing data are listed in Table 4-1. A ½-inch wellbore was drilled in the

cement cores using a drill press, and then top and bottom caps were attached to the cement cores using epoxy.

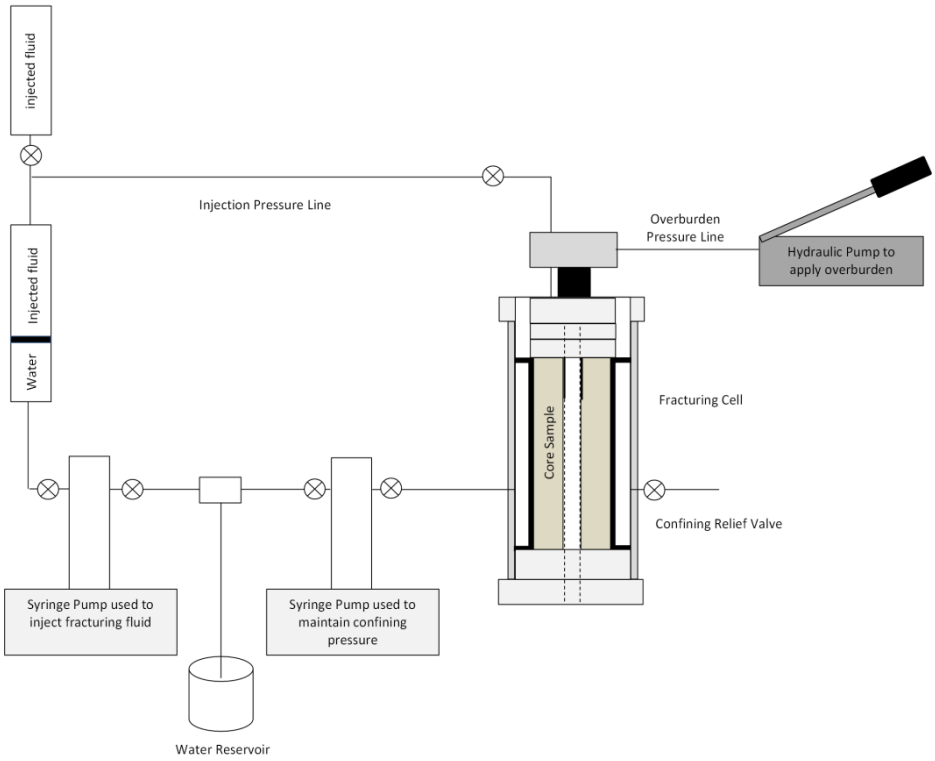

Figure 4-1. Hydraulic fracturing apparatus schematic

Table 4-1. Cement properties and experimental data

Parameter		Value	Unit
Minimum horizontal stress	σ_h	100	psi
Maximum horizontal stress	σ_H	100	psi
Young's Modulus	E	1450377	psi
Poisson's ratio	v	0.25	
Fracture length	L	2.65	inches
Wellbore radius	r_w	0.275	inches
Pressure along the fracture	P_f	0	psi

The first test was conducted using EDC95-11, which is a solid-free, clear base fluid used to prepare the pre-mixed OBM. The second test was conducted with the pre-mixed OBM without LCM to serve as a control sample. Tests # 3, 4, and 5 were conducted using the pre-mixed OBM mixed with 3 different LCM mixtures. The LCM mixtures were based on recommendations of previously published research. 20 ppb graphite and nutshells blend (G & NS) was used for test # 3 as suggested by Hettema et al. [17]. 30 ppb graphite and sized calcium carbonate blend was studied in test #4, following the recommendations of Aston et al. [18]. 55 ppb graphite, sized calcium carbonate, and cellulosic fibers blend was used in test #5, as recommended by Kumar et al. [19]. A confining pressure of 100 psi and an overburden pressure of 400 psi were applied. An injection rate of 5 ml/min was used to pressurize the wellbore until reaching the breakdown and propagation pressure. The injection is stopped for a 10-minute period before running the re-opening cycle. The test is stopped after the second cycle has peaked.

4.2. PARTICLE SIZE DISTRIBUTION (PSD) ANALYSIS

Dry sieve analysis was used to analyze the particle size distribution (PSD) of the evaluated LCM mixtures. Samples of LCM treatment were filtered through a series of stacked sieves using a mechanical sieve shaker. The cumulative weight percent retained for each sieve size was calculated from the measured weight retained in each sieve and then plotted versus the sieve sizes. The five main parameters of interest for the different blends were obtained from the resulting plot; they are the D10, D25, D50, D75, and D90, measured in mm and converted to microns where 1 mm = 1000 microns.

5. RESULTS AND DISCUSSION

Figure 5-1 and Figure 5-2 show the results from the hydraulic fracturing experiment. The blue line represents the first injection cycle, which is used to estimate the breakdown pressure. The red line represents the second injection cycle, which is used to estimate the re-opening pressure after the 10- minute fracture healing period. The peak pressure at the first cycle shows the breakdown pressure, and the peak pressure of the second cycle shows the fracture re-opening pressure. More details about experiments and the results can be found in [21]. Table 5-1 and Table 5-2 give an overview for comparing the results of the hydraulic fracturing experiment for the breakdown and re-opening pressures for every fluid mixture. Figures 5-3 to 5-7 show the actual fractures and the measured fracture width of concrete cores under a microscope. The lowest breakdown and re-opening pressures (843 and 571 psi) were observed for the first test (Table 5-1), which was conducted using EDC95-11 base fluid. The small size of fracture (15 to 22 microns) from the microscopy image (Figure 5-3) could be due to using clear fluid without solid content. The highest breakdown pressure (2372 psi) resulted from the test with an LCM blend containing graphite (G), sized calcium carbonate (SCC), and cellulosic fiber (CF) (Table 5-1). The highest re-opening pressure (1834 psi) was obtained using a combination of graphite (G) and sized calcium carbonate (SCC) (Figure 5-6 and Table 5-1). Traces of LCM particles were visible on the fracture opening for tests #3, 4 and 5 (Figures 5-5 to 5-7). In general, the addition of LCM enhanced both the fracture breakdown and re-opening pressures.

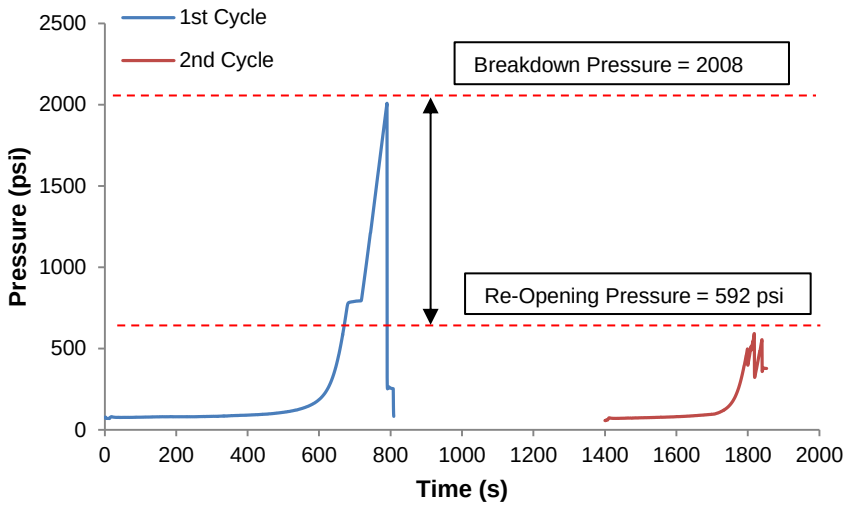

Figure 5-1. Pressure vs. Timer for Test # 2

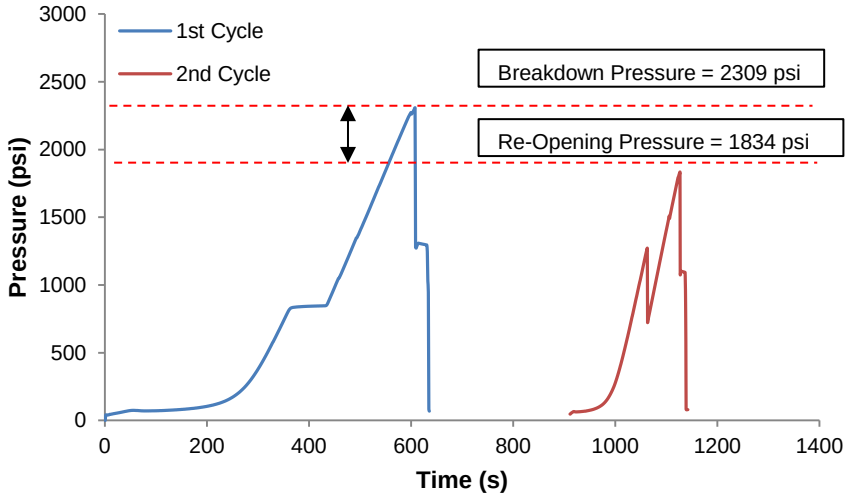

Figure 5-2. Pressure vs. Timer for Test # 4

Table 5-1. Summary of Testing Results

Test #	Fluid Used	Density (ppg)	LCM Blend	Concentration (ppb)	Breakdown Pressure (psi)	Re-Opening Pressure (psi)
1	EDC95-11	6.8	N/A	N/A	843	571
2	VERSATEC OBM	11	N/A	N/A	2008	592
3	VERSATEC OBM	11	G&NS	20	2199	1334
4	VERSATEC OBM	11	G & SCC	30	2309	1834
5	VERSATEC OBM	11	G, SCC, & CF	55	2375	1717

When comparing the solid-free base fluid (EDC95-11) from test #1 with the pre-mixed OBM control sample (test # 2), the breakdown pressure was reduced from 2008 psi to 843 psi, and the re-opening pressure was reduced from 592 psi to 571 psi (Table 5-1). The breakdown pressure of test #1 was the lowest compared to other tests since the solid-free base fluid did not build a filter cake around the wellbore wall. The 20 ppb graphite (G) and nutshells (NS) blend used in test #3 enhanced the breakdown pressure from 2008 psi to 2199 psi while the re-opening pressure was enhanced from 592 psi to 1334 psi, compared to the results of test #2 (Table 5-1). The enhancement in both the breakdown and the re-opening pressure is attributed to the formation of a stronger filter cake with the presence of LCM. The increases also suggest that LCM sealed the fracture, which occurred in the first cycle, and improved the wellbore integrity, resulting in higher re-opening pressure in the second injection cycle. The 30 ppb graphite and sized calcium carbonate blend in test #4 also resulted in enhancing both the breakdown and re-opening pressures from 2199 psi to 2309 psi and from 1334 psi to 1834 psi, respectively (Table 5-1). Test #5 containing 55 ppb graphite, sized calcium carbonate, and cellulosic fiber resulted in the highest enhancement in the breakdown pressure from 2309 psi to 2375 psi (Table 5-1).

Based on the measured range of the fracture width under an optical microscope for the five core samples (Figures 5-3 to 5-7 and Table 5-2), the fracture width increased as the wellbore pressure increased (breakdown pressure). The first test has the lowest range of the fracture widths (15 - 22 microns) (Figure 5-3 and Table 5-2), and tests #4 & 5 have the highest range of the estimated fracture width (40 - 85 microns and 50 - 140 microns) (Figures 5-6 &5.7 and Table 5-2).

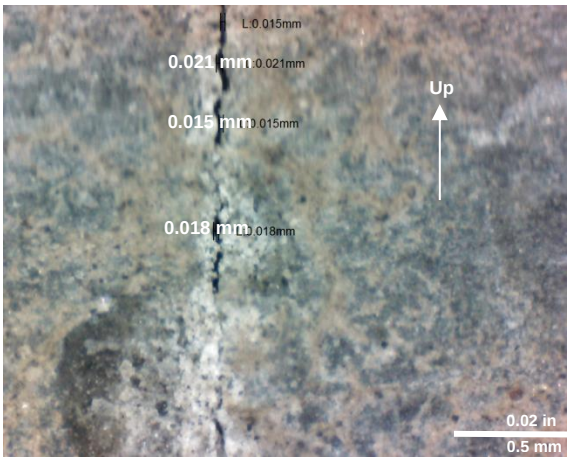

Figure 5-3. The resulting fracture under a microscope (200x magnification) for Test #1 showing the fracture widths ranging between 15 – 21 microns

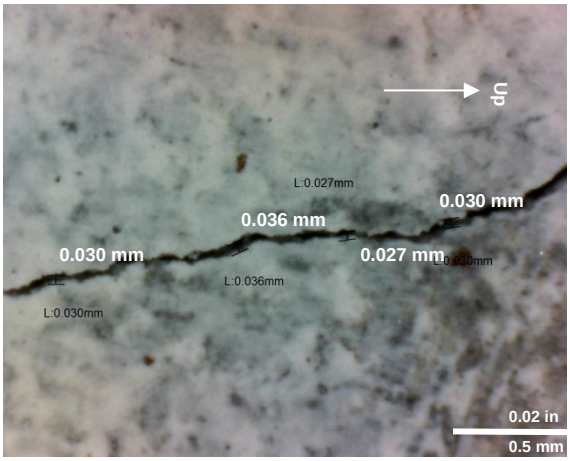

Figure 5-4. The resulting fracture under a microscope (200x magnification) for Test #2 showing the fracture widths ranging between 27 – 36 microns

Table 5-2. The estimated fracture width of cores under a microscope

Test #	Fluid Used	LCM Blend	Breakdown Pressure (psi)	Re-Opening Pressure (psi)	Estimated Fracture Width (Microns)
1	EDC95-11	N/A	843	571	15 - 22
2	VERSATEC OBM	N/A	2008	592	27 - 36
3	VERSATEC OBM	G&NS	2199	1334	40 - 85
4	VERSATEC OBM	G & SCC	2309	1834	40- 145
5	VERSATEC OBM	G, SCC, & CF	2375	1717	50 - 140

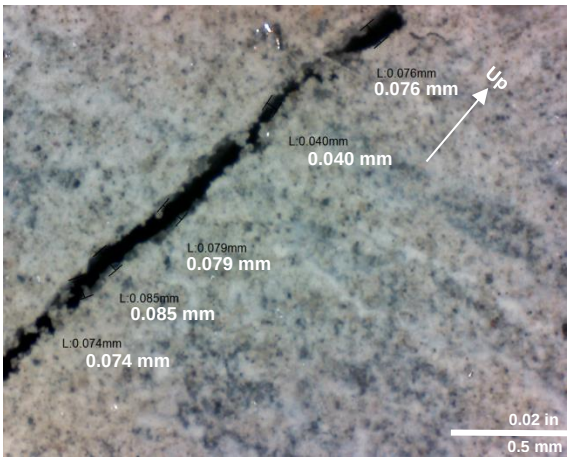

Figure 5-5. The resulting fracture under a microscope (200x magnification) for Test #3 showing the fracture widths ranging between 40 – 85 microns

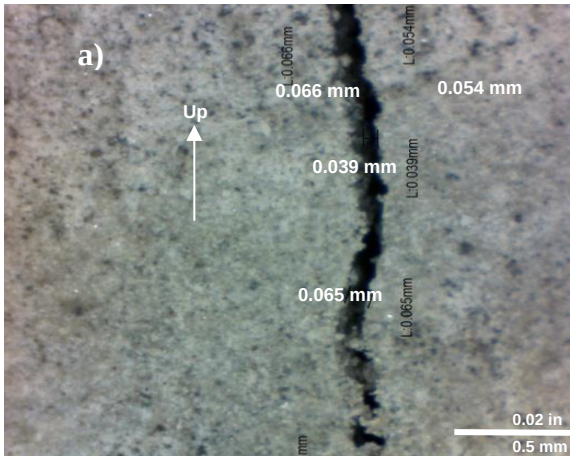

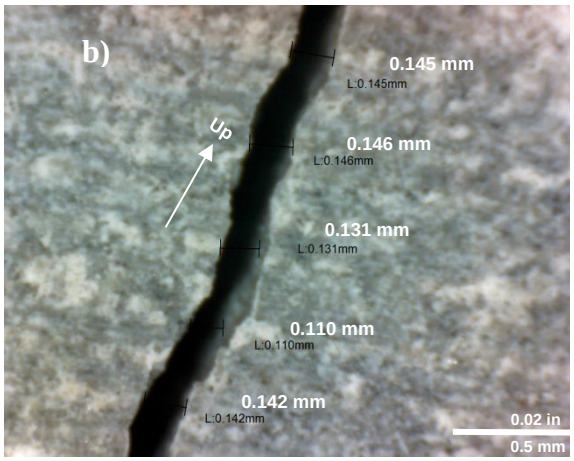

Figure 5-6. The resulting fracture under a microscope (200x magnification) for Test #4 showing the fracture widths ranging between 40 – 145 microns

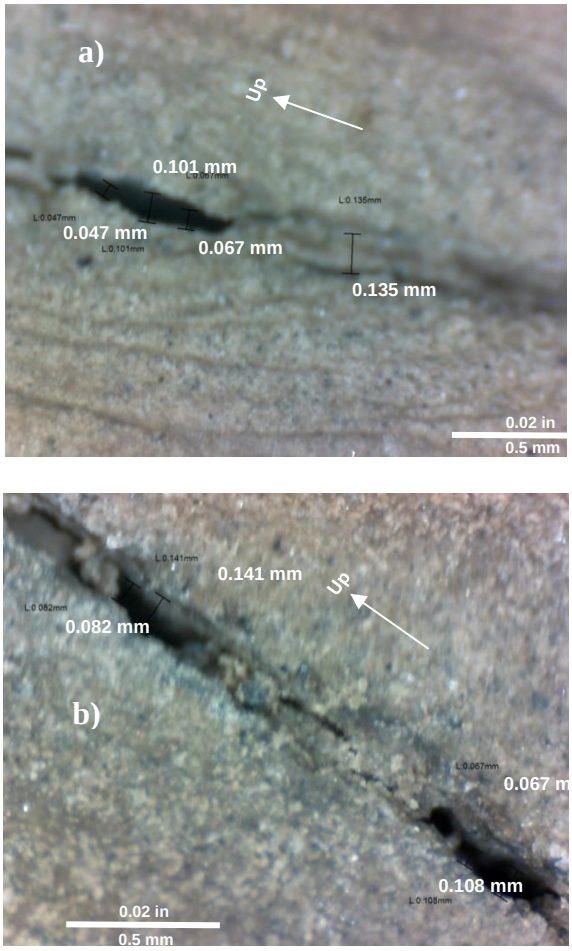

Figure 5-7. The resulting fracture under a microscope (200x magnification) for Test # 5 showing fracture widths ranging between 50 – 140 microns

The mechanical properties of concrete samples and hydraulic fracturing results (Table 3-1) were used to estimate the fracture width using the five analytical fracture models (Table 5-2). According to the results of analytical fracture models (Table 5-2), the highest size of the fracture width was estimated by Alberty and McLean's model. Wang et al.'s model estimated the lowest fracture width for all tests with significant difference in results from other models (Table 5-2). Morita and Fuh's model estimated a constant fracture for all tests (Table 5-2), since the pressure along the fracture was assumed to be negligible due to perfect sealing of fracture mouth by LCM plug. The estimated fracture

width by Carbonell and Detournay's model is in the middle range of results for all models (Table 5-2). Comparing the measured fracture width of core samples under a microscope with the results of analytical models, Carbonell and Detournay's model estimated a more realistic size of the fracture width (Table 5-2). The estimated fracture width from the analytical models increased as the wellbore pressure (breakdown pressure) increased (Table 5-1). The estimated D10, D25, D50, D75, and D90 values from particle size distribution (PSD) analysis are presented in Table 5-3. The particle size analysis of barite is reported in Tehrani et al. [20]. Based on PSD analysis, the LCM blend of graphite (G) and nutshells (NS) has the highest size of all D10, D25, D50, D75, and D90 parameters (Table 5-3). An LCM blend containing graphite (G) and sized calcium carbonate (SCC) has the lowest particle sizes (Table 5-4) and yet resulted in the highest breakdown pressure (Table 5-1). Based on the measured fracture width from the optical microscope for the tests using the pre-mixed OBM that contained LCM with the PSD analysis of the tested blends, the fracture widths were within the range of the D10 and D25 of particle sizes (Table 5-3).

Table 5-3. Comparison of PSD with the estimated fracture width using two methods

Test #	Particle Size Distribution (microns)			Estimated Fracture Width Using Analytical Model (Micron)					Estimated Fracture Width Using Microscopic Image (Micron)
	D10	D50	D90	Wang et al.	Hillerborg et al.	Morita and Fuh	Carbonell and Detournay	Alberty and McLean	
1				0.082	2.5	20	22.9	145	15 - 22
2	3	21	64	0.2	7.6	20	29.5	368	27 - 36
3	65	500	1900	0.21	8.1	20	30.5	404	40 - 85
4	80	460	1300	0.21	8.5	20	31.3	424	40- 145
5	55	450	1200	0.23	8.8	20	31.7	437	50 - 140

Table 5-4. PSD analysis results using dry sieve analysis

Particle Size Distribution (microns)						
LCM Blend	Concentration (ppb)	D10	D25	D50	D75	D90
G&NS	20	65	180	500	1300	1900
G & SCC	30	80	100	460	900	1300
G, SCC, & CF	55	55	100	450	850	1200

6. CONCLUSIONS

In this paper, the effect of LCM in enhancing the fracture breakdown and re-opening pressures was investigated. The five analytical fracture models were studied and compared, and a sensitivity analysis of the input parameters on the result of the estimated fracture width was conducted. The experimental results and the mechanical properties of concrete cores were used to estimate the fracture width from different analytical models, and the results were compared with the measured fracture width from the optical microscope. According to the findings of this paper, the addition of different LCM blends enhanced the breakdown and re-opening pressures up to 18% and 210%, respectively, compared to the control sample that contained no LCM. The cores fractured with fluid-containing solids had a larger fracture size compared to the fractured core using the base fluid. Morita and Fuh's model estimated a constant fracture width for all cases, which is smaller than the measured size of fractures for tests with fluid-containing solids. The estimated fracture widths by Wang et al.'s and Hillerborg et al.'s models are smaller compared to the measured fracture widths. Larger fracture widths were predicted by Alberty and McLean's model. Carbonell and Detournay's model estimated comparable fracture widths to the measured widths on the fractured cores, indicating that this analytical fracture model reflects more realistic fracture width behavior.

REFERENCES

[1] Fuh GH, Morita N, Byod PA, McGoffin SJ. A New Approach to Preventing Lost Circulation While Drilling. In: Proceedings of the SPE Annual Technical Conference and Exhibition, Washington DC, USA, October 4-7, 1992. SPE-157032.

[2] Alberty MW, McLean MR. A Physical Model for Stress Cages. In: Proceedings of the SPE Annual Technical Conference and Exhibition, Houston, Texas, September 26-29, 2004. SPE-90493.

[3] Tehrani A, Friedheim J, Cameron J, Reid B. Designing Fluids for Wellbore Strengthening – Is It an Art? In: Proceedings of the AADE National Technical Conference and Exhibition, Houston, Texas, April 10-12, 2007. AADE-07-NTCE-75.

[4] Van Oort E, Friedheim J, Pierce T, Lee J. Avoiding Losses in Depleted and Weak Zones by Constantly Strengthening Wellbores. Journal of Drilling & Completion 2011; 26(4): 519–530.

[5] Morita N, Black AD, Fuh GF. Borehole Breakdown Pressure with Drilling Fluids I. Empirical Results. Int J of Rock Mech Min Sci 1996; 33(1): 39–51.

[6] Morita N, Black AD, Fuh GF. Borehole Breakdown Pressure with Drilling Fluids II. Semi-analytical Solution to Predict Borehole Breakdown Pressure. Int J of Rock Mech Min Sci 1996; 33(1): 53–69.

[7] Morita N, Fuh GF. Parametric Analysis of Wellbore-Strengthening Methods from Basic Rock Mechanics. SPE Drill & Complet 2012; 27(2): 315-327.

[8] Deeg WFJ, Wang H. Changing Borehole Geometry and Lost-Circulation Control. In: Proceedings of the 6th North America Rock Mechanics Symposium, Houston, Texas, June 5-9, 2004.

[9] Wang H, Sweatman R, Engelman B, Deeg W, Whitfill D, Soliman M, Towler BF. Best Practice in Understanding and Managing Lost Circulation Challenges. SPE Drill & Complet 2008; 23(2): 168-175.

[10] Guo Q, Feng YZ, Jin ZH. Fracture Aperture for Wellbore Strengthening Applications. In: Proceedings of the 45th US Rock Mechanics / Geomechanics Symposium, San Francisco, CA, June 26-29, 2011.

[11] Shahri MP, Trevor TO, Safari R, Karimi M, Mutlu O. Advanced Semianalytical Geomechanical Model for Wellbore-Strengthening Applications. SPE Drill & Complet 2015. SPE-167976.

[12] Carbonell RJK, Detournay, EJK. Modeling Fracture Initiation and Propagation from a Pressurized Hole: A Dislocation-Based Approach. In: Proceedings of the 35th U.S. Symposium on Rock Mechanics (USRMS), Reno, Nevada, June 5-7, 1995.

[13] Hillerborg A, Modeer M, Petersson PE. 1976. Analysis of crack formation and crack growth in concrete by means of fracture mechanics and finite elements. Division of Building Materials Lund Institute of Technology, Lund, vol. 6. Pergamon, Sweden, pp. 773– 782.

[14] Warren WE. The quasi-static stress field around a fractured wellbore. Int J of Fracture 1982; 18(2): 113–124.

[15] Erdogan F, Gupta GD. 1972. On the Numerical Solution of Singular Integral Equations. Quarterly of Applied Mathematics 1972; 29: 525–534.

[16] Tada H, Paris PC, Irwin GR. The Stress Analysis of Cracks Handbook. 3d ed. Wiley publication; 2000.

[17] Hettema M, Horsrud P, Taugbol K, Friedheim J, Huynh H, Sanders MW, Young S. Development of an Innovative High-Pressure Testing Device for the Evaluation of Drilling Fluid Systems and Drilling Fluid Additives within Fractured Permeable Zones. In: Proceedings of the Offshore Mediterranean Conference and Exhibition, Ravenna, Italy, March 28-30, 2007.

[18] Aston MS, Alberty MW, McLean MR, Jong HJD, Armagost K. Drilling Fluid for Wellbore Strengthening. In: Proceedings of the IADC/SPE Conference, Dallas, Texas, March 2-4, 2004. SPE-87130-MS.

[19] Kumar A, Savari S, Jamison DE, Whitfill DL. Application of Fiber Laden Pill for Controlling Lost Circulation in Natural Fractures. In: Proceedings of the AADE National Technical Conference and Exhibition, Houston, Texas, April 12-14, 2011.

[20] Tehrani A, Cliffe Angleika, Hodder MH, Young S, Lee J, Stark J, Seale S. Alternative Drilling Fluid Weighting Agents: A Comprehensive Study on Ilmenite and Hematite. In: Proceedings of the IADC/SPE Conference, Dallas, Texas, March 4-6, 2014. SPE-167937-MS.

[21] Rahimi R, Alsaba M, Nygaard R. Can Particle Size Distribution of Lost Circulation Materials Affect the Fracture Gradient?. In: Proceedings of the AADE National Fluid Conference and Exhibition, Houston, Texas, April 12-13, 2016.

IV. CAN PARTICLE SIZE DISTRIBUTION OF LOST CIRCULATION MATERIALS AFFECT THE FRACTURE GRADIENT?

Reza Rahimi, Mortadha Alsaba, and Runar Nygaard

Department of Geosciences and Geological and Petroleum Engineering,

Missouri University of Science and Technology, Rolla, MO, United States

ABSTRACT

The purpose of preventive treatment of fluid losses, i.e. wellbore strengthening, is to deliberately enhance the fracture gradient by creating and curing fractures while drilling. The effectiveness of such treatments can be affected by the lost circulation material (LCM) type, size distribution, and the fracture width. This paper investigates if the particle size distribution of preventive LCMs can change the breakdown or re-opening pressure. Hydraulic fracturing experiments were performed on concrete cores as a proxy for impermeable rocks with a low-toxicity oil-based fluid and LCM blends with different particle size distributions. Two injection cycles were performed to measure the breakdown and fracture re-opening pressures. Microscopic analysis of the fractured cores was performed to estimate the fracture width. The fracture pressure and re-opening pressure were greatly increased by including LCMs in the fluid compared to the basic drilling fluid. The experimental results indicate that selecting fluids with LCM of certain range will enhance the fracture gradient and widen the available drilling fluid window.

1. INTRODUCTION

Lost circulation events, defined as the loss of drilling fluids into the formation, are challenging problems to prevent or mitigate while drilling [1]. Losses can occur when drilling through natural fractures, or into drilling induced fractures initiated when the drilling fluid pressure exceeds the formation breakdown pressure. Preventive lost circulation material (LCM) treatments can be used to cure losses on natural fractures before lost circulation occur or increase the breakdown pressure before drilling induced fracture is created. This preventive method will effectively widen the fluid weight window or in other words, enhance the fracture gradient. Experimental LCM performance studies have focused on reducing fluid loss [2] or increase fracture sealing pressure (i.e. fracture re-opening pressure) [3–7]. Fluid loss reduction is studied in high pressure high temperature (HPHT) filter press and plug particle apparatus (PPA) tests2. Creating a seal in fractures causing an increased sealing pressure has been experimentally studied on both permeable and impermeable fractures [3, 4, 6]. A broader distribution of particle sizes was recommended by [3] to get better fracture sealing efficiency (i.e. increased re-opening pressure) of drilling induced or natural fractures based on the results of permeable fracture test. Proposed procedure for wellbore strengthening fluid design by [4] focused on importance of particle sizes in bridging fracture aperture. According to [6], smaller sized particles and narrow particle size distribution (well sorted) gives a better fracture sealing efficiency. The results of the impermeable fracture tests showed that the particle size distribution should be a function of the type of formation to be strengthened. Using of slotted discs with different fracture aperture and fracture tip was one of the other methods used to evaluate LCM performance 8. Based on the results of different LCM blends

evaluation using a high pressure LCM testing apparatus, [8] observed that blends with a wide range of particle sizes exhibited the lowest fluid loss. Large scale fracturing experiments suggested large and uniform particle size of LCMs for a better sealing efficiency [9, 10]. Based on fracturing experiments, [11] concluded that coarser particles should be used for bridging the fracture mouth while smaller particles should prevent fluid loss through the bridge. According to fracturing experiment on shale cores using a block test set up with 5 in. rock cubes, [12] suggested particle size distribution and size of lost circulation materials should be selected based on fracture aperture. There are other studies which theoretically investigated the effect of LCM particle sizes [13-15]. The importance of the particle size distribution in improving sealing efficiency was emphasized by [13] without specifically addressing how to select the size distribution. According to [14], LCM particle sizes are relatively unimportant since any pill will develop into an immobile mass but particle sizes smaller than 100 microns should be used to block pore throats to stop matrix seepage and not as a LCM for minimizing fluid losses. [15] indicated that the design of particle sizes in wellbore strengthening pills is a function of fracture width while the effect of shearing at the bit face on particle size degradation should be considered.

The results from [3-15] show that particle size distribution is a critical parameter to effectively seal fracture either shown as reduced fluid losses, increased fracture breakdown or re-opening pressure. However, there are still limited published results on how particle size distribution could affect the performance of different LCM's. The majority of tests conducted have been with slotted/tapered discs, which do not simulate the process of inducing and propagation of fractures while drilling. The previous hydraulic fracturing experiments shows adding LCM increases the fracture gradient but no agreement has been

achieved on how LCM strength, particle size, and size distribution affect the fracture sealing efficiency (i.e. strengthening).

The main objective of this paper is to investigate the effect of particle size distribution of conventional LCMs in enhancing the fracture gradient (fracture breakdown and re-opening pressure). Hydraulic fracturing experiments were carried out on concrete cores as a proxy for non-permeable rocks using low toxicity oil based fluid and LCM mixtures. These experiments were used a) to investigate the strengthening effect as a result of adding LCM to an oil based fluid, b) to investigate the effect of LCM particle sizes on enhancing fracture gradient (breakdown and re-opening pressure) c) find a relation between the particle sizes, the fracture size and the wellbore pressure.

2. EXPERIMENTAL PROCEDURE

Hydraulic fracturing experiments were performed on nine concrete cores using nine different oil based drilling fluid formulations. Figure 2-1 shows a schematic drawing of the hydraulic fracturing apparatus. Two pumps are used to apply confining and injection pressure, while a hydraulic hand pump is used to apply overburden stress on the core sample. A metal accumulator was used to inject fluids into the core. Injection pressures was recorded using LabVIEW© software. Cement core samples were prepared using Portland cement (Class H) to simulate impermeable formations. Class H cement was mixed with API recommended water requirements of 38% by weight of cement in a large batch following the standard mixing procedures to ensure the same physical properties of the fractured cores. The cement mixture was poured into 5 7/8 inch (diameter) x 9 inch (height) molds and left to cure for at least 7 days. A ½ inch wellbore was drilled in the cement cores using a drill press, and then a steel cap were attached to the top and bottom of the cement cores using epoxy. The first test was conducted using EDC95-11 solid free clear base fluid used to prepare the pre-mixed drilling fluid. The second test was conducted with the pre-mixed oil based drilling fluid without LCM to serve as a control sample. Tests # 3, 4, and 5 were conducted using the oil based fluid mixed with 3 different LCM mixtures. The LCM mixtures were based on recommendations of previously published research. 20 ppb graphite and nutshells blend (G & NS) was used for test # 3 as suggested by [3]. 30 ppb graphite and sized calcium carbonate blend was investigated in test # 4 to follow the recommendations by [16]. 55 ppb graphite, sized calcium carbonate, and cellulosic fibers blend was used in test # 5 as recommended by [17]. Tests #6 to 9 were conducted using Graphite with different D50 of particle size distribution, 50, 100, 400, and 1000 microns

respectively. A confining pressure of 100 psi and an overburden pressure of 400 psi were applied. An Injection rate of 5 ml/min was used to pressurize the wellbore until reaching the breakdown pressure where an increase in the confining pressure is observed due to fluid pushing against the rubber sleeve. The injection is stopped to allow for 10 minutes period before running the re-opening cycle. The test is stopped after the second cycle when an increase in the confining pressure is observed; indicating that the fluid has already propagated through the fracture. The retrieved fractured cores from the fracturing apparatus were examined under optical microscopy and fracture opening was measured perpendicular to the fracture side at several locations to estimate the range of fracture widths observed.

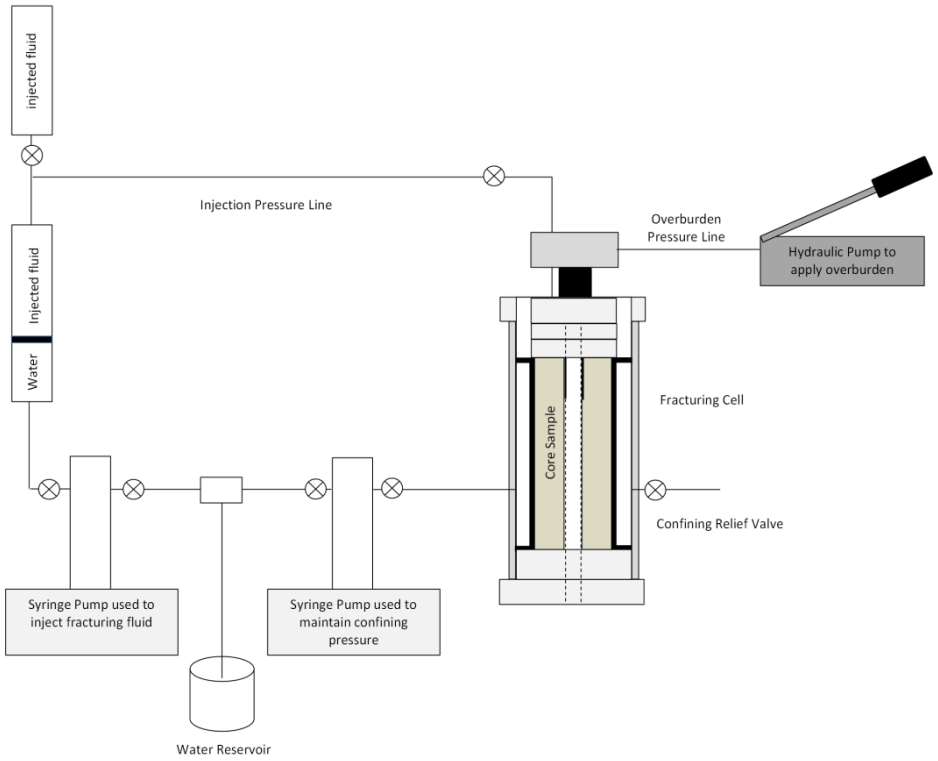

Figure 2-1. Schematic of the hydraulic fracturing apparatus

3. RESULTS

Figure 3-1 shows the cross section of a concrete core for one of the test after the hydraulic fracturing experiment, a symmetric and bi-wing fracture created around the wellbore. Figure 3-2 shows micrographs of the actual fractures and the measured fracture width of the concrete cores for all tests. Figures 3-3 to 3-11 are the pressure versus time results from the hydraulic fracturing experiments. The blue line represents the first injection cycle, which is used to estimate the breakdown pressure. The red line represents the second injection cycle, which is used to estimate the re-opening pressure (after the 10 minutes fracture healing period). The peak pressure at first cycle shows the breakdown pressure and the peak pressure of the second cycle shows the fracture re-opening pressure.

Figure 3-1. Symmetric and bi-wing fracture created around the wellbore for Test #7

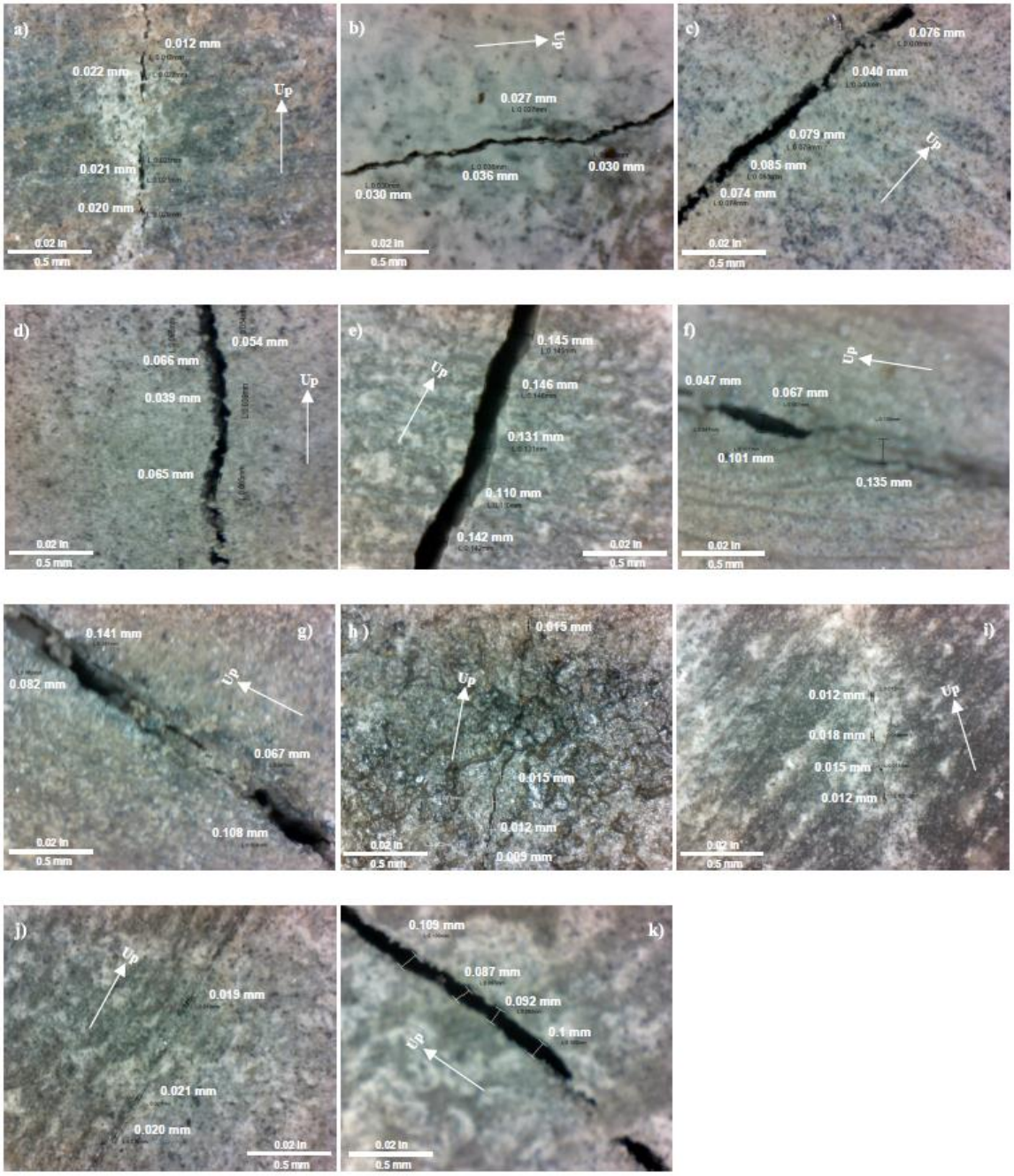

Figure 3-2. The fracture width for: a) Test #1 (15 – 22 microns),
b) Test #2 (27 – 36 microns), c) Test #3 (40 – 85 microns),
d) & e) Test #4 (40 – 145 microns), f) & g) Test #5 (50 – 145 microns),
h) Test #6 (9 – 15 microns), i) Test #7 (12 – 18 microns)
j) Test #8 (19 – 21 microns), k) Test #9 (92 – 109 microns)

The lowest breakdown and re-opening pressures (843 and 571 psi) were observed for the first test (Figure 3-3), which was conducted using EDC95-11 base fluid. The small size of fracture (15 to 22 microns) from microscopy image (Figure 3-2.a) could be because of using clear fluid without solid content.

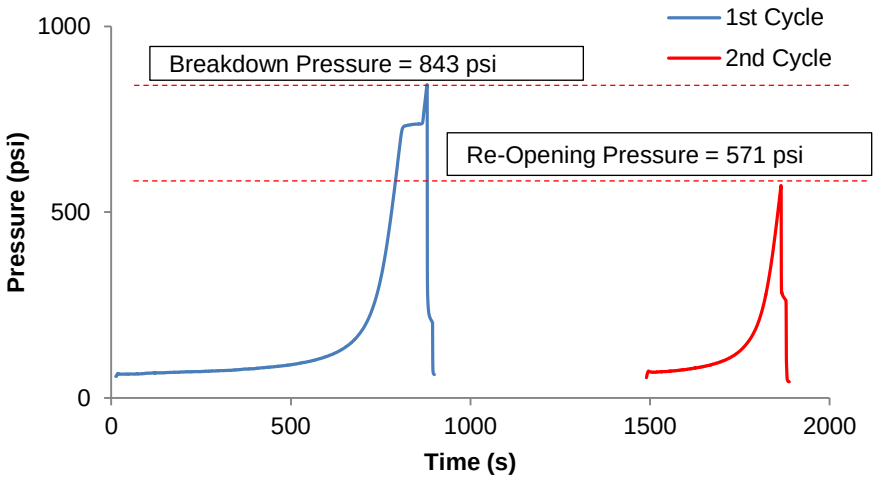

Figure 3-3. Pressure vs. Time for Test # 1

The results of the second test (Figure 3-4) with the pre-mixed OBM containing barite particles shows significant increase in breakdown pressure (From 843 psi to 2008 psi) compared to the results of the first test (Figure 3-3), however there is small difference between the fracture re-opening pressure for both test (Figures 3-3 &3-4). The measured range of fracture width for the second test (Figure 3-2.b) (27 to 36 microns) is higher compared to the first test using the solid free fluid. Adding LCM blend of G &NS in test #3 increased the fracture re-opening about 125% (Figure 3-5) (From 592 psi to 1334 psi) compared to the results of test #2 with no LCM. Increasing of the breakdown pressure in test #3 (Figure 3-5) (From 2008 psi to 2199 psi) compared to the results of test #2 is not notable as the fracture re-opening pressure. The measured range of fracture width in Figure

3-1.c (40 to 85 microns) shows broader range of measured fracture widths compared to the results test #1 and test #2 (Figures 3-2.a & 3-2.b).

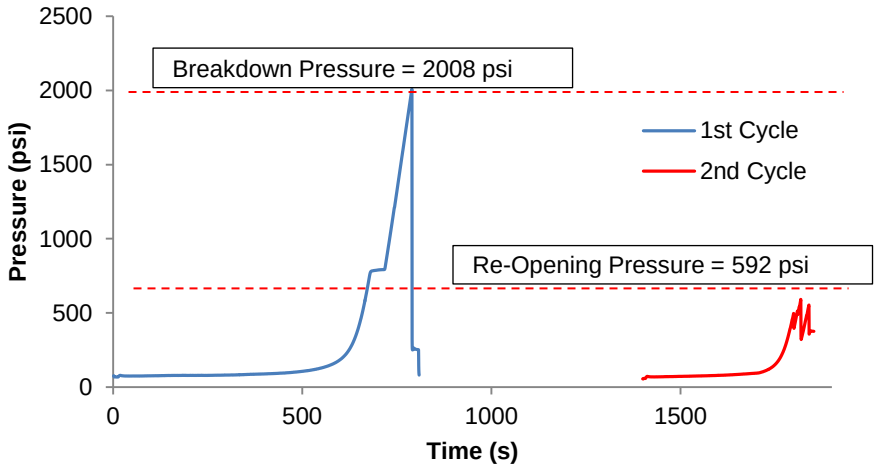

Figure 3-4. Pressure vs. Time for Test # 2

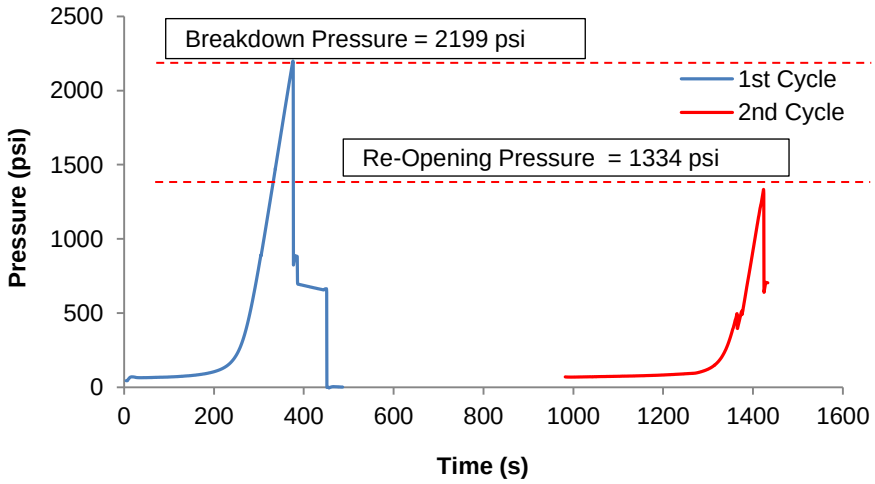

Figure 3-5. Pressure vs. Time for Test # 3

Replacing NS in LCM blend of test #4 with SCC and increasing concentration of LCM from 20 ppb to 30 ppb increased both the breakdown and the fracture re-opening pressure (Figure 3-6). Comparing the results of test #3 with the test #4, the fracture re-

opening was increased form 1334 psi to 1834 psi. The increase of breakdown pressure is not remarkable as fracture re-opening pressure (Figures 3-2.d & 3-2.e) (From 2199 psi to 2309 psi).

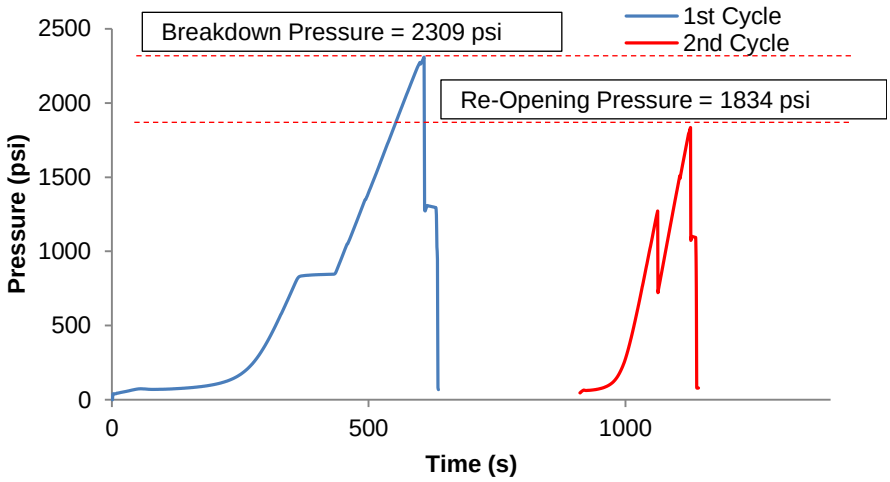

Figure 3-6. Pressure vs. Time for Test # 4

Test # 5 containing 55 ppb graphite, sized calcium carbonate, and cellulosic fiber resulted in highest breakdown pressure (2372 psi) (Figure 3-7) compared to the previous tests. However, the fracture re-opening pressure (1717 psi) is lower than the LCM blend used in test # 4. The range of the measured fracture width (Figure 3-2.f & 3-2.g) (50 to 145 microns) for test #5 is broader than previous tests (Figures 3-2.a to 3-2.e).

Second set of tests (Tests #6 to 9) were conducted with a single LCM (Graphite) with different particle sizes range. Using the same premixed OBM, Graphite with D50 values of 50, 100, 400, and 1000 microns were used. According to the results of the second set of tests, increasing the D50 value of LCM (Graphite) particle size distribution from 50 microns to 100 microns increased both breakdown (From 2085 psi to 2725 psi) and fracture re-opening pressure (From 840 psi to 1292 psi) (Figures 3-8 &3-9). The wider fracture

width (12 to 15 microns) was observed for test #7 (Figure 3-1.i) compared to the measured fracture width (9 to 12 microns) of test #6 (Figure 3-2.h). Increasing the D50 of the Graphite (test# 8 and 9) resulted in a lower breakdown and fracture re-opening pressure (Figures 3-10 and 3-11) compared to test #7 (Figure 3-9).

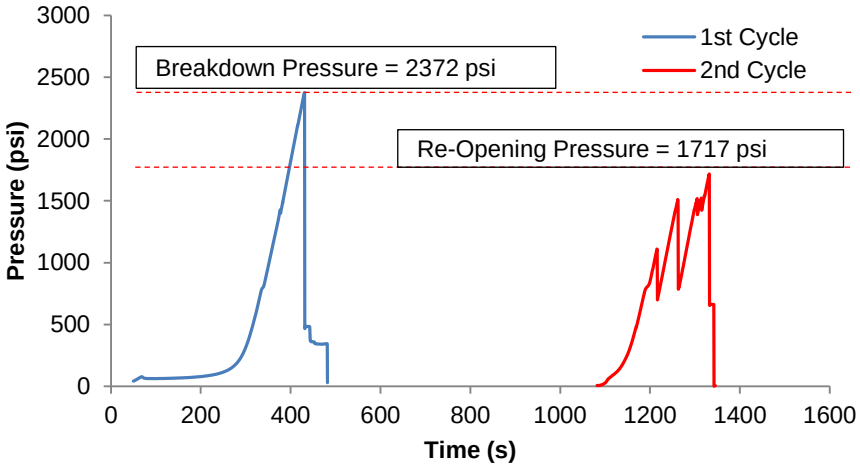

Figure 3-7. Pressure vs. Time for Test # 5

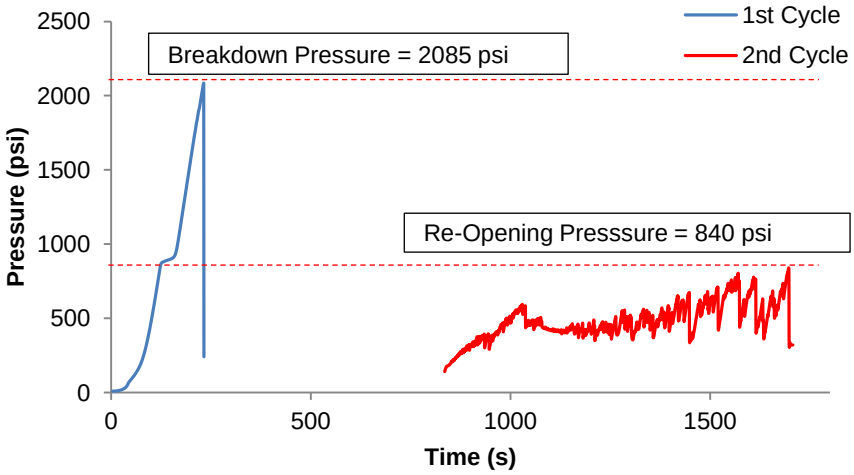

Figure 3-8. Pressure vs. Time for Test # 6 (D50: 50 microns)

For test #8 with D50 of 400 microns for Graphite particle sizes, the breakdown pressure (2004 psi) (Figure 3-10) is lower than the results of test #7 (2725 psi) with D50 of 100 microns for Graphite particle sizes. In the same situation, the fracture re-opening pressure for test #8 (1216 psi) (Figure 3-10) is lower than the fracture re-opening pressure for test #7 (1292 psi), but this difference is not significant breakdown pressure. The measured fracture width for test #7 (12 to 15 microns) (Figure 3-2.i) with D50 of 100 microns for Graphite particle sizes is lower than the measured fracture width for test #8 (19 to 21 microns) (Figure 3-2.j). Test #9 was conducted using larger particle sizes of Graphite with D50 of 1000 microns. The recorded breakdown pressure for test #9 (2415 psi) (Figure 3-11) is less than the results of test #7 (Figure 3-9) but higher than test #8 (Figure 3-10), however the fracture re-opening pressure for test #9 (1020 psi) (Figure 3-11) is lower than the fracture re-opening pressure for test # 7 &8 (Figures 3-9 & 3-10). The measured range of fracture width for test #9 (92 to 109 microns) (Figure 3-2.k) is higher than the measured fracture width for tests #6, 7, and 8 (Figures 3-2.h, 3-2.i, & 3-2.j).

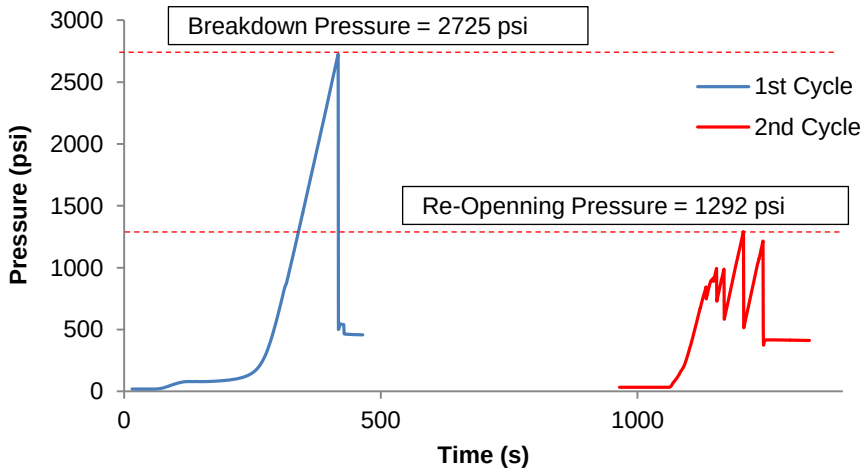

Figure 3-9. Pressure vs. Time for Test # 7 (D50: 100 microns)

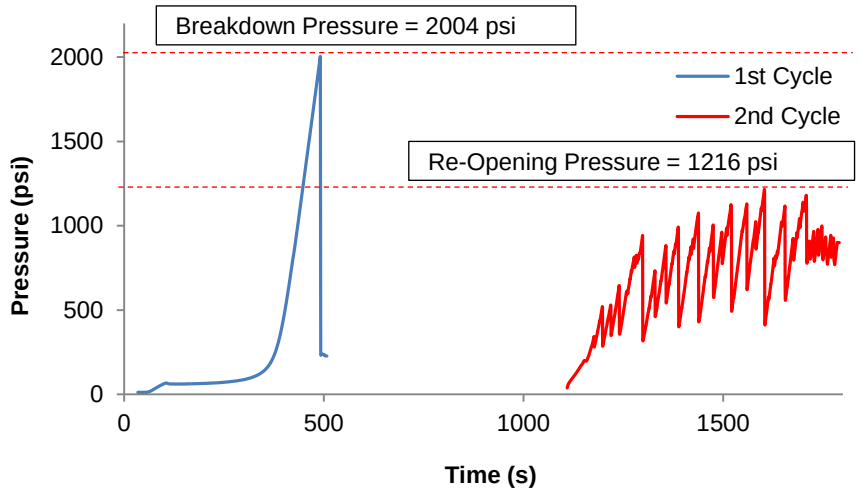

Figure 3-10. Pressure vs. Time for Test # 8 (D50: 400 microns)

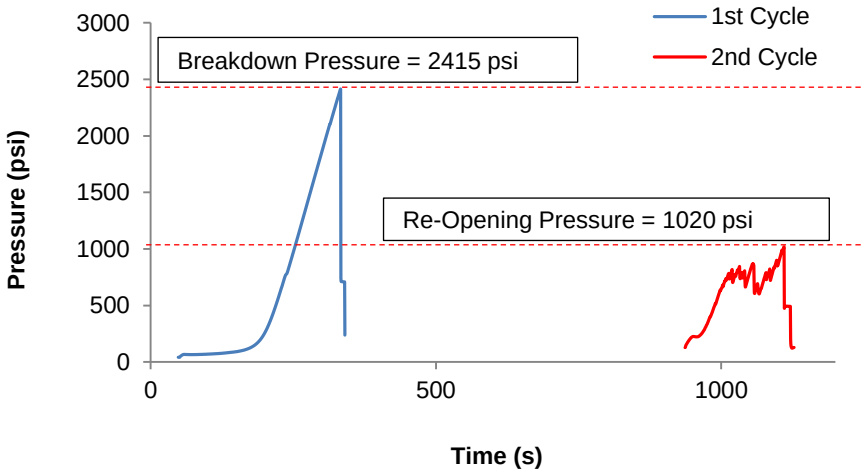

Figure 3-11. Pressure vs. Time for Test # 9 (D50: 1000 microns)

4. DISCUSSIONS

Analysis of the results from the first set of tests (#1 to 5) (Table 4-1) showed that including LCM blend in fluid (Test #3, 4, &5) can enhance both breakdown and fracture re-opening pressure compared to solid free fluid (test #1) and also pre-mixed OBM (test #2) which only contained barite as weighting agent. The blend of G & SCC LCMs resulted in the highest fracture reopening pressure (1834 psi), while the highest breakdown pressure was observed with G, SCC, and CF blend of LCMs (Table 4-1). There is a significant difference in breakdown pressure of test #1 &2 but the fracture re-opening pressure is almost the same (Table 4-1). The barite particles containing in the fluid of test #2 are able to block pore throats on the borehole wall which resulted in an increase in the breakdown pressure, however the small sizes of barite particles (Table 4-1) are not able of bridging the fracture aperture. The highest breakdown pressure resulted from the blend of G, SCC, &CF could be due to the same reason (Table 4-1). The blend of G, SCC, & CF in test #5 has smaller particle sizes compared to the LCM blends of test #3 &4, especially smaller range of particles (Table 4-3).

Table 4-1. Summary of results for tests 1 to 5

Test #	Fluid Used	LCM Blend	Conc (ppb)	Breakdown Pressure (psi)	Re-Opening Pressure (psi)
1	EDC95-11	N/A	N/A	843	571
2	VERSATEC OBM	N/A	N/A	2008	592
3	VERSATEC OBM	G&NS	20	2199	1334
4	VERSATEC OBM	G & SCC	30	2309	1834
5	VERSATEC OBM	G, SCC, & CF	55	2375	1717

These smaller particles could block pore throats and create a sealing that result in higher breakdown pressure (Table 4-1), however enhancing fracture re-opening pressure is a function of bridging the fracture aperture and also filling the fracture itself. Thus, broader range of particle sizes is required to reach higher fracture re-opening pressure. The second set of the tests (#6 to 9) was conducted using a single LCM with same concentration to specifically investigate how LCM particle sizes can enhance fracture gradient. Test #7 with D50 of 100 microns of Graphite particle size distribution resulted in the highest breakdown pressure among all other tests (Tables 4-1 & 4-2) and also the highest fracture re-opening pressure among the second set of experiments (Table 4-2). Considering D10 of 25 microns and D90 of 210 microns (Table 4-3), LCM particles of test #7 were capable of blocking the pore throats, which increased the breakdown pressure and also the fracture aperture was sealed resulting in a higher fracture re-opening pressure (Table 4-2). The fine Graphite particle sizes, D50 of 50 microns, of test # 6 (Table 4-3) were not able to bridge the fracture aperture, causing the fracture re-opening pressure to be the lowest among the second set of tests (Table 4-2).

Table 4-2. Summary of results for tests #6 to 9

Test #	Fluid Used	LCM	D50 (microns)	Conc (ppb)	Breakdown Pressure (psi)	Re-Opening Pressure (psi)
6	VERSATEC OBM	G	50	30	2080	840
7	VERSATEC OBM	G	100	30	2725	1292
8	VERSATEC OBM	G	400	30	2004	1216
9	VERSATEC OBM	G	1000	30	2415	1020

The particle sizes of test #8 have a broader range compared to test #6 &7 (Table 4-3). The fracture re-opening from test #8 is not as high as the fracture re-opening in test #7 but much higher than test #6. Although the fracture aperture was bridged, the barrier was not strong enough as the particles barrier created in the test #7. This might be due to the lack of the presence of the finer particles as used in test #7. The particle sizes of test #9 are even broader than the test #9 (D50 of 1000 microns (Table 4-3)), the fracture re-opening pressure in this case is lower than the results of test #7 &8 since particles are not capable of bridging the fracture aperture and create a fluid barrier as particles in test #7 or 8 (Table 4-2).

Table 4-3. LCMs particle size distributions

Particle Size Distribution (microns)				
Test #	LCM Blend	D10	D50	D90
2	Barite	3	21	64
3	G&NS	65	500	1900
4	G & SCC	80	460	1300
5	G, SCC, & CF	55	450	1200
6	G (50)	25	50	130
7	G (100)	35	100	210
8	G (400)	250	400	1000
9	G (1000)	300	1000	1700

The experimental analysis verified the importance of the particle sizes despite the conclusion of [14], which believed particle sizes are unimportant. Also, coarser particles and broader size distribution of LCMs recommended by [3] and [10] would not result in

the highest sealing efficiency of the fracture, according to the results of this paper. Moreover, designing the LCM particle sizes to only bridge the fracture aperture as suggested by [4] and [12] do not cause high fracture sealing efficiency. Furthermore, small range of particle sizes [6] cannot effectively bridge the fracture aperture, so enhancement of fracture re-opening pressure would not be significant. Based on the results of this study, range of particle sizes which could effectively bridge the fracture aperture and also create a strong and impermeable seals within the fracture would result in the highest sealing efficiency, which agrees with [11] findings.

5. CONCLUSIONS

Two sets of hydraulic fracturing experiments were conducted with an oil based drilling fluid containing either a blend of LCMs or a single LCM with different particle size distributions. The results verified the effect of lost circulation material in enhancing fracture gradient of fracture wellbores however; the particle size distribution of lost circulation material has a significant effect on the sealing efficiency of fractured wellbores and also enhancing the breakdown pressure of intact wellbores. Smaller range of fine particles (<100 microns) were capable of blocking the pore throats and increasing the breakdown pressure; however they cannot create a strong barrier for enhancing the fracture re-opening pressure. Broad range of coarse particle sizes, in order of hundreds to thousands of microns, could bridge fracture aperture but the barrier would not be as strong toward fluid pressure. LCMs with particle sizes range of few hundred microns were capable of bridging the fracture aperture and creating a strong seal to enhance fracture re-opening pressure significantly. The measured range of fracture width increased by increasing the particle size distribution.

REFERENCES

[1] Messenger, J. U., and McNiel, J. S. "Lost Circulation Corrective: Time-Setting Clay Cement". Journal of Petroleum Technology, Vol. 4 (3), (1952) pp. 59-64.

[2] Savari, S., Kumar, A., Whitfill, D. L., Miller, M., Murphy, R. J., and Dale E. Jamison. "Engineered LCM Design Yields Novel Activating Material for Potential Application in Severe Lost Circulation Scenarios." SPE-164748-MS, SPE North Africa Technical Conference and Exhibition, Cairo, Egypt, April 15-17, 2013.

[3] Hettema, M., Horsrud, P., Taugbol, K., Friedheim, J., Huynh, H., Sanders, M. W., and Young, S. "Development of an Innovative High-Pressure Testing Device for the Evaluation of Drilling Fluid Systems and Drilling Fluid Additives within Fractured Permeable Zones." OMC-2007-082, Offshore Mediterranean Conference and Exhibition, Ravenna, Italy, March 28-30, 2007.

[4] Tehrani, A., Friedheim, J., Cameron, J., and Reid, B. "Designing Fluids for Wellbore Strengthening – Is It an Art?" AADE-07-NTCE-75, AADE National Technical Conference and Exhibition, Houston, Texas, USA, April 10-12, 2007.

[5] Kaageson-Loe, N. M., Sanders, M. W., Growcock, F., Taugbol, K., Horsrud, P., Singelstad, A. V., and Omland, T. H. "Particulate-Based Loss-Prevention Material - The Secrets of Fracture Sealing Revealed!". SPE Drilling & Completion, Vol. 24(4), (2009) pp. 581-589.

[6] Van Oort, E., Friedheim, J., Pierce, T., and Lee, J. "Avoiding Losses in Depleted and Weak Zones by Constantly Strengthening Wellbores." SPE Drilling & Completion, Vol. 26 (4), (2011) pp. 519-530.

[7] Mostafavi, V., Hareland, G., Belayneh, M. and Aadnoy, B. S. "Experimental and Mechanistic Modeling of Fracture Sealing Resistance with Respect to Fluid and Fracture Properties." ARMA 11-98, the 45th US Rock Mechanics Symposium, San Francisco, USA, June 26-29, 2011.

[8] Alsaba, M.T., Nygaard, R., Saasen, A., and Nes, O.M. "Lost Circulation Materials Capability of Sealing Wide Fractures." SPE-170285-MS, SPE Deepwater Drilling and Completions Conference, Galveston, Texas, USA, September 10-11, 2014.

[9] Morita N., Black A., and Fuh G.F. "Theory of Lost Circulation Pressure." SPE-20409-MS, SPE Annual Technical Conference and Exhibition, New Orleans, Louisiana, USA, September 23-26, 1990.

[10] Fuh, G. F., Morita, N., Byod, P. A., and McGoffin, S. J. "A New Approach to Preventing Lost Circulation While Drilling." SPE-24599-MS, SPE Annual Technical Conference and Exhibition, Washington D.C., USA, October 4-7, 1992.

[11] Aadnoy, B. S. and Belayneh, M. “Elasto-Plastic Fracturing Model for Wellbore Stability Using Non-Penetrating Fluids.” Journal of Petroleum Science and Engineering, Vol. 45 (3), (2004) pp. 179-192.

[12] Guo, Q., Cook, J., Ji, L., and Friedheim, J. E. “A Comprehensive Experimental Study on Wellbore Strengthening.” SPE- 167957-MS, ADC/SPE Drilling Conference and Exhibition, Fort Worth, Texas, USA, March 4-6, 2014.

[13] Alberty, M. W. and McLean, M. R. “A Physical Model for Stress Cages.” SPE- 90493-MS, SPE Annual Technical Conference and Exhibition, Houston, USA, September 26-29, 2004.

[14] Dupriest, F. E. “Fracture Closure Stress (FCS) and Lost Returns Practices.” SPE-92192-MS, SPE/IADC Drilling Conference, Amsterdam, Netherlands, February 23-25, 2005.

[15] Salehi, S. and Nygaard, R. “Developing a Full Fluid-Solid Finite-Element Model to Simulate near Wellbore Fractures for Wellbore Strengthening Applications.” ASME Journal of Energy Resources Technology, Vol. 137 (1), (2015).

[16] Aston, M. S., Alberty, M. W., McLean, M. R., Jong, H., and Armagost, K. SPE-87130-MS, “Drilling Fluids for Wellbore Strengthening.”, IADC/SPE Drilling Conference, Dallas, Texas, March 2-4, 2004.

[17] Kumar, A., Savari, S., and Jamison, D. E., and Whitfill, D. 2011. Application of Fiber Laden Pill for Controlling Lost Circulation in Natural Fractures. AADE-11 NTCE-19, AADE National Technical Conference and Exhibition, Houston, Texas, USA, April 12-14, 2011.

V. EXPERIMENTAL EVALUATION ON USING FINE GRAINED COAL COMBUSTION RESIDUALS FOR CONTROLLING FLUID INVASION IN SHALES

Reza Rahimi, Runar Nygaard

Department of Geosciences and Geological and Petroleum Engineering

Missouri University of Science and Technology, Rolla, MO

Geir Hareland

Department of Chemical and Petroleum Engineering

Oklahoma State University, Stillwater, OK

ABSTRACT

Drilling fluid invasion into shales is one reason for instabilities while drilling. Invaded drilling fluid affects near wellbore stresses, rock strength, and overbalance wellbore pressure. The fluid invasion is a coupled-transport phenomena mainly due to hydraulic drive and chemical potential drive. The invaded fluid will increase near wellbore pore pressure and reduce effective stresses, therefore the likelihood of wellbore instabilities arise. The flow of fluid through shales' pores and micro fractures should be mitigated using an effective additives in a water-based drilling fluid system. This paper will experimentally evaluate using of Combusted Carbon Residuals (CCRs) as a shale inhibitor additive. Combusted Carbon Residuals were mechanically grinded. Pressure transient testing was

used to evaluate CCRs in a water-based drilling fluid system for controlling fluid invasion into Catoosa shale samples. Also, two chemically made nano silica, AEROSIL & AERODISP were tested in comparison to fine grained CCRs. The testing results shows the positive impact of using fine grained CCRs in controlling fluid invasion rate compared to the conventional water based drilling fluid and the two other nano products were tested.

1. INTRODUCTION

Time-dependent drilling fluid invasion in shales causes wellbore instabilities [1-7]. Fluid invasion in shales is believed to be a physiochemical process mainly due to hydraulic potential drive and chemical potential drive [6, 8]. The Darcy flow of water is driven by hydraulic potential gradients (pressure imbalance), and diffusion of solutes are driven by chemical potential gradients (chemical imbalance) between the drilling fluid and the shales' pore fluid. Increase of near wellbore pore pressure, reduction of near wellbore rock strength, increase of hydration stress in pore space, and shales swelling or wellbore size shrinkage are the main consequences of shale hydration [3, 9, 10]. Invaded drilling fluid increases pore pressure since shales have a low permeability and cannot dissipate excess pore pressure [1, 2, 6, and 7]. The shale hydration causes differential micro-strains and weakens the cohesive bonds between clay platelets which results in strength reduction [11]. There are different theories that have been developed to describe the shales swelling process, such as hydraulic pressure balance, capillary suction (surface hydration), and osmosis pressure [6, 8, 12]. However, shales swelling phenomena is not well-understood and there is no agreement as to which mechanism is dominant in the shale hydration.

In In order to prevent and control drilling fluid invasion into shales, proper drilling fluid should be designed [3-7]. One of the primary solutions is using oil-based fluid instead of water-based fluid [3-6]. Oil-based fluid acts as a semi-permeable membrane and creates high capillary pressure, so clay hydration would be significantly mitigated compared to water-based fluid [4, 5]. However, oil-based fluids are expensive, have environmental footprints, and can change wettability of reservoirs under overburden shales [13, 14]. An alternative solution for preventing fluid invasion in shales is including different additives

such as salts to water-based drilling fluid systems [3, 15]. The purpose of using additives is to block pore throats and control factors such as ionic exchange, the chemical potential of drilling fluid, and the hydraulic flow of fluid into shales [3, 6]. Effectiveness of these additives depends on shale properties since the chemical potential of shales changes with the chemical composition of the formation [16]. Moreover, ionic concentration is not uniform throughout the pore space and high cationic concentration on the particles would lead to surface charges [8]. Thus, the effectiveness of drilling fluid additives for preventing and controlling swelling pressures will be changed for different shales. Furthermore, drilling fluid additives for controlling clay hydration have advantages and disadvantages; for example, one might decrease osmosis potential but accelerate ionic exchange [9]. Also, isolation of the membrane on the wellbore wall is difficult due to shales' low permeability and low filtration rate. Hydrodynamic forces of the drilling fluid will wear any solid deposition on the wellbore wall. Drilling fluid additives cannot completely prevent swelling in shales; there will always be a residual repulsion between the platelets due to hydration of the clay surfaces and interference between hydrated ions and water molecules [8].

There are different types of experiments to evaluate the effectiveness of drilling fluid additives for controlling shales swelling [19-22]. Shale-fluid interaction could be analyzed in these different ways: weight, volume, pressure, and rock surface hardness index [6, 19, and 20]. Indentation tests, scratch tests, swelling tests, pressure transient tests, and hydraulic fracturing tests are the main categories of experiments to evaluate the effectiveness of drilling fluid additives for controlling swelling in shales [20]. Also, some tests are designed to evaluate the effect of drilling fluid additives on chemical potentials or

hydraulic potentials of clay hydration [21-22]. However, the most common experiment is the pressure transient test (PTT) [6, 19, and 20]. Basically, PTT measures the amount of pressure transmitted to the shale samples. One of the challenges with shales experiments is keeping the in situ water content. Different interaction of shale-fluid will be observed if in situ water content is altered [19]. Thus, in situ water content of shales sample should be preserved.

The main objective of this paper is to evaluate Coal Combustion Residuals (CCRs) as a drilling fluid additive for controlling fluid invasion into shales. To reach this objective, mechanically grinded CCRs were used in a water-based bentonite drilling fluid system. Performance of CCRs for controlling fluid invasion into shales has been evaluated using pressure transient testing on Catoosa shale samples. Two different types of chemically made nano silica were tested in comparison to nano CCRs. The pressure transient testing results were analyzed to investigate the effect of using drilling fluid containing micro sized CCRs on fluid invasion into shales compared to the conventional water-based drilling fluid and also fluids containing two other used nano products.

2. COAL COMBUSTION RESIDUALS

Coal Combustion Residuals (CCRs) or coal ash is the main waste product of coal fired power plants. CCRs are mixture of different by-products including fly ash, bottom ash, boiler slag, and flue gas desulfurization material [23]. The fly ash is the most dominant by-products of CCRs. Fly ash is fine material with grey or blackish grey color mainly composed of Silica produced by burning ground coal in a burner [23]. The bulk composition of fly ash might be different depends on the coal source and combustion type (suspension firing or fluidized bed combustion) which will affect their physiochemical properties. Particle sizes of fly ash are typically in order of few to hundred microns [24] and particles have spherical and hollow shapes [25]. Although fly ash has been used for different purposes such as cement concrete, the main portion of annual produced fly ash is still disposed in landfills [23].

3. EXPERIMENTAL PROCEDURE

The testing plan was based on using of fly ash with smaller range of particle size distribution potentially in order of nanometers. The fly ash powder was mechanically grinded in order to get smaller range of particle sizes. A mixture of fly ash, surfactant, distilled water, and 2 millimeter grinding balls were placed in a high speed ball grinder at rotational speed of 1500 RPM. The X-Ray diffractometer was used to investigate any potential difference in the bulk composition of mechanically grinded fly ash compared to the fly ash. Investigation of particles sizes of mechanically grinded fly ash compared to fly ash was done using the laser diffraction particle size analyzer. The standard particle settling test was conducted to understand fine grinded fly ash particles settling rate. Pennsylvanian age Catoosa shale [26] obtained from Catoosa, Oklahoma with porosity value of 0.0773 (fraction) and permeability values of 0.007 md [27] was used for experimental analysis. The bulk composition of Catoosa shale is listed in Table 3-1 [28]. Disk shape samples of 2” diameter by 0.25” thickness were prepared from Catoosa shale cores. Coring and cutting of shale samples was done under exposure of synthetic oil and prepared samples were stored in a synthetic oil filled container. The 2” shale samples were secure in a 2.5” casing using epoxy and then were place in a humid chamber for couple of hours before the experiment for keeping the moisture content of samples while epoxy is curing (Figure 3-2). A pressure transient testing (PTT) setup (Figure 3-1) was designed to evaluate different designed fluids for controlling fluid invasion into shales. The shale samples were placed at the bottom of the high pressure high temperature PTT cell. Drilling fluid was injected hydraulically using a piston was pressurized by water (Figure 3-1).

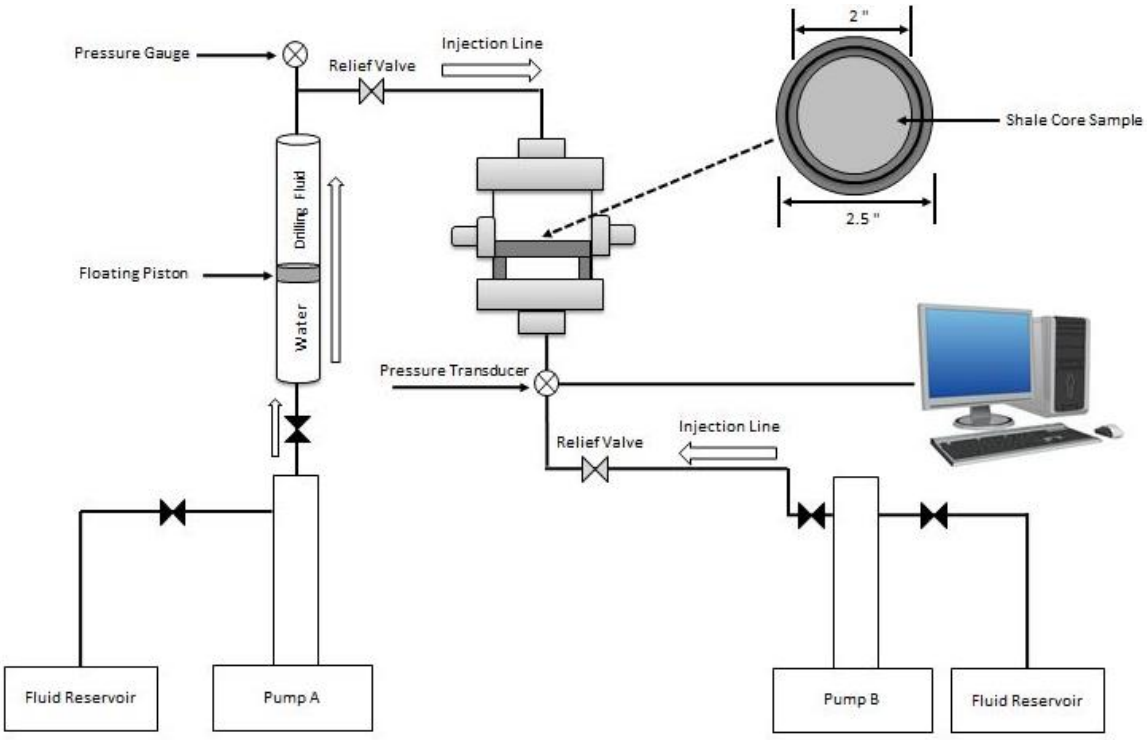

Figure 3-1. Pressure transient testing setup schematic

Table 3-1. Catoosa Shale Composition [28]

Mineral	**%**
Quartz	47
Feldspar	9
Calcite	Trace
Dolomite	0
Chlorite	15
Illite/Mica	29
Smectite	0

Figure 3-2. A shale sample were secured with epoxy in a casing and were placed in humid chamber couple of hours before PTT experiment

A top pressure of 100 psi was maintained during experiments and back pressure of 50 psi was applied on the bottom of shale sample by injecting of water. A pressure transducer was installed on the bottom of the cell to record the gradual transmission of pressure on the lower side of shale samples. Each experiment was conducted for five hours. A total of five tests were planned and each test was repeated three times. Two chemically made nano products were used in comparison to fine grained fly ash; AEROSIL and AERODISP. AEROSIL is hydrophilic fumed silica and AERODISP is a low viscosity water dispersion of fumed silica. Water-based bentonite drilling fluid with total of 6% solid particles weight percentage was designed for all tests. Sufficient amount of deflocculant (Q-Broxin) was used to reduce viscosity and prevent flocculation of bentonite clays for each fluid. The fluid of test #1 is conventional water-based bentonite drilling fluid. The fluids of test #2 and 3 are consisting of 4% & 2% Nano fly ash respectively. 4% of AEROSIL was included in the fluid of test #4 and 4% AERODISP in the fluid of test #5. Table 3-2 shows the testing matrix.

Table 3-2. Pressure Transient Testing Matrix

Test No	Drilling Fluid Composition
1	6% Bentonite
2	2% Bentonite + 4% Fly Ash
3	4% Bentonite + 2% Fly Ash
4	2% Bentonite + 4% AEROSIL
5	2% Bentonite + 4% AERODISP

4. RESULTS AND DISCUSSION

The results of the particle size analysis of fly ash and the mechanically grinded fly ash is presented in Figure 4-1. The horizontal axis shows particle sizes in microns and two vertical axis are presenting normal distribution of sizes and likelihood of each particle size for fly ash (blue data series) and mechanically grinded fly ash (red data series). The results showed that 70% of mechanically grinded fly ash has particle size of less than 1 microns and the D50 value of normal distribution of particle sizes is around 600 nanometers while the D50 value of normal distribution of particle sizes for regular fly ash is around 30 microns. Figure 4-2 shows the results of X-Ray diffraction analysis on the fly ash and the fine grained fly ash samples. Orange line shows the intensity of X-Ray diffraction for the fly ash sample at different angles and the red line represents the same for the grinded fly ash sample. According to the results, both samples have a similar amount of quartz since there is a good match on the peak of curves for the quartz. Grinded fly ash has a higher Calcite content compared to the fly ash as the higher peak could be observed for fine grained fly ash (Figure 4-2). Aluminum silicate content is more in fly ash compared to the fine grained fly ash because of the higher peak.

Figure 4-3 shows the fine grained fly ash particles settling test results. The vertical axis represents the percentage of remaining particles level in the fluid column and the horizontal axis represents time in minutes. Based on the results represented in Figure 4-3, 15% of fine grained fly ash particles were settled after 90 minutes.

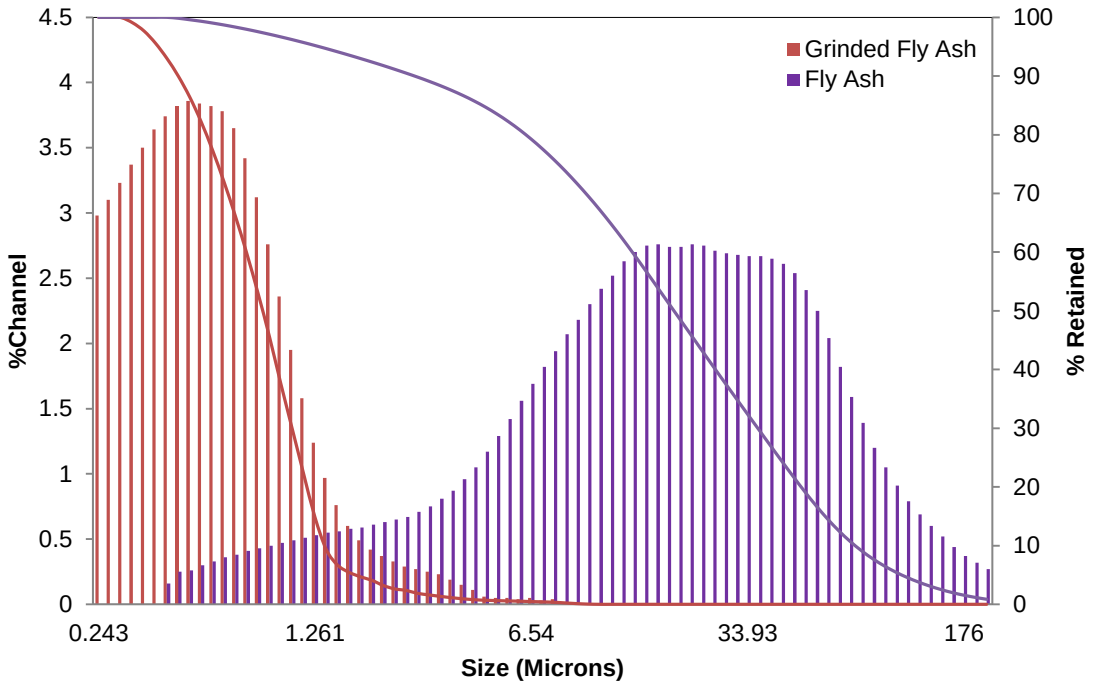

Figure 4-1. Particle size analysis of fly ash and mechanically grinded fly ash

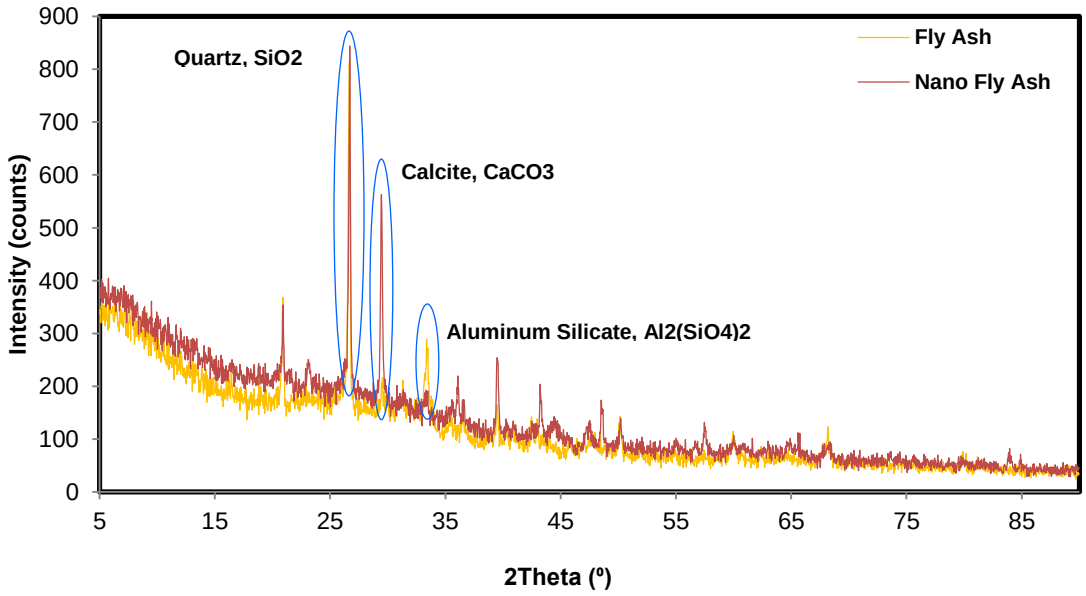

Figure 4-2. X-Ray diffraction analysis of fly ash and grinded fly ash samples

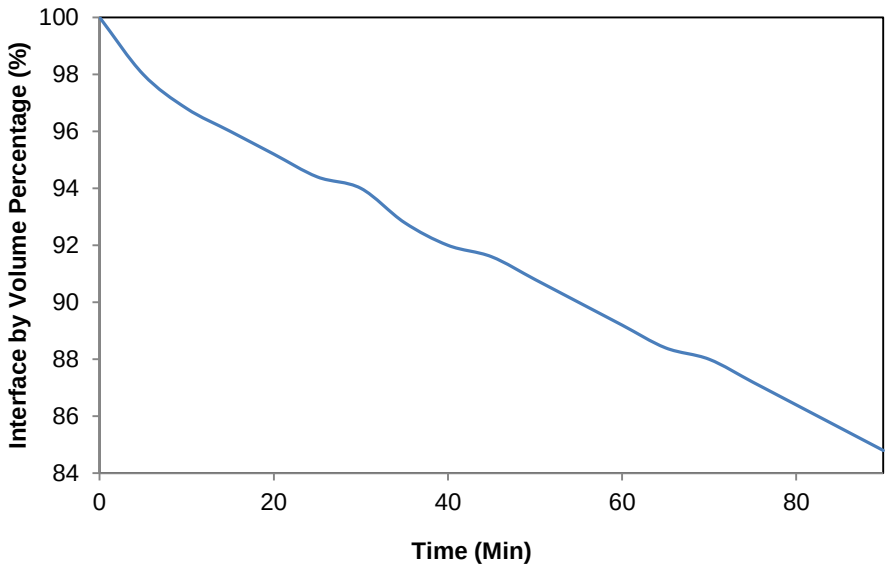

Figure 4-3. Fine grained fly ash standard settling test results

The shale sample was exposed to the fluid of test #2 (2% Bentonite + 4% Fly Ash) is shown in Figure 4-4. Figures 4-5 to 4-9 show the results of pressure transient tests. The vertical axis represents the pressure in psi and the horizontal axis indicates time in hour. As indicated by results for all three runs of test #1 (6% Bentonite), the final transmitted pressure and pressure transient rate for the first run and the second run are similar (Figure 4-5). However, the results for third run of test #1 shows a different pressure transient rate and final transmitted pressure compare the results of the first run and the second run (Figure 4-5). Although, the pressure transient rate of third run is higher than two other runs but the final transmitted pressure is lower (Figure 4-5). Based on the results for all three runs of test #2 (2% Bentonite + 4% Fly Ash), the third run of test shows higher pressure transient rate compared to the first two runs (Figure 4-6). The first run of test #2 shows different pressure transient pattern compared to the second and third runs.

Figure 4-4. A shale sample was exposed to the fluid of test #2
(2% Bentonite + 4% Fly Ash)

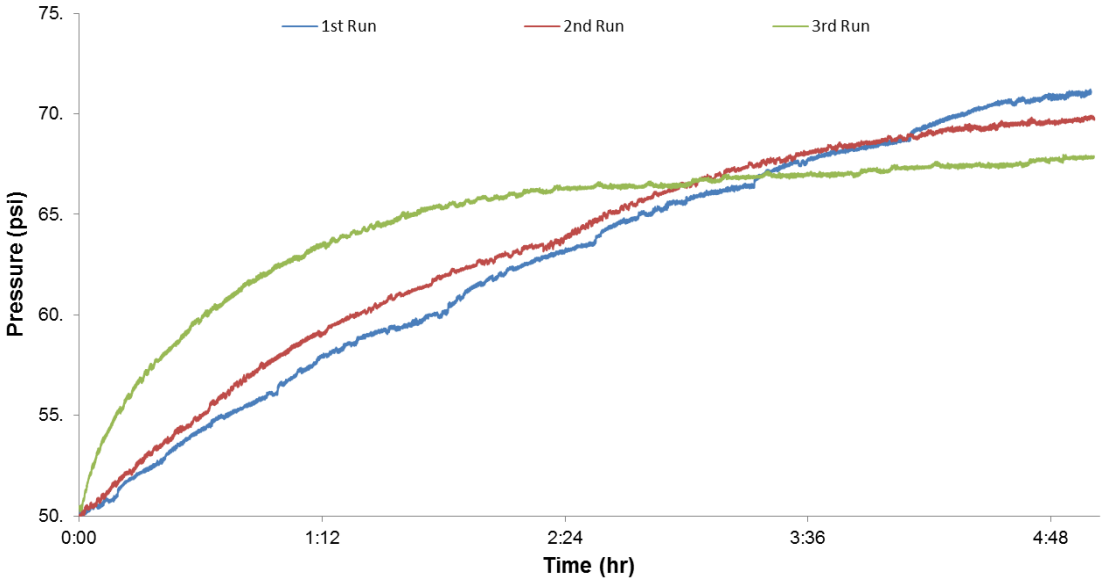

Figure 4-5. Results from all three runs of test #1 (6% Bentonite)

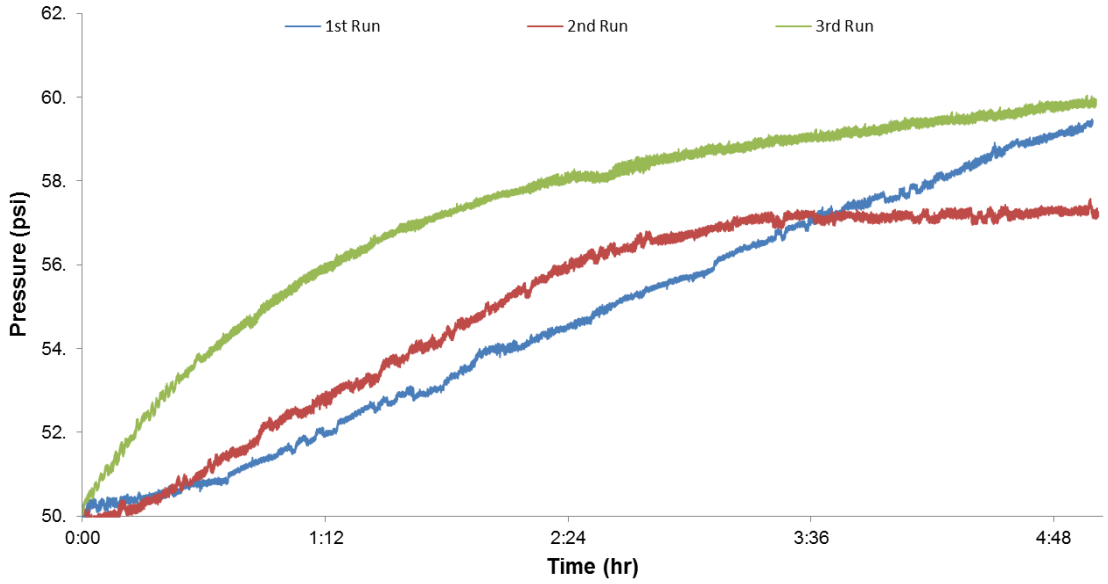

Figure 4-6. Results from all three runs of test #2 (2% Bentonite + 4% Fly Ash)

The final transmitted pressure by all three runs has small difference (2 psi) (Figure 4-6). The first run of test #3 (4% Bentonite + 2% Fly Ash) shows a significant difference compared to other two runs with higher pressure transient rate and higher final transmitted pressure (Figure 4-7). The second run of test #3 (4% Bentonite + 2% Fly Ash) has higher early pressure transient rate compared to the third run but lower final transmitted pressure (Figure 4-7). The final transmitted pressure from the second and third run of test #3 (4% Bentonite + 2% Fly Ash) shows small difference (2 psi) (Figure 4-7). The pressure transient rate from third run of test #4 (2% Bentonite + 4% AEROSIL) is higher compared to the first two runs (Figure 4-8). All three runs of test #4 (2% Bentonite + 4% AEROSIL) have a similar pressure transient pattern compared to other tests (Figures 4-5 to 4-8). There is a small difference (3 psi) between the final transmitted pressure by all three runs of test #4 (Figure 4-8).

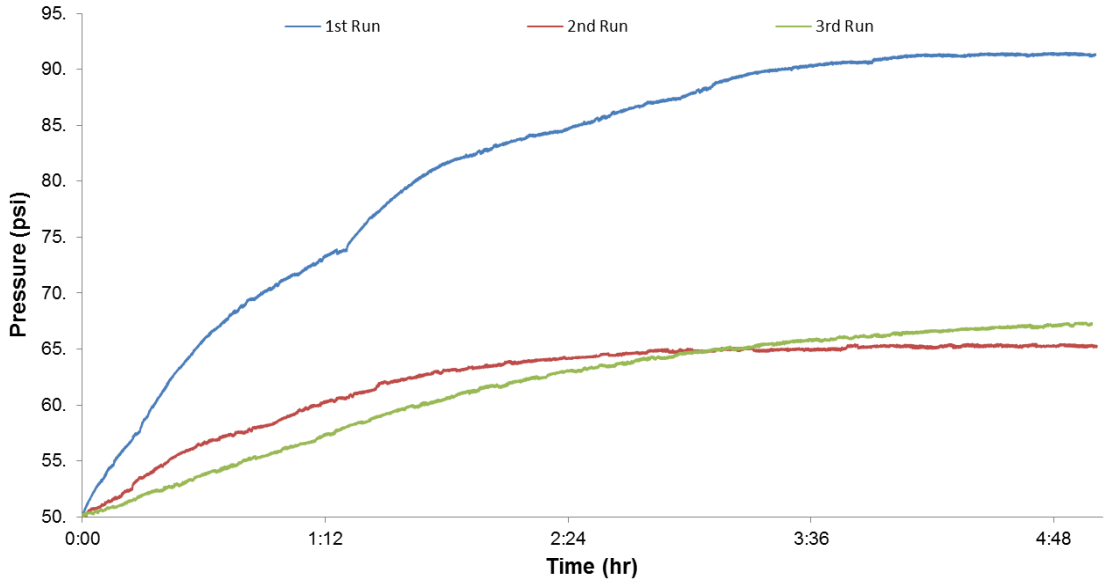

Figure 4-7. Results from all three runs of test #3 (4% Bentonite + 2% Fly Ash)

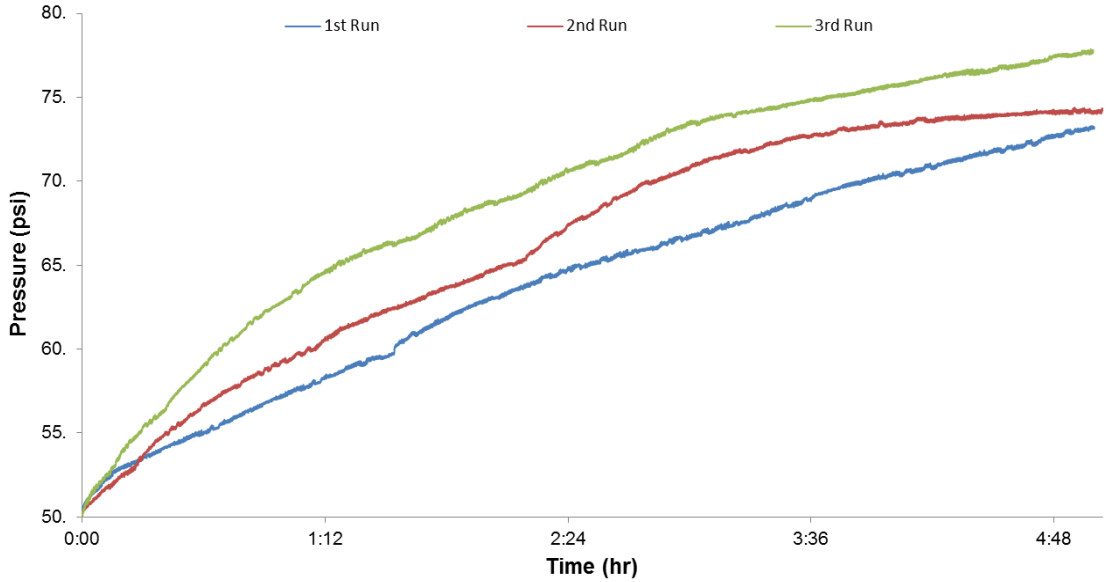

Figure 4-8. Results from all three runs of test #4 (2% Bentonite + 4% AEROSIL)

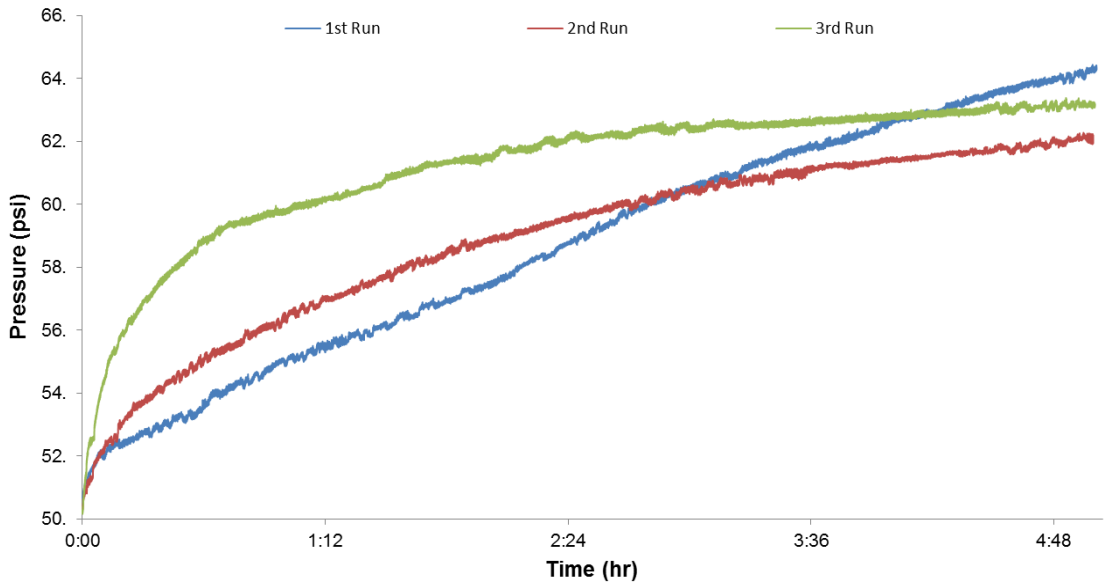

Figure 4-9. Results from all three runs of test #5 (2% Bentonite + 4% AERODISP)

The third run of test #5 (2% Bentonite + 4% AERODISP) has higher early pressure transient rate compared to the first and second runs (Figure 4-9). The first run of the test #5 resulted in the highest transmitted pressure and the second run gave the lowest. However, the final transmitted pressure by all three runs is in small difference range of (3 psi). The second run and the third run of test #5 (2% Bentonite + 4% AERODISP) have similar pressure transient pattern (Figure 4-9).

Table 4-1 summarizes all testing results. According to the summary of results for the first run of tests, the transmitted pressure from the fluid of test # 1 (6% Bentonite) (21 psi) and the fluid of test #4 (2% Bentonite + 4% AEROSIL) (23 psi) are comparable. The transmitted pressure (14 psi) from fluid in test #5 (2% Bentonite + 4% AERODISP) is lower than fluids of tests #1, 3, and 4 but higher than the transmitted pressure from the fluid of test #2 (Table 4-1).

Table 4-1. Summary of Testing Results

	Test #1			Test #2			Test #3			Test #4			Test #5		
	1st	2nd	3rd	1st	2nd	3rd	1st	2nd	3rd	1st	2nd	3rd	1st	2nd	3rd
P_i (psi)	50	50	50	50	50	50	50	50	50	50	50	50	50	50	50
P_F (psi)	71	70	68	59	58	60	92	65	67	73	74	74	64	62	63
ΔP (psi)	21	20	18	9	8	10	42	16	17	23	24	24	14	12	13
ΔP (%)	43	40	35	19	16	20	83	31	35	45	48	48	27	24	26

Based on the results for the second set of the experiments, the transmitted pressure (24 psi) by fluid of test #4 (2% Bentonite + 4% AEROSIL) is the highest (Table 4-1). The fluid of test #2 (2% Bentonite + 4% Fly Ash) resulted in the lowest transmitted pressure (8 psi). The final transmitted pressure (12 psi) by the fluid of test #5 was less than the result for the fluids of test #1 (20 psi), test #3 (16 psi), and test #4 (24 psi). Looking at the results from the third set of tests (Table 4-1), the fluid of test #2 (2% Bentonite + 4% Fly Ash) resulted in the lowest transmitted pressure (10 psi) and the highest transmitted pressure (24 psi) by the fluid of test #4. The fluid of test #3 resulted in the higher transmitted pressure (17 psi) compared to the transmitted pressure (10 psi) by fluid of test #3 (Table 4-1).

Figure 4-10 represents the transmitted pressure range from all three runs of each test after 30 min, one hour, and five hours. The final transmitted pressure result from the first run of test #3 was excluded as an outlier since there is major difference compared to the two other runs of test #3 and results of all other tests (Table 4-1). As indicated by data presented in Figure 4-10, the transmitted pressure range from all three runs of each test is smaller after 5 hours compare the range of transmitted pressure after the first 30 minutes

and also the first hour. The range of final transmitted pressure for all three runs of tests #1 to 5 is small which indicates the repeatability of tests (Figure 4-10.c) but the larger range of transmitted pressure for the first 30 minutes and also the first hour shows different pressure transient rate (Figure 4-10.a and Figure 4-10.b). The final transmitted pressure from all three runs of test #2 (2% Bentonite + 4% Fly Ash) is the smallest compared to the results of other test (Figure 4-10.c).

The highest recorded transmitted pressure (42 psi) was from the fluid of test #3 in the first run of experiments. However, the results of the fluid of test #3 in the second run (16 psi) and third run (17 psi) of experiments were not as high as the results of test #3 in the first set of experiment (Table 4-1). This difference might be due to presence of small fracture in the shale sample of test #3 in the first set of experiments which enhanced the permeability of sample. The transmitted pressure by fluid of test #4 (2% Bentonite + 4% AEROSIL) was higher than the conventional bentonite drilling fluid (test #1) in all three sets of experiments (Table 4-1). This indicates that AEROSIL particles (test #4) are not capable of controlling fluid invasion not even to level of bentonite clay particles of conventional drilling fluid of test #1. AEROSIL Nano particles are very soft and deformable compare to other fluid additives were used such a bentonite clay, fine grained fly ash and AERODISP particles. The transmitted pressure by fluid of test #5 is less than the results of tests #1, 3, and 4 for all three sets of experiments. This fact concludes that using of AERODISP particles has positive impact in controlling fluid invasion in shales compare to the conventional bentonite drilling fluid (test #1) (Table 4-1).

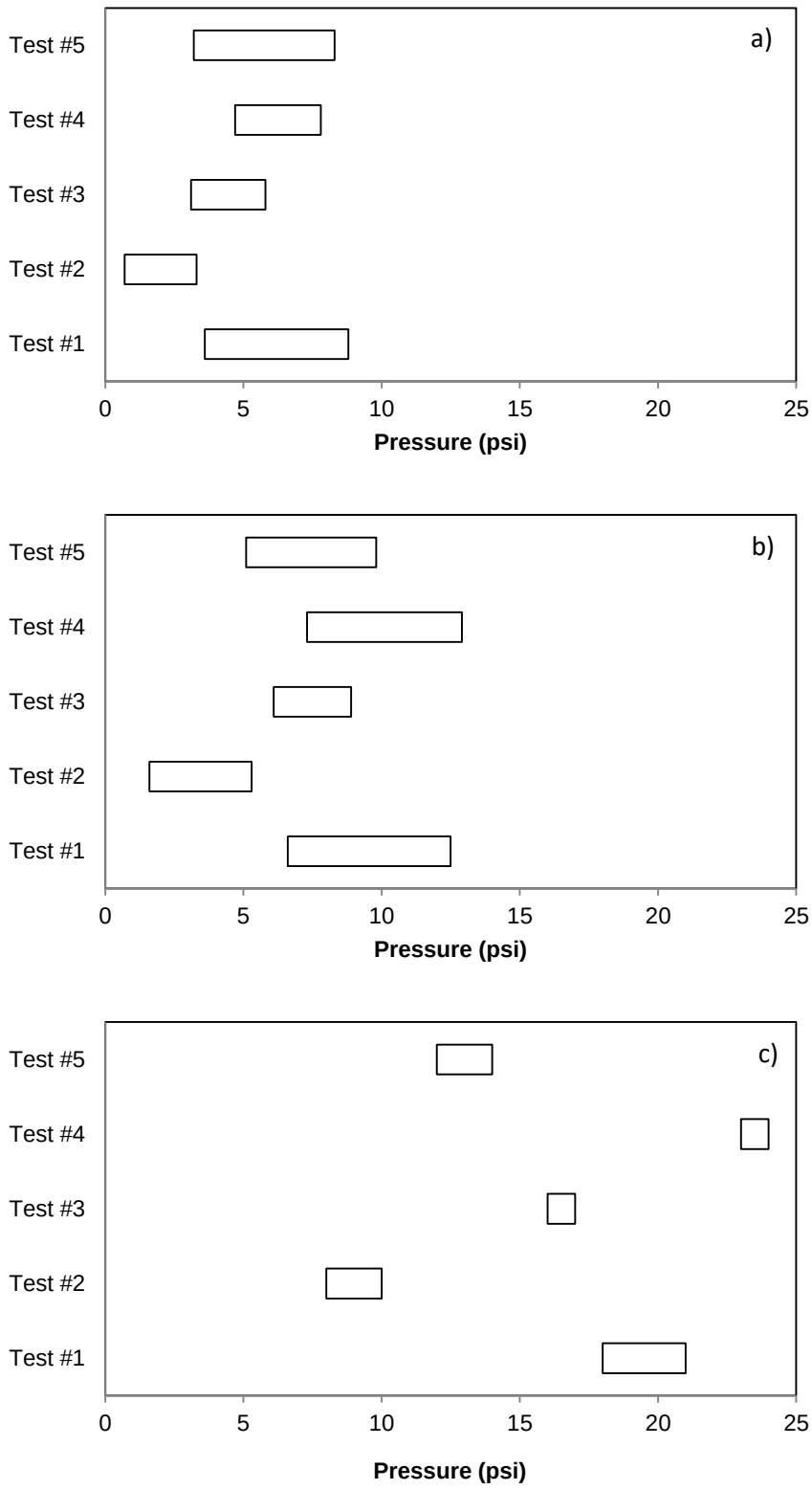

Figure 4-10. Range of transmitted pressure from all three runs of each test after a) 30 min b) one hour c) five hours

The fluid of test #2 (2% Bentonite + 4% Fly Ash) resulted in the lowest transmitted pressure and also the lowest pressure transient rate compared to the results of fluids of other tests in all three sets of experiments (Table 4-1). Fine grained fly ash particles are capable of blocking surface pores on the shale samples and control the hydraulic flow of fluid into the Catoosa shale samples. Also fine grained fly ash particles are (silica) are stronger than chemical made silica (fumed silica in AEROSIL and AERODISP). Although the fluid of test #3 included fly ash but the percentage of the particles in the fluid were not enough to sufficiently block the surface pores on the shale samples as good as the fluid of test #2 with higher percentage of fine grained fly ash particles. It should be noted that these experiments has been conducted for five hours which is only good to evaluate the performance of fluid additives for controlling the hydraulic flow of fluids in shale. Evaluating the efficiency of these additives in controlling other fluid drive mechanism requires conducting these experiments in a longer time (24 Hours). Also, these experiments have been conducted on a single type of shale with a low clay content (Catoosa shale). More extensive testing is required on different shales with different composition to draw a general conclusion about the performance of these additives in controlling fluid invasion in shales. Potential usage of CCRs as shale inhibitors for water-based drilling fluids could be one solution for the growing concern about landfill disposal of coal fired power plants wastes.

5. CONCLUSIONS

In this paper, the effect of using fly ash for controlling fluid invasion in shales has been experimentally evaluated. Mechanically grinded fly ash particles and two other Nano products (AEROSIL and AERODISP) were evaluated as a shale inhibitor additive using pressure transient testing setup. Five different water-based fluids were designed with different combination of additives all with total particles weight percentage of 6 %. As indicated by testing results, the fluid containing the 2% bentonite and 4% Fine grained fly ash particles resulted in the lowest transmitted pressure and also the lowest pressure transient rate. So, fly ash can potentially be an effective additive for controlling fluid invasion in shales and addressing the environmental concern regarding disposing of fly ashes. However, further analysis is required to have a better understanding of fly ash performance as shale inhibitor additive for water-based drilling fluid compared to other commercially available products.

REFERENCES

[1] Chenevert, M.E. 1970. Shale alteration by water adsorption. Journal of Petroleum Technology, 22(09), pp. 1,141 - 1,148.

[2] Chenevert, M. E. 1989. Lecture: Diffusion of water and ions into shales. ISRM International Symposium, Pau, France, 30 August-2 September.

[3] Hale, A.H., Mody, F.K., Salisbury, D.P. 1993. The influence of chemical potential on wellbore stability. SPE-23885-PA. Journal of Drilling & Completion; 8(3): 207–216.

[4] Ballard, T.J., Beare, S.P. and Lawless, T.A. 1994. Fundamentals of shale stabilisation: water transport through shales. SPE Formation Evaluation; 9(02), pp.129-134.

[5] Bol, G.M., Wong, S.W., Davidson, C.J., Woodland, D.C., 1994. Borehole stability in shales. SPE Drilling & Completion, 9(02), pp.87-94.

[6] Van Oort, E., Hale, A.H., Mody, F.K., Roy, S. 1996. Transport in shales and the design of improved water-based shale drilling fluids. SPE-28309-PA. SPE Drilling & Completion, Vol. 11(3), pp. 137-146.

[7] Horsud, P. and Bostrom, B. 1998. Interaction between shale and water-based drilling fluids: laboratory exposure tests give new insight into mechanisms and field consequences of KC1 content. SPE-48986.

[8] Karaborni, S., Smit, B., Heidug, W., Urai, J., Van Oort, E. 1996. The swelling of clays: molecular simulations of the hydration of montmorillonite. Science, 271(EPFL-ARTICLE-200818), pp.1102-1104.

[9] Ghassemi, A., Diek, A. 2001. Effects of ion transfer on stress and pore pressure distributions around a borehole in shale. The 38th U.S. Symposium on Rock Mechanics (USRMS), Washington, D.C., 7-10 July.

[10] Mody, F. K., Tare, U. A., Tan, C. P., Drummond, C. J., & Wu, B. 2002. Development of novel membrane efficient water-based drilling fluids through fundamental understanding of osmotic membrane generation in shales. SPE-77447-MS. SPE Annual Technical Conference and Exhibition, San Antonio, Texas. 29 September-2 October.

[11] Fam, M. A., Dusseault, M. B. 1998. Borehole stability in shales: a physico-chemical perspective. SPE-47301-MS. SPE/ISRM Rock Mechanics in Petroleum Engineering, Trondheim, Norway, 8-10 July.

[12] Forsans, T.M. and Schmitt, L. 1994. Capillary forces: The neglected factor in shale instability studies? SPE-28029-MS. Rock Mechanics in Petroleum Engineering Conference. Delft, Netherlands, 29-31 August.

[13] Ballard, T.J. and Dawe, R.A., 1988, January. Wettability alteration induced by oil-based drilling fluid. SPE-17160-MS. SPE Formation Damage Control Symposium, 8-9 February, Bakersfield, California.

[14] Van Oort, E. 1994. A novel technique for the investigation of drilling fluid induced borehole instability in shales. SPE-28064. Rock Mechanics in Petroleum Engineering, Delft, Netherlands, 29-31 August.

[15] Sherwood, J.D., Bailey, L. 1994. Swelling of shale around a cylindrical wellbore. In Proceedings of the Royal Society of London A: Mathematical, Physical and Engineering Sciences; 444 (1920), pp. 161-184.

[16] Schmitt, L., Forsans, T., Santarelli, F.J. 1994. Shale testing and capillary phenomena. International Journal of Rock Mechanics and Mining Sciences, 31(5); pp. 411-427.

[17] Van Oort, E. 2003. On the physical and chemical stability of shales. Journal of Petroleum Science and Engineering, Vol. 38(3-4), pp. 213-235.

[18] Steiger, R.P. 1993. Advanced triaxial swelling tests on preserved shale cores. International Journal of Rock Mechanics and Mining Sciences, 30(7); pp. 681-685.

[19] Guo, Q., Blue, A., Friedheim, J. 2015. Testing methods for evaluating drilling fluid effects on gas shale stability. 49th U.S. Rock Mechanics/Geomechanics Symposium, San Francisco, California, 28 June-1 July.

[20] Salisbury, J.W., D'Aria, D.M., Jarosewich, E. 1991. Midinfrared (2.5–13.5 μm) reflectance spectra of powdered stony meteorites. Icarus, 92(2), pp.280-297.

[21] Chenevert, M.E.K., Osisanya, S.O.K. 1992. Shale swelling at elevated temperature and pressure. ARMA-92-0869. The 33th U.S. Symposium on Rock Mechanics (USRMS), Santa Fe, New Mexico, 3-5 June.

[22] Santos, H., Diek, A., Da Fontoura, S., Roegiers, J.C. 1997. Shale Reactivity test: a novel approach to evaluate shale-fluid interaction. International Journal of Rock Mechanics and Mining Sciences, 34(3); pp.268-e1-e11.

[23] Asokan, P., Saxena, M. and Asolekar, S.R., 2005. Coal combustion residues—environmental implications and recycling potentials. Resources, Conservation and Recycling, 43(3), pp.239-262.

[24] Wigley, F. and Williamson, J., 1998. Modelling fly ash generation for pulverised coal combustion. Progress in energy and combustion science, 24(4), pp.337-343.

[25] Kolay, P.K. and Singh, D.P. 2001. Physical, chemical, mineralogical, and thermal properties of cenospheres from an ash lagoon. Cement and Concrete Research, 31(4), pp.539-542.

[26] Shewalla, M., 2007. Evaluation of Shear Strength Parameters of Shale and Siltstone Using Single Point Cutter Tests. M.Sc. Thesis. Louisiana State University, Baton Rouge LA, USA.

[27] Reyes, L., and Osisanya, S.O. 2000. Empirical Correlation of Effective Stress Dependent Shale Rock Properties. Petroleum Society of Canada Paper 1000-038 presented at the Canadian International Petroleum Conference, Calgary, AB, Canada, 4-8 June.

[28] Andersen, E.E., and Azar, J.J. 1990. PDC Bit Performance under Simulated Borehole Conditions. SPE Drilling and Completion 8 (3): 184-188.

SECTION

2. CONCLUSIONS AND RECOMMENDATIONS

2.1. CONCLUSIONS

Thirteen of the most common rock failure criteria were evaluated based on prediction of borehole failure using the data set from four field cases. The results of failure criteria were compared with actual field case shear failure in order to investigate using which of these failure criteria could be a safe approach in wellbore stability analysis. The effect of rock strength variation and strength anisotropy on estimated borehole breakout by different criteria was studied using data from main North American shale plays. The fracture width estimate of five analytical fracture models were analyzed and the effect of different input parameters on the estimated fracture width, including rock properties, in-situ stresses, anisotropy, borehole size and fracture geometry was studied. Hydraulic fracturing experiments were conducted to investigate the effect of adding different LCM for enhancing the fracture breakdown pressure and the fracture re-opening pressure, the effect of LCM particle sizes on enhancing fracture gradient (breakdown and re-opening pressure), and to find a relation between the particle sizes, the fracture size and the wellbore pressure. Fine grained Coal Combustion Residuals (CCRs) were experimentally evaluated as drilling fluid additive for controlling fluid invasion into shales.

Based on this work the following conclusions can be drawn;

- Tresca, Von Mises, and Inscribed Drucker-Prager overestimate the breakout of rock and over predict the minimum required drilling fluid density; therefore, they are too conservative for wellbore stability analysis. Also, the estimated drilling fluid density by these three criteria is always higher than other criteria.

- Circumscribed Drucker-Prager criterion underestimates the breakout of rock and under predicts the minimum required drilling fluid density for the analyzed field cases, so using this criterion is an unsafe approach in wellbore stability analysis. Circumscribed Drucker-Prager estimates a lower bound of results except for formations with low frictional angle.
- Using of Mohr-Coulomb is not suggested because of overestimating rock breakout and a conservative prediction of the minimum required drilling fluid density.
- Strength anisotropy can affect the estimated minimum required drilling fluid density by some criteria more than others. This effect depends on the rock strength and the level of strength anisotropy.
- Estimated minimum required drilling fluid density by Modified Lade, Modified Wiebols-Cook, and Mogi-Coulomb criteria are close to the field reported onset of shear failure. Hence, using these three failure criteria is recommended.
- Morita and Fuh's model estimated a constant fracture width for all cases, which is smaller than the measured size of fractures for tests with fluid-containing solids.
- The estimated fracture widths by Wang et al.'s and Hillerborg et al.'s models are smaller compared to the measured fracture widths.
- Larger fracture widths were predicted by Alberty and McLean's model compared to the measured fracture widths.
- Carbonell and Detournay's model estimated comparable fracture widths to the measured widths on the fractured cores, indicating that this analytical fracture model reflects more realistic fracture width behavior.

- The addition of different LCM blends enhanced the breakdown and re-opening pressures up to 18% and 210%, respectively, compared to the control sample that contained no LCM.
- The cores fractured with fluid- containing solids had a larger fracture size compared to the fractured core using the base fluid.
- The particle size distribution of lost circulation material has a significant effect on the sealing efficiency of fractured wellbores and also enhancing the breakdown pressure of intact wellbores.
- Smaller range of fine particles (<100 microns) were capable of blocking the pore throats and increasing the breakdown pressure; however they cannot create a strong barrier for enhancing the fracture re-opening pressure.
- Broad range of coarse particle sizes, in order of hundreds to thousands of microns, could bridge fracture aperture but the barrier would not be as strong toward fluid pressure.
- LCMs with particle sizes range of few hundred microns were capable of bridging the fracture aperture and creating a strong seal to enhance fracture re-opening pressure significantly.
- The measured range of fracture width increased by increasing the particle size distribution.
- Fine grained fly ash particles lowered the pressure transient rate into Catoosa shale samples compared to the conventional water-based drilling fluid and the two other Nano products were tested.

2.1. RECOMMENDATION AND FUTURE WORK

Borehole breakout estimation of rock failure criteria were evaluated based only four field reported failure cases. Upon availably of good field data set of failure cases this work can be expanded to have a better understanding of failure criteria.

The fracture widths of the fractured cores were measured after removing the applied overburden and confining stresses. Therefore, the measured width represent the relaxed fracture width rather than the actual stressed width. For a better measurement, future work should consider in-situ fracture width estimation.

Five hydraulic fracturing experiments were carried out in this study using OBM on concrete core samples, where 3 tests were performed using LCMs. Future work should include further investigation using permeable and impermeable rocks using WBM and different LCM treatments to identify the relationship between the maximum sealing pressure and the enhancement in the breakdown and re-opening pressure.

Only one kind of shale (Catoosa) was used in the pressure transient testing. Further testing should be conducted using different shales to establish a better understanding of fly ashes performance as shale inhibitor additives. Also, the testing apparatus could be modified by installing a flow loop that circulates drilling fluids across the shale sample to simulate in situ wellbore condition. Furthermore, fly ashes performance should be compared with all commercially available shale inhibitors products.

APPENDIX A

ROCK FAILURE CRITERIA

This section will describe the rock failure criteria which were used in this study:

A.1. Mohr-Coulomb

Linear Mohr-Coulomb is the most commonly used failure criterion in geomechanics. Following is the governing equation for Mohr-Coulomb criterion based on the shear and normal stress components:

$$\tau = \mu\sigma + c \tag{A.1}$$

$$\mu = \tan\phi \tag{A.2}$$

The parameter c is the cohesion of rock and μ is the coefficient of the internal angle of friction. In terms of principal stresses, Mohr-Coulomb failure criterion can be expressed in the following form:

$$\sigma_1 = q\sigma_3 + C_0 \tag{A.3}$$

where C_0 is the uniaxial compressive strength (UCS) and q is the flow factor parameter which is a function of the internal angle of friction:

$$q = \frac{1+\sin\phi}{1-\sin\phi} \tag{A.4}$$

$$C_0 = \frac{2c\cos\phi}{1-\sin\phi} \tag{A.5}$$

Mohr-Coulomb criterion does not consider the effect of intermediate principal stress in contrast to the triaxial stress state of rock.

A.2. Mogi-Coulomb

Based on the Mogi's theory on the effect of intermediate principal stress on the rock strength, Al-Ajmi and Zimmerman found a linear relation which can fit polyaxial test data in $\tau_{oct} - \sigma_{m,2}$ space:

$$\tau_{oct} = a + b\sigma_{m,2} \tag{A.6}$$

$$\sigma_{m,2} = \frac{1}{3}(\sigma_1 + \sigma_3) \tag{A.7}$$

$$\tau_{oct} = \frac{1}{3}\sqrt{(\sigma_1 - \sigma_2)^2 + (\sigma_1 - \sigma_3)^2 + (\sigma_2 - \sigma_3)^2} \tag{A.8}$$

The τ_{oct} is octahedral shear stress and $\sigma_{m,2}$ is mean normal stress. Parameters a and b can be evaluated based on the Mohr-Coulomb parameter C_0 and q:

$$a = \frac{2\sqrt{2}}{3}\frac{C_0}{q+1} \tag{A.9}$$

$$b = \frac{2\sqrt{2}}{3}\frac{q-1}{q+1} \tag{A.10}$$

A.3. Tresca

The simplest failure criterion based on the Mohr's theory is Tresca which assumes failure would occur if maximum shear failure inside any plane of rock reaches a critical value, c.

$$\frac{(\sigma_1 - \sigma_3)}{2} = c = \tau_{max} \tag{A.11}$$

$$\frac{C_0}{2} = c \tag{A.12}$$

Tresca can be considered a special case of the Mohr-Coulomb failure criterion when the internal angle of friction is equal to zero.

$$\sigma_1 = q\sigma_3 + C_0$$

$$When\ \phi = 0, \quad q = \frac{1+sin\,\phi}{1-sin\,\phi} = 0$$

$$\sigma_1 - \sigma_3 = C_0 \tag{A.13}$$

A.4. Von Mises

Von Mises proposed his failure criterion by assuming that rock fails when the invariant of the deviatoric stress (J_2) reaches a critical value:

$$\sqrt{J_2} = \frac{C_0}{3} \tag{A.14}$$

$$\sqrt{J_2} = \sqrt{\frac{(\sigma_1-\sigma_3)^2+(\sigma_2-\sigma_3)^2+(\sigma_1-\sigma_3)}{6}} = \frac{C_0}{3} \quad \text{(A.15)}$$

Von Mises hypothetically included the effect of intermediate principal stress by using rotational symmetry in the three dimensional stress space.

A.5. Drucker-Prager

As an extension of Von Mises theory, Drucker and Prager presented their failure criterion in the following form:

$$\sqrt{J_2} = k + \alpha J_1 \quad \text{(A.16)}$$

The parameters k and α are the material constants and J_1 is the mean effective confining stress:

$$J_1 = \frac{(\sigma_1+\sigma_2+\sigma_3)}{3} \quad \text{(A.17)}$$

The material parameters α and k can be determined from the slope and the intercept of the failure envelope plotted in the (J_1) and $(\sqrt{J_2})$ space. The parameter α is related to the frictional angle of rock and k is related to the cohesion of rock. Therefore Mohr-Coulomb criterion parameters could be used to determine Drucker-Prager criterion parameters. Based on comparison with the Mohr-Coulomb criterion in a three dimensional stress space, the Drucker-Prager criterion can be divided into Circumscribed Drucker-Prager and Inscribed Drucker-Prager. The solution of α and k parameters for Inscribed Drucker-Prager presented by Vekeens and Walters (1989):

$$\alpha = \frac{3\sin\phi}{\sqrt{9+3\sin\phi^2}} \quad \text{(A.18)}$$

$$k = \frac{3C_0\cos\phi}{2\sqrt{q}\sqrt{9+3\sin\phi^2}} \quad \text{(A.19)}$$

Zhou (1994) found the following solution for α and k parameters in the Circumscribed Drucker-Prager:

$$\alpha = \frac{\sqrt{3}(q-1)}{(2+q)} \tag{A.20}$$

$$k = \frac{\sqrt{3}C_0}{2+q} \tag{A.21}$$

A.6. Hoek-Brown

Hoek and Brown (1982) presented their empirical rock failure criterion for fractured rocks based on the wide range of experimental data in following form:

$$\sigma_1 = \sigma_3 + \sqrt{mC_0\,\sigma_3 + s{C_0}^2} \tag{A.22}$$

Where m and s are constant depending on both rock and fracture properties and parameter s for intact rock is equal to 1. Although there is a relation between parameter m and internal angle of friction, there is no mathematical relation presented for that. Different references provided the range of parameter m for different rock lithology. It should be noted that Hoek-Brown failure criterion does not consider the effect of the intermediate principal stress.

A.7. Modified Lade

Lade developed his criterion in terms of the first and third stress invariants:

$$\left(\frac{{I_1}^3}{I_3} - 27\right)\left(\frac{I_1}{P_a}\right)^m = \eta_1 \tag{A.23}$$

The parameter m and η_1 are material constants and P_a is atmospheric pressure. The stress invariant parameters, I_1 and I_3 are defined as:

$$I_1 = (\sigma_1 + \sigma_2 + \sigma_3) \tag{A.24}$$

$$I_3 = (\sigma_1.\sigma_2.\sigma_3) \tag{A.25}$$

The Modified Lade criterion was developed by Ewy (1999). He neglected material constant m in order to obtain a criterion that predicts linear shear strength increases with increasing first stress InvariantI_1. Furthermore, Ewy considered the effect of pore pressure and included effective stress components in the criterion. Since the original Lade criterion was for cohesionless soil, Ewy introduced parameter S as the function of cohesion to extend application of the Lade criterion to cohesive rocks. The Modified Lade criterion was presented in following form:

$$\frac{I"_1{}^3}{I"_3} = \eta_1 + 27 \tag{A.26}$$

where the appropriate stress Invariants $I"_1$ and $I"_3$ are in following form:

$$I"_1 = (\sigma_1 + S) + (\sigma_2 + S) + (\sigma_3 + S) \tag{A.27}$$

$$I"_3 = (\sigma_1 + S).(\sigma_2 + S).(\sigma_3 + S) \tag{A.28}$$

The parameters S and η can be determined by Mohr-Coulomb criterion parameters, cohesion and internal angle of friction:

$$S = \frac{c}{\tan\phi} \tag{A.29}$$

$$\eta = \frac{4\tan^2\phi(9-7\sin\phi)}{(1-\sin\phi)} \tag{A.30}$$

A.8. Modified Wiebols-Cook

Wiebols and Cook (1968) developed a model that describes the impact of the σ_2 on the rock strength. By considering shear strain energy of microcracks in the rock, they provided a physical description of sliding microcrack surfaces that cause failure when the stress condition meets the frictional criterion. Zhou developed a nonlinear criterion as an extension of circumscribed Drucker-Prager that is named Modified Wiebols-Cook due to similarities to the original model by Wiebols and Cook:

$$\sqrt{J_2} = A + BJ_1 + CJ_1^{\,2} \tag{A.31}$$

The Mohr-Coulomb criterion parameters, including uniaxial compressive strength (C_0) and flow factor (q), can be used as input data to determineA, B, and C parameters:

$$C = \frac{\sqrt{27}}{2C_1+(q-1)\sigma_3-C_0}\left(\frac{C_1+(q-1)\sigma_3-C_0}{2C_1+(2q-1)\sigma_3-C_0} - \frac{q-1}{q+2}\right) \tag{A.32}$$

The parameter C_1 is the function of frictional angle and uniaxial compressive strength (C_0):

$$C_1 = (1 + 0.6\,\mu)C_0 \tag{A.33}$$

where μ is the coefficient of internal angle of friction.

$$B = \frac{\sqrt{3}(q-1)}{q+2} - \frac{C}{3}[2C_0 + (q+2)\sigma_3] \tag{A.34}$$

and parameter A is a function of B and C:

$$A = \frac{C_0}{\sqrt{3}} - \frac{C_0}{3}B - \frac{C_0^{\,2}}{9}C \tag{A.35}$$

A.9. Griffith

Analysis of microcracks in a two dimensional model was Griffith's idea for developing his failure model. Expansion of microcracks as the onset of failure is a function of tensile stress at the tip of a crack. Original Griffith criterion has been developed in Mohr space and in terms of principal stresses and uniaxial tensile strength, T_0:

$$(\sigma_1 - \sigma_3)^2 = 8T_0(\sigma_1 + \sigma_3) \tag{A.36}$$

$$\sigma_3 = -T_0 \quad \text{if} \;\; \sigma_1 + 3\sigma_3 < 0$$

$$T_0 = \frac{C_0}{8} \tag{A.37}$$

In $\tau-\sigma$ plane, Griffith criterion is presented in the following form:

$$\tau^2 = 4T_0(\sigma + T_0) \tag{A.38}$$

The constant ratio of uniaxial compressive strength to uniaxial tensile strength, which has been presented by Griffith, is lower but close to the typical range of this ratio, 10 to 15, from experimental observation. One of the disadvantages of this failure criterion is its dependence on a single variable which makes it harder to fit polyaxial test data. The second shortcoming of the Griffith criterion is the lack of consideration of the effect that intermediate principal stress has on the rock strength.

A.10. Modified Griffith

Under compression, shear failure due to the closure of a crack can occur before tensile stress reaches a critical level at the tip of a crack to initiate fracture. McClintock and Walsh included the effect of friction between crack faces, and Modified Griffith was presented. By neglecting the stress required to close cracks, Modified Griffith would be reduced to the following form:

$$\sigma_1\left[\sqrt{\mu^2+1}-\mu\right]-\sigma_3\left[\sqrt{\mu^2+1}+\mu\right]=4T_0 \tag{A.39}$$

$$\frac{C_0}{T_0}=\frac{4}{\sqrt{\mu^2+1}-\mu} \tag{A.40}$$

By including the frictional behavior, Modified Griffith shows similarity to the Mohr-Coulomb Criterion. As it is shown in Eq.40, the ratio of uniaxial compressive strength to tensile strength is a function of internal angle of friction. The effect of intermediate principal stress is not considered in the Modified Griffith criterion since failure theory has been modeled in two-dimensional space.

A.11. Murrell

Murrell introduced a new criterion based on Griffith theory by including the intermediate principal stress as a contributing factor in the rock strength. He extended the Griffith criterion to three-dimensional stress space:

$$(\sigma_1 - \sigma_3)^2 + (\sigma_1 - \sigma_2)^2 + (\sigma_2 - \sigma_3)^2 = 24T_0(\sigma_1 + \sigma_2 + \sigma_3) \quad \text{(A.41)}$$

The ratio between uniaxial compressive strength and uniaxial tensile strength in the Murrell criterion is close to the typical range of the experimental observation:

$$T_0 = \frac{C_0}{12} \quad \text{(A.42)}$$

In terms of octahedral stresses, the Murrell criterion can be written in the following form. The σ_{oct} is equal to mean confining stress, J_1.

$$\tau^2{}_{oct} = 8T_0\sigma_{oct} \quad \text{(A.43)}$$

A.12. Stassi d'Alia

Stassi d'Alia (1967) developed his failure criterion in terms of tensile strength and uniaxial compressive strength.

$$(\sigma_1 - \sigma_3)^2 + (\sigma_1 - \sigma_2)^2 + (\sigma_2 - \sigma_3)^2 = 2(C_0 - T_0)(\sigma_1 + \sigma_2 + \sigma_3) + 2C_0T_0 \quad \text{(A.44)}$$

In this study, the Modified Griffith assumption (Eq.40) was used for determination of tensile requirement in Eq.44.

APPENDIX B

PRESSURE TRANSIENT TESTING PROCEDURE

CORE PREPARATION

1- 2 in diameter cores of Catoosa shale was prepared using coring machine. Synesthetic oil was used as drilling fluid (Figure B-1.a & Figure B-1.b).

2- 2 in diameters cores were cut into disk shape sample with thickness of 0.25 in (Figure B-1.c, Figure B-1.d, and Figure B-1.e).

3- Prepared samples persevered in a bucket of synthetic oil.

4- Prepared samples were secured in a casing (2.5 in OD X 2 in ID) using epoxy (Figure B-1.f).

5- Cased sample was placed in a humid chamber 5 hours before each experiment to maintain water content while epoxy is curing (Figure B-1.f).

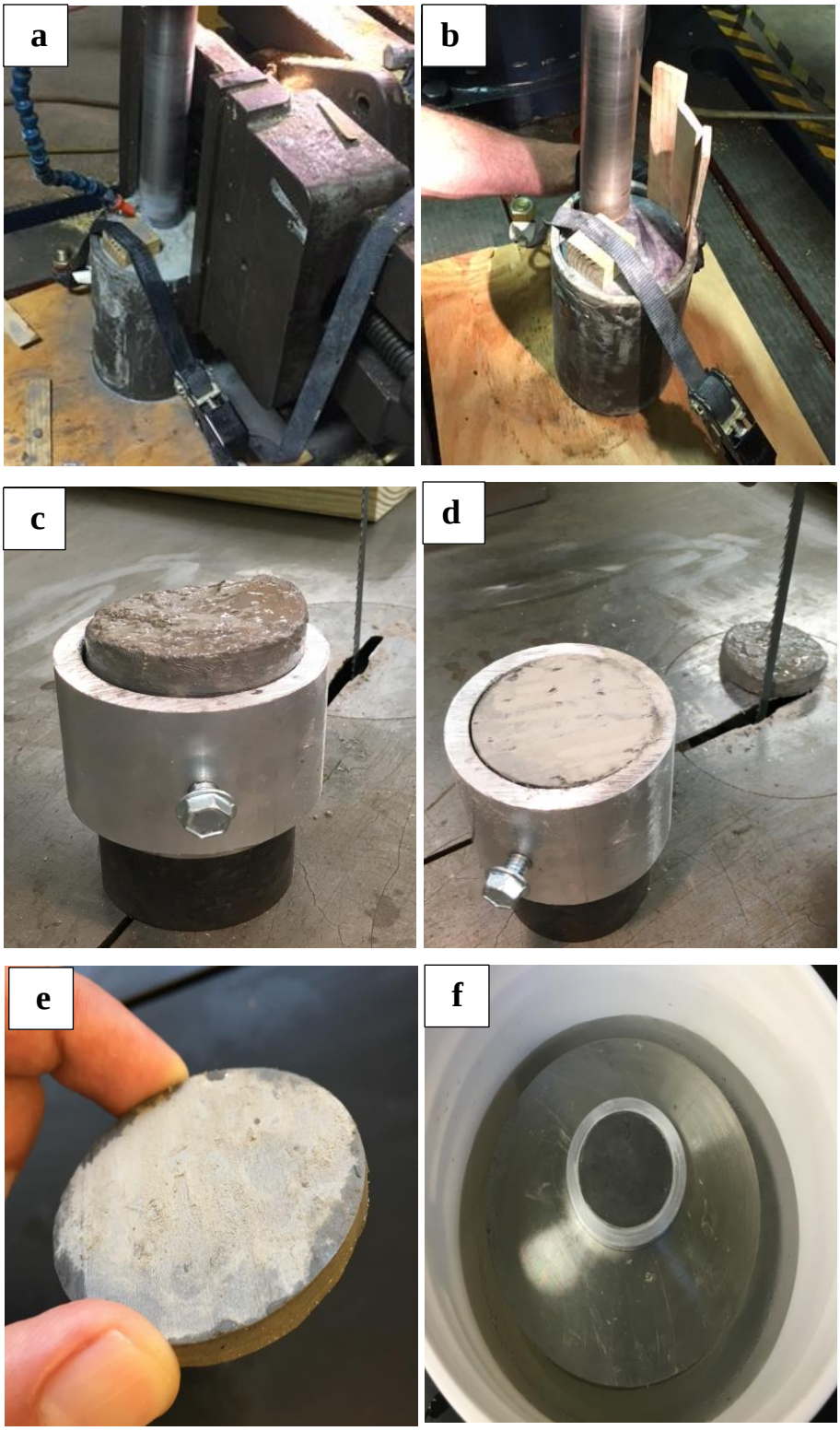

Figure B-0-1. Shale samples preparation

TEST PROCEDURES

1- Place the cased shale sample at the bottom of high pressure high temperature (HPHT) testing cell.

2- Install the lower cap and screw pins in place.

3- Place the HPHT cell in the cell holder (heating chamber).

4- Connect the lower injection line (Including the pressure transducer).

5- Fill the HPHT cell with the testing fluid.

6- Install the upper cap and screw pins in place.

7- Connect the upper injection line and pressure gauge and tighten it.

8- Install the hydraulic cylinder on top of the upper injection line and tighten it with proper sealing tape.

9- Push the floating piston inside the hydraulic cylinder.

10- Connect the hydraulic cylinder to the Isco pump injection line. Use strong sealing tape at the fitting to prevent any leakage.

11- Make sure all two relief valves are closed.

12- Start injecting water into hydraulic cylinder until the testing fluid pressure in the HPHT cell reaches to 50 psi.

13- Start injecting the water through the lower injection line using the Isco pump until you see the pressure transducer reading of 50 psi.

14- Start pressurizing the testing fluid in the HPHT cell from the upper injecting line using Isco pump until pressure of 100 psi observed.

15- Record the pressure log from the Omega transducer during testing time (5 Hours).

16- Stop data logging after 5 hours of testing time and open the upper and the lower relief valves.

17- Stop the pump and stop the data logging, at this point the test is complete.

18- Loosen the upper and the lower injecting line and remove the HPHT cell.

19- Unscrew the upper and the lower caps in the HPHT cell.

20- Drain the testing fluid and remove the shale sample carefully.

21- Clean the system, including the cell inside.

Figure B-0-2. Pressure transient testing setup.

APPENDIX C

HYDRAULIC FRACTURING TEST PROCEDURE

CORE PREPARATION

1- Mix cement in a large container to ensure the consistency of the cores (Figure C-1.1)

2- A 94 lbs sack of Portland cement Class-H was mixed with 38% of water (35 lbs of water) following the recommended mixing procedures.

3- Apply grease or any kind of lubricants inside the molds to easily extract the samples after the dry.

4- Pour the cement mixture into 5 7/8 inch (diameter) x 9 inch (height) molds (Figure C-1.2) while hitting on the molds outside to get rid of the air bubbles.

5- Let the concrete to cure for at least 7 days.

6- Drill ½ inch wellbore in the cement cores using the drill press (Figure C-1.3)

7- Screw casings into the top and bottom cap.

8- Attach top and bottom caps to the cement cores using epoxy (Figure C-1.4) and let the epoxy dry for 24 hrs. Note that each cap needs to be attached on a different day.

9- Grind the core sample or use sanding papers to remove excess dried epoxy and ensure a smooth surface to avoid damaging the confining rubber sleeve.

10- Screw the injection nipple into the top cap (Figure C-1.5)

(1) Mix Cement

(2) Pour cement in molds

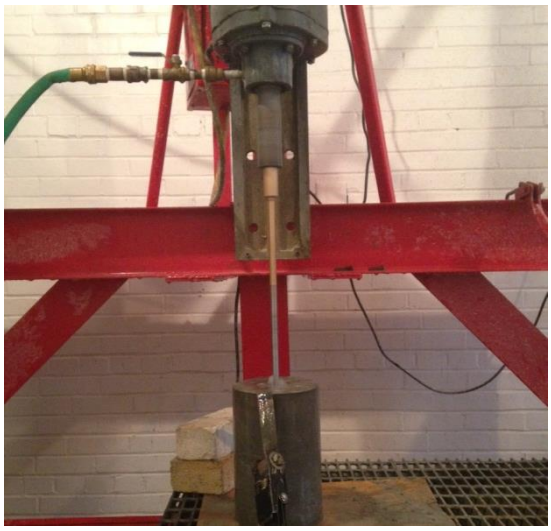

(3) Drill wellbore

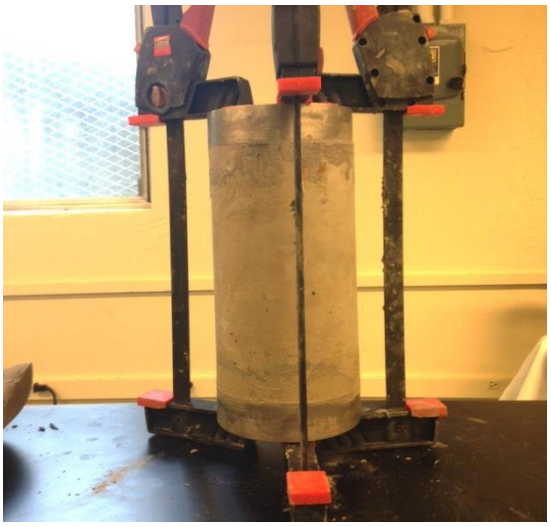

(4) Attach top and bottom cap

(5) Screw Injection Nibble

Figure C-1. Concrete Core Sample Preparation Steps

TEST PROCEDURES

1- Raise the pressure cell and remove the clevis pins after removing the safety cutter pins.

2- Lower the pressure cell (Figure C-2).

3- Place an O-ring inside the pressure cell at the bottom.

4- Place the prepared core in the fracturing cell carefully.

5- Place the three top spacers with O-rings between them on the core sample.

6- Raise the pressure cell and place the clevis pins back again with the safety cutter pins.

7- Once the clevis pins are in place, drop the cell on the clevis until the hoist cables are no longer in tension.

8- Close the cell exit valve.

9- Fill up wellbore with drilling fluid containing LCM

10- Connect the injection line into the injection nipple.

11- Connect the confining line to the cell and close the confining exit line.

12- Apply 400 psi overburden on the core, which reads 7000 psi in the upper gauge, using the hydraulic hand pump.

13- Apply 100 psi confining pressure using the Isco Pump.

14- Fill up accumulator with drilling fluid (without LCM) using the upper plastic accumulator.

15- Open the Isco pump software and assign a name to file and take the injection pump into the remote control.

16- Change the flow rate to 5ml/min and start recording the data (Logging ON) and hit the start button to start injection.

17- Continue injection until a dramatic decrease in the injection pressure is observed, which indicates the sample is fractured. Note that the confining pump will show an increase in the pressure above too.

18- Stop the injection and open the mud exit valve to relief wellbore pressure

19- Close the mud exit valve and start timing (10 minute for fracture healing) before the second cycle.

20- Refill injection pump if needed.

21- Start the second injection cycle until another drop in the injection pressure is observed.

22- Stop the pump and stop the data logging, at this point the test is complete.

23- Open the mud exit valve again to release the wellbore pressure.

24- Remove the overburden pressure and open the confining exit valve to remove confining pressure.

25- Unscrew both injection and confining lines from the pressure cell.

26- Raise the pressure cell and remove the clevis pins after removing the safety cutter pins.

27- Lower the pressure cell.

28- Remove the three top spacers.

29- Pull the core sample out carefully.

30- Clean the system, including the cell inside.

31- Clean both plastic and metal accumulator before the next test if different fluid will be used.

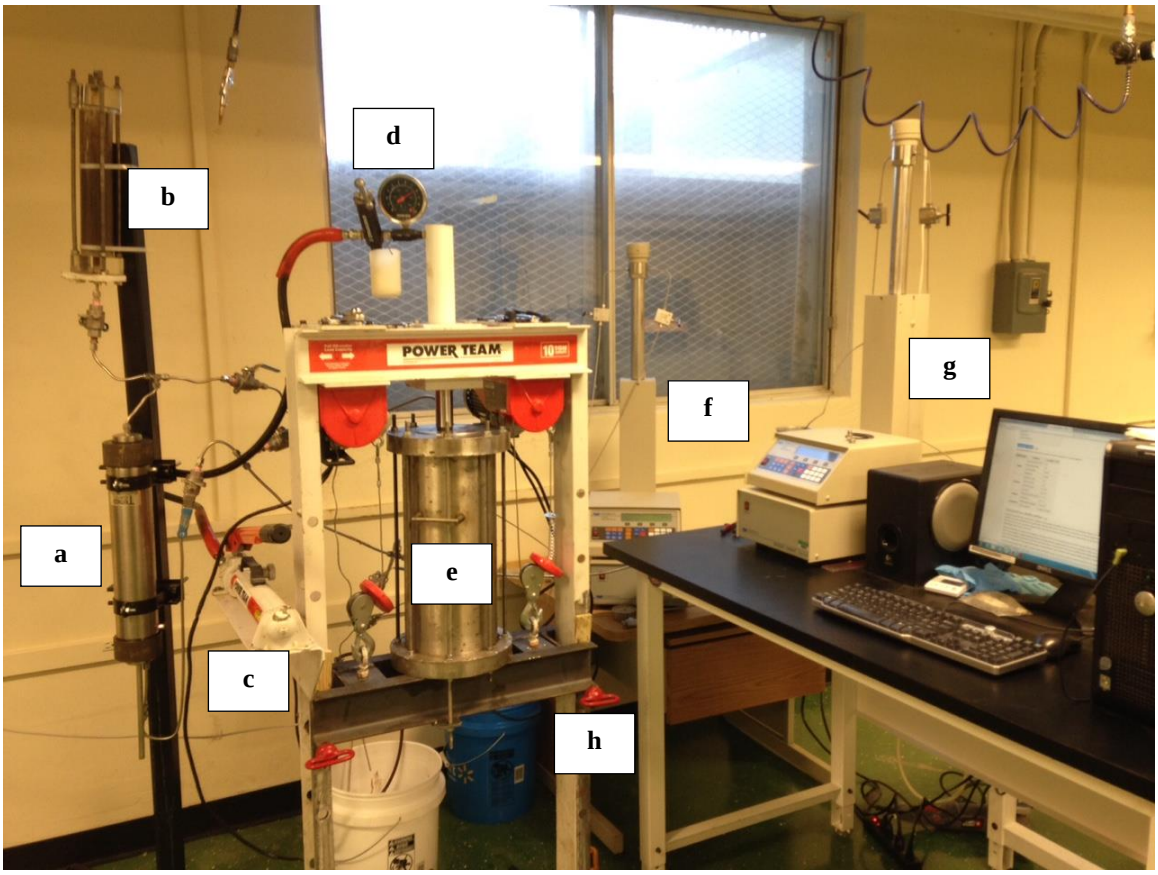

Figure C-2. Hydraulic Fracturing Apparatus; (a) Metal Accumulator, (b) Plastic Accumulator, (c) Hydraulic Hand Pump, (d) Overburden Gauge, (e) Pressure Cell, (f) Confining Pump, (g) Injection Pump, (h) Clevis Pin

APPENDIX D

PUBLICATION FROM THIS DISSERTATION

PUBLISHED PAPERS

Rahimi, R., Nygaard, R. 2015. Comparison of rock failure criteria in predicting borehole shear failure. International Journal of Rock Mechanics and Mining Sciences, Vol 79, P 29-40.

Rahimi, R., Alsaba, M., Nygaard, R. 2016. Can Particle Size Distribution of Lost Circulation Materials Affect the Fracture Gradient? AADE-16-FTCE-80, AADE Fluids Technical Conference and Exhibition, Houston, USA, 12-13 April.

Rahimi, R., Nygaard, R. 2014. What Difference Does Selection of Failure Criteria Make in Wellbore Stability Analysis? 48th U.S. Rock Mechanics/Geomechanics Symposium, Minneapolis, Minnesota, USA, 1–4 June.

PAPERS IN REVIEW

Rahimi, R., Alsaba, M., Nygaard, R. 2016. Analysis of Analytical Fracture Models for Wellbore Strengthening Applications, an Experimental Approach. Submitted to the Journal of Natural Gas Science & Engineering. (Under Review).

Rahimi, R., Nygaard, R. 2016. Effect of Rock Strength Variation on the Estimated Borehole Breakout Using Shear Failure Criteria. Submitted to the Journal of Rock Mechanics and Rock Engineering.

Rahimi, R., Nygaard, R., Akhtarmanesh, S., Hareland, G. Experimental Evaluation on Using Fine Grained Coal Combustion Residuals for Controlling Fluid Invasion in Shales. Intend for submitting to the 2017 Offshore Technology Conference.

BIBLIOGRAPHY

[1] Aadnoy, B.S., Chenevert, M.E. 1987. Stability of highly inclined boreholes. SPE Drilling Engineering, 2(04): 364-374.

[2] Aadnoy, B. S. and Belayneh, M. 2004. Elasto-plastic fracturing model for wellbore stability using non-penetrating fluids. Journal of Petroleum Science and Engineering, 45: 179-192.

[3] Al-Ajmi AM, Zimmerman RW. 2005. Relation between the Mogi and the Coulomb failure criteria. Int J of Rock Mech Min Sci, 42(3): 431–439.

[4] Al-Ajmi AM, Zimmerman RW. 2006. Stability analysis of deviated boreholes using the Mogi-Coulomb failure criterion, with applications to some North Sea and Indonesian reservoirs. SPE-104035. IADC/SPE Asia Pacific Drilling Technology Conference and Exhibition, Bangkok, Thailand, 13-15 November.

[5] Alberty, M. W. and McLean, M. R. 2004. A physical model for stress cages. SPE-90493. SPE Annual Technical Conference and Exhibition, Houston, USA, 26-29 September.

[6] Alsaba, M.T., Nygaard, R., Saasen, A., and Nes, O.M. 2014. Lost circulation materials capability of sealing wide fractures. SPE-170285. SPE Deepwater Drilling and Completions Conference, Galveston, Texas, USA, 10-11 September.

[7] Asokan, P., Saxena, M. and Asolekar, S.R., 2005. Coal combustion residues—environmental implications and recycling potentials. Resources, Conservation and Recycling, 43(3): 239-262.

[8] Babcock, E. A. 1978. "Measurement of subsurface fractures from dipmeter logs." AAPG Bulletin 62.7: 1111-1126.

[9] Ballard, T.J. and Dawe, R.A. 1988. Wettability alteration induced by oil-based drilling fluid. SPE-17160. SPE Formation Damage Control Symposium, 8-9 February, Bakersfield, California.

[10] Ballard, T.J., Beare, S.P. and Lawless, T.A. 1994. Fundamentals of shale stabilisation: water transport through shales. SPE Formation Evaluation, 9(02):129-134.

[11] Beihoffer, T.W., Dorrough, D.S., Schmidt, D.D. 1990. The development of an inhibitive cationic drilling fluid for slim-hole coring applications. SPE-19953. SPE/IADC Drilling Conference, Houston, Texas, 27 February-2 March.

[12] Benz T, Schwab R. 2008. A quantitative comparison of six rock failure criteria. Int J of Rock Mech Min Sci, 45(7): 1176–1186.

[13] Bol, G.M., Wong, S.W., Davidson, C.J. and Woodland, D.C. 1992. Borehole stability in shales. SPE 24975. SPE European Petroleum Conference.

[14] Bol, G.M., Wong, S.W., Davidson, C.J., Woodland, D.C. 1994. Borehole stability in shales. SPE Drilling & Completion, 9(02): 87-94.

[15] Bradley, W.B. 1979. Failure of inclined boreholes. Journal of Energy Resources Technology, 101(4): 232-239.

[16] Brudy, M. and Zoback, M. 1999. Drilling-induced tensile wall-fractures: implications for determination of in-situ stress orientation and magnitude. International Journal of Rock Mechanics and Mining Sciences, 36(2): 191-215.

[17] Cai, J., Chenevert, M.E., Sharma, M.M. and Friedheim, J.E. 2012. Decreasing water invasion into Atoka shale using nonmodified silica nanoparticles. SPE Drilling & Completion, 27(01): 103-112.

[18] Carbonell RJK, Detournay, EJK. 1995. Modeling Fracture Initiation and Propagation from a Pressurized Hole: A Dislocation-Based Approach. 35th U.S. Symposium on Rock Mechanics (USRMS), Reno, Nevada, 5-7 June.

[19] Chen X, Tan CP., Haberfield CM. 1998. A comprehensive practical approach for wellbore instability management. SPE-48898. SPE International Oil and Gas Conference and Exhibition, Beijing, China, 3-6 October.

[20] Chenevert, M.E. 1970. Shale alteration by water adsorption. Journal of Petroleum Technology, 22(09): 1,141 - 1,148.

[21] Chenevert, M. E. 1989. Lecture: Diffusion of water and ions into shales. ISRM International Symposium, Pau, France, 30 August-2 September.

[22] Chenevert, M.E.K., Osisanya, S.O.K. 1992. Shale swelling at elevated temperature and pressure. ARMA-92-0869. The 33th U.S. Symposium on Rock Mechanics (USRMS), Santa Fe, New Mexico, 3-5 June.

[23] Chenevert, M. E., Sharma, A. K. 1993. Permeability and effective pore pressure of shales. SPE- 21918. SPE Drill & Completion, 8(1): 28–34.

[24] Chenevert, M.E. and Pernot, V. 1998. Control of shale swelling pressures using inhibitive water-base muds. SPE-49263. SPE Annual Technical Conference and Exhibition, New Orleans, Louisiana, 27-30 September.

[25] Colmenares LB, Zoback MD. 2002. A statistical evaluation of intact rock failure criteria constrained by polyaxial test data for five different rocks. Int J of Rock Mech Min Sci, 39: 695–729.

[26] Contreras, O., Hareland, G., Husein, M., Nygaard, R. and Al-Saba, M.T. 2014. Experimental investigation on wellbore strengthening in shales by means of nanoparticle-based drilling fluids. SPE-170589. SPE Annual Technical Conference and Exhibition, 27-29 October, Amsterdam, The Netherlands.

[27] Deeg WFJ, Wang H. 2004. Changing borehole geometry and lost-circulation control. 6th North America Rock Mechanics Symposium, Houston, Texas, 5-9 June.

[28] Denis, J.H., Keall, M.J., Hall, P.L., Meeten, G.H. 1991. Influence of potassium concentration on the swelling and compaction of mixed (Na, K) ion-exchanged montmorillonite. Clay Minerals, 26(2): 255-268.

[29] Downs, J.D., Van Oort, E., Redman, D.I., Ripley, D., Rothmann, B. 1993. TAME: A new concept in water-based drilling fluids for shales. SPE-26699. Offshore Europe, Aberdeen, United Kingdom, 7-10 September.

[30] Dupriest, F. E. 2005. Fracture closure stress (FCS) and lost returns practices. SPE-92192. SPE/IADC Drilling Conference, Amsterdam, Netherlands, 23-25 February.

[31] Dupriest, F. E., Smith, M. V., Zeilinger, C. S. and Shoykhet, I. N. 2008. Method to eliminate lost returns and build integrity continuously with high-filtration-rate fluid. SPE-112656. SPE/IADC Drilling Conference, Orlando, Florida, USA, 4-6 March.

[32] Ewy RT. 1999. Wellbore-stability predictions by use of a Modified Lade criterion. SPE-56862. SPE Drill & Completion, 14(2): 85–91.

[33] Ewy, R. T., Stankovich, R. J. 2000. Pore pressure change due to shale-fluid interactions: measurements under simulated wellbore conditions. 4th North American Rock Mechanics Symposium, Seattle, Washington, 31 July-3 August.

[34] Fam, M. A., Dusseault, M. B. 1998. Borehole stability in shales: a physico-chemical perspective. SPE-47301-MS. SPE/ISRM Rock Mechanics in Petroleum Engineering, Trondheim, Norway, 8-10 July.

[35] Fjaer E, Holt RM, Horsrud P, Raaen AM, Risnes R. 2008. Petroleum related rock mechanics. 2rd ed. Oxford. Elsevier.

[36] Forsans, T.M. and Schmitt, L. 1994. Capillary forces: The neglected factor in shale instability studies? SPE-28029. Rock Mechanics in Petroleum Engineering Conference. Delft, Netherlands, 29-31 August.

[37] Fuh, G. F., Morita, N., Byod, P. A., and McGoffin, S. J. 1992. A New approach to preventing lost circulation while drilling. SPE-24599. SPE Annual Technical Conference and Exhibition, Washington D.C., USA, 4-7 October.

[38] Ghassemi, A., Diek, A. 2001. Effects of ion transfer on stress and pore pressure distributions around a borehole in shale. The 38th U.S. Symposium on Rock Mechanics (USRMS), Washington, D.C., 7-10 July.

[39] Griffith, A.A. 1921. The phenomena of rupture and flow in solids. Philosophical transactions of the royal society of London. Series A, containing papers of a mathematical or physical character, 221: 163-198.

[40] Guo Q, Feng YZ, Jin ZH. 2011. Fracture aperture for wellbore strengthening applications. 45th US Rock Mechanics / Geomechanics Symposium, San Francisco, CA, June 26-29.

[41] Guo, Q., Cook, J., Ji, L., and Friedheim, J. E. 2014. A comprehensive experimental study on wellbore strengthening. SPE-167957. IADC/SPE Drilling Conference and Exhibition, Fort Worth, Texas, USA, March 4-6.

[42] Guo, Q., Blue, A., Friedheim, J. 2015. Testing methods for evaluating drilling fluid effects on gas shale stability. 49th U.S. Rock Mechanics/Geomechanics Symposium, San Francisco, California, 28 June-1 July.

[43] Hale, A.H., Mody, F.K., Salisbury, D.P. 1993. The influence of chemical potential on wellbore stability. SPE-23885. Journal of Drilling & Completion, 8(3): 207–216.

[44] Hettema, M., Horsrud, P., Taugbøl, K., Friedheim, J., Huynh, H. Sanders, M. W. and Young, S. 2007. Development of an innovative high-pressure testing device for the evaluation of drilling fluid systems and drilling fluid additives within fractured permeable zones, Paper N. 041/dlg2, Offshore Mediterranean Conference and Exhibition in Ravenna, Italy, 28-30 March.

[45] Hillerborg A, Modeer M, Petersson PE. 1976. Analysis of crack formation and crack growth in concrete by means of fracture mechanics and finite elements. Division of Building Materials Lund Institute of Technology, Lund, vol. 6. Pergamon, Sweden, pp. 773– 782.

[46] Himes, R. E., Vinson, E. F., Simon, D. E. 1989. Clay stabilization in low-permeability formations. SPE Production Operations Symposium, Oklahoma City, Oklahoma, 13-14 March.

[47] Hoek, E., Brown, E.T. 1980. Empirical strength criterion for rock masses. Journal of Geotechnical and Geoenvironmental Engineering, 106(9): 1013–1035.

[48] Hoelscher, K.P., De Stefano, G., Riley, M. and Young, S. 2012. Application of nanotechnology in drilling fluids. SPE International Oilfield Nanotechnology Conference and Exhibition, 12-14 June, Noordwijk, Netherlands. SPE-157031.

[49] Horsud, P. and Bostrom, B. 1998. Interaction between shale and water-based drilling fluids: laboratory exposure tests give new insight into mechanisms and field consequences of KC1 content. SPE-48986.

[50] Horsud, P. 2001. Estimating mechanical properties of shale from empirical correlations. SPE-56017. SPE Drill & Completion, 16(2): 68–73.

[51] Howard, S. K. 1995. Formate brines for drilling and completion: state of the art. SPE-30498. SPE Annual Technical Conference and Exhibition, Dallas, Texas, 22-25 October.

[52] Jaeger J.C., Cook N.G.W., Zimmerman R.W. 2007. Fundamentals of rock mechanics. 4rd ed. Oxford. Blackwell Publishing.

[53] Kaageson-Loe, N. M., Sanders, M. W., Growcock, F., Taugbol, K., Horsrud, P., Singelstad, A. V., and Omland, T. H. 2009. Particulate-based loss-prevention material - the secrets of fracture sealing revealed! SPE Drilling & Completion, 24(4): 581-589.

[54] Karaborni, S., Smit, B., Heidug, W., Urai, J., Van Oort, E. 1996. The swelling of clays: molecular simulations of the hydration of montmorillonite. Science, 271(EPFL-ARTICLE-200818), pp.1102-1104.

[55] Labenski, F., Reid, P., Santos, H. 2003. Drilling fluids approaches for control of wellbore instability in fractured formations. SPE-85304. SPE/IADC Middle East Drilling Technology Conference and Exhibition, Abu Dhabi, United Arab Emirates, 20-22 October.

[56] Marine, I.W., Fritz, S.J. 1981. Osmotic model to explain anomalous hydraulic heads. Water Resources Research, 17(1): 73-82.

[57] Mese, A.I. 1995. Effects of water content and stress state on the mechanical and chemical properties of shale (Doctoral dissertation, Ph. D. Dissertation, The University of Texas at Austin).

[58] McClintock, F.A., Walsh, J.B. 1962. Friction on Griffith cracks in rocks under pressure. 4th US Nat. Congr. Appl. Mech., 2: 1015-1022.

[59] McLean MR, Addis MA. 1990. Wellbore Stability Analysis: A review of current methods of analysis and their field application. SPE-19941. IADC/SPE Drilling Conference, Houston, Texas, February 27- March 2.

[60] Mody, F.K., Hale, A.H. 1993. Borehole-stability model to couple the mechanics and chemistry of drilling-fluid/shale interactions. Journal of Petroleum Technology, 45(11): 1-093.

[61] Mody, F. K., Tare, U. A., Tan, C. P., Drummond, C. J., & Wu, B. 2002. Development of novel membrane efficient water-based drilling fluids through fundamental understanding of osmotic membrane generation in shales. SPE-77447. SPE Annual Technical Conference and Exhibition, San Antonio, Texas. 29 September-2 October.

[62] Morita, N., Black, A. D., and Fuh, G. F. 1990. Theory of lost circulation pressure. SPE 20409. SPE Annual Technical Conference and Exhibition, New Orleans, Louisiana, USA, 23-26 September.

[63] Morita, N., Fuh, G. F., and Black, A. D. 1996a. Borehole breakdown pressure with drilling fluids-I. Empirical results. International Journal of Rock Mechanics and Mining Sciences & Geomechanics, 39-51.

[64] Morita, N., Fuh, G. F., and Black, A. D. 1996b. Borehole breakdown pressure with drilling fluids-II. Semi-analytical solution to predict borehole breakdown pressure. International Journal of Rock Mechanics and Mining Sciences & Geomechanics, 53-69.

[65] Morita N, Fuh GF. 2012. Parametric Analysis of Wellbore-Strengthening Methods from Basic Rock Mechanics. SPE Drill & Completion, 27(2): 315-327.

[66] Mostafavi, V., Hareland, G., Belayneh, M. and Aadnoy, B. S. 2011. Experimental and mechanistic modeling of fracture sealing resistance with respect to fluid and fracture properties. ARMA 11-98. 45th US Rock Mechanics Symposium, San Francisco, USA, 26-29 June.

[67] Murrell, S.A.F. 1963. A criterion for brittle fracture of rocks and concrete under triaxial stress and the effect of pore pressure on the criterion. Rock mechanics, pp.563-577.

[68] Nawrocki PA. 2010. Critical wellbore pressures using different rock failure criteria. ISRM International Symposium and 6th Asian Rock Mechanics Symposium, New Delhi, India, 23–27 October.

[69] Nygaard, R., Salehi, S. 2011. Critical review of wellbore strengthening: physical model and field deployment. AADE-11-NTCE-24, AADE National Technical Conference and Exhibition, Houston, Texas, USA, 12-14 April.

[70] ODCE. 2012. Ocean Discharge Criteria Evaluation. For The General Permit GMG290000. 2 February.

[71] Okland D, Cook JM. 1998. Bedding-related borehole instability in high-angle wells. SPE-47285. SPE/ISRM Rock Mechanics in Petroleum Engineering, Trondheim, 8-10 July.

[72] Olphen, H.V. 1977. An introduction to clay colloid chemistry, for clay technologists, geologists, and soil scientists. An introduction to clay colloid chemistry, for clay technologists, geologists, and soil scientists, 2nd edition.

[73] Retz, R.H., Friedheim, J., Lee, L.J., Welch, O.O. 1991. An environmentally acceptable and field-practical, cationic polymer mud system. SPE-23064. Offshore Europe, 3-6 September, Aberdeen, United Kingdom.

[74] Russel KA, Ayan C, Hart NJ, Rodriguez JM, Scholey H, Sugden C, Davidson JK. 2006. Predicting and preventing wellbore instability: Tullich field development, North Sea. SPE Drill & Complet, 14(1): 12-22

[75] Salisbury, J.W., D'Aria, D.M., Jarosewich, E. 1991. Midinfrared (2.5–13.5 μm) reflectance spectra of powdered stony meteorites. Icarus, 92(2): 280-297.

[76] Santos, H., Diek, A., Roegiers, J.C., Fontoura, S. Can shale swelling be (easily) controlled? ISRM-EUROCK-1996-014. ISRM International Symposium- EUROCK 96, Turin – Italy, 2-5 September.

[77] Santos, H., Diek, A., Da Fontoura, S., Roegiers, J.C. 1997. Shale Reactivity test: a novel approach to evaluate shale-fluid interaction. International Journal of Rock Mechanics and Mining Sciences, 34(3): 268-e1-e11.

[78] Savari, S., Kumar, A., Whitfill, D. L., Miller, M., Murphy, R. J., and Dale E. Jamison. 2013. Engineered LCM design yields novel activating material for potential application in severe lost circulation scenarios. SPE-164748. SPE North Africa Technical Conference and Exhibition, Cairo, Egypt, 15-17 April.

[79] Schmitt, L., Forsans, T., Santarelli, F.J. 1994. Shale testing and capillary phenomena. International Journal of Rock Mechanics and Mining Sciences, 31(5): 411-427.

[80] Sensoy, T., Chenevert, M.E. and Sharma, M.M. 2009. Minimizing water invasion in shales using nanoparticles. SPE-124429. SPE Annual Technical Conference and Exhibition, New Orleans, Louisiana, 4-7 October.

[81] Shahri MP, Trevor TO, Safari R, Karimi M, Mutlu O. 2015. Advanced semianalytical geomechanical model for wellbore-strengthening applications. SPE-167976. SPE Drill & Completion.

[82] Sharma, M.M., Chenevert, M.E., Guo, Q., Ji, L., Friedheim, J. and Zhang, R. 2012. A new family of nanoparticle based drilling fluids. SPE-160045. SPE Annual Technical Conference and Exhibition, San Antonio, Texas, USA, 8-10 October.

[83] Sherwood, J.D., Bailey, L. 1994. Swelling of shale around a cylindrical wellbore. In Proceedings of the Royal Society of London A: Mathematical, Physical and Engineering Sciences, 444 (1920): 161-184.

[84] Stassi-D'Alia, F. 1967. Flow and fracture of materials according to a new limiting condition of yielding. Meccanica, 2(3): 178-195.

[85] Steiger, R.P. 1982. Fundamentals and use of potassium/polymer drilling fluids to minimize drilling and completion problems associated with hydratable clays. Journal of Petroleum Technology, 34(08): 1661 - 1670.

[86] Steiger, R.P., Leung, P.K. 1991. Critical state shale mechanics. ARMA-91-293. The 32nd U.S. Symposium on Rock Mechanics (USRMS), Norman, Oklahoma, 10-12 July.

[87] Steiger, R.P. 1993. Advanced triaxial swelling tests on preserved shale cores. International Journal of Rock Mechanics and Mining Sciences, 30(7): 681-685.

[88] Tan CP, Willoughby DR. 1999. A pragmatic approach to managing wellbore instability in extended reach wells in the Goodwyn field. SPE-56565. SPE Annual Technical Conference and Exhibition, Houston, Texas, 3-6 October.

[89] Tehrani, A., Friedheim, J., Cameron, J. and Bill Reid. 2007. Designing fluids for wellbore strengthening – Is It an Art? AADE-07-NTCE-75, AADE National Technical Conference and Exhibition, Houston, Texas, USA, 10-12 April.

[90] Van Oort, E. 1994. A novel technique for the investigation of drilling fluid induced borehole instability in shales. SPE-28064. Rock Mechanics in Petroleum Engineering, Delft, Netherlands, 29-31 August.

[91] Van Oort, E., Hale, A.H., Mody, F.K. 1995. Manipulation of coupled osmotic flows for stabilisation of shales exposed to water-based drilling fluids. SPE-30499. SPE Annual Technical Conference and Exhibition, Dallas, Texas, 22-25 October.

[92] Van Oort, E., Hale, A.H., Mody, F.K., Roy, S. 1996. Transport in shales and the design of improved water-based shale drilling fluids. SPE-28309. SPE Drilling & Completion, 11(3): 137-146.

[93] Van Oort, E., Ripley, D., Ward, I., Chapman, J. W., Williamson, R., Aston, M. 1996. Silicate-Based Drilling Fluids: Competent, Cost-effective and Benign Solutions to Wellbore Stability Problems. SPE-35059. SPE/IADC Drilling Conference, New Orleans, Louisiana, 12-15 March.

[94] Van Oort, E. 1997. Physico-chemical stabilization of shales. SPE-37263. International Symposium on Oilfield Chemistry, Houston, Texas 18-21 February.

[95] Van Oort, E. 2003. On the physical and chemical stability of shales. Journal of Petroleum Science and Engineering, 38(3-4): 213-235.

[96] Van Oort E, Friedheim J, Pierce T, Lee J. 2011. Avoiding losses in depleted and weak zones by constantly strengthening wellbores. Journal of Drilling & Completion, 26(4): 519–530.

[97] Veeken C.A.M., Walters J.V., Kenter C.J., Davies D.R. 1989. Use of plasticity models for predicting borehole stability. ISRM International Symposium, Pau, France, August 30-September 2.

[98] Yi X., Ong S.H., Russel JE. 2005. Improving borehole stability analysis by quantifying the effects of intermediate principal stress using polyaxial rock strength test data. 40th U.S. Symposium on Rock Mechanics (USRMS), Anchorage, Alaska, 25–29 June.

[99] Young, S. and Friedheim, J. 2013, March. Environmentally friendly drilling fluids for unconventional shale. Offshore Mediterranean Conference and Exhibition, 20-22 March, Ravenna, Italy.

[100] Wang H, Sweatman R, Engelman B, Deeg W, Whitfill D, Soliman M, Towler BF. 2008. Best practice in understanding and managing lost circulation challenges. SPE Drill & Completion, 23(2): 168-175.

[101] Ward, I., Chapman, J.W. and Williamson, R. 1997. Silicate based muds: Chemical optimization Based on field Experience. SPE-37266. International Symposium on Oilfield Chemistry, Houston, Texas, 18-21 February.

[102] Zhang L, Cao P, Radha KC. 2010. Evaluation of rock strength criteria for wellbore stability analysis. Int J of Rock Mech Min Sci, 47(8): 1304–1316.

[103] Zhou, S. 1994. A program to model the initial shape and extent of borehole breakout. Computers & Geosciences, 20(7-8): 1143-1160.

VITA

Reza Rahimi entered Petroleum University of Technology in Abadan, Iran in 2005 and completed his Bachelor's degree in 2009. He has completed two summer internships with Iranian Offshore Oil Company (IOOC) and National Iranian Oil Company (NIOC) in 2007 and 2008. After finishing his Bachelor's degree, he was employed by PETROPRAS Oil and Gas Institute (POGI) as a Research Engineer. Later he was hired by MAPSA ENG Co. and PETROPARS Ltd to work on the offshore drilling project of the South Pars gas field in the Persian Gulf. In August 2012, he entered the graduate school of Missouri University of Science and Technology as a Master's student in Petroleum Engineering program. Reza completed his MS in the Petroleum Engineering in May, 2014. Reza served as an instructor for the drilling fluid laboratory and also as a teaching assistant for multiple undergraduate and graduate petroleum engineering courses. He established the American Rock Mechanics Association (ARMA) Missouri S&T student chapter and served as a president of the organization. Also, he was an active member of the Society of Petroleum Engineer (SPE) and American Association of Drilling Engineer (AADE) student chapters. Reza received his Ph.D. in Petroleum Engineering from Missouri University of Science and Technology in December, 2016.